R. & M. No. 3581

MINISTRY OF TECHNOLOGY

AERONAUTICAL RESEARCH COUNCIL
REPORTS AND MEMORANDA

Co-ordinated Experimental and Theoretical Research on the Oscillatory Airforces for Selected Planforms at Subsonic and Supersonic Speeds

By D. L. Woodcock

Structures Dept., R.A.E., Farnborough

LONDON: HER MAJESTY'S STATIONERY OFFICE

1969

PRICE £2 10*s.* 0*d.* NET

Co-ordinated Experimental and Theoretical Research on the Oscillatory Airforces for Selected Planforms at Subsonic and Supersonic Speeds

By D. L. Woodcock

Structures Dept., R.A.E., Farnborough

Reports and Memoranda No. 3581[φ]
February, 1968

Summary.

Oscillatory heave and pitch derivatives have been determined experimentally and theoretically for a set of eight planforms – three cropped delta wings, three arrowhead wings, and two unswept tapered wings. Three experimental procedures of widely different type were used. These were a free oscillation technique for a wall-mounted half-span wind-tunnel models. A similar technique for models mounted on rocket-boosted test vehicles and an inexorable forcing technique of the internal rigid drive type applied to half-span wind-tunnel model wings. The theoretical values were obtained by various forms of lifting-surface theory. All these results are tabulated and compared. They cover a Mach number range of approximately 0·8 to 2·5. Some theoretical values of control-surface derivatives are included in the Tables, and a few other miscellaneous experimental or theoretical results are also described.

CONTENTS

[φ]Replaces R.A.E. Tech. Report 68 033—A.R.C. 30 105.

LIST OF TABLES

LIST OF ILLUSTRATIONS

41–47 Free flight results compared with theory-subsonic – wings A–G ($A = 4$ version)

48–50 Variation of l_θ with $A\sqrt{1-M^2}$ – wings A, B and F

51–52 Variation of $(-m_\theta)$, $(-m_{\dot{\theta}})$ with M – wing G ($A = 3$ version)

53–54 Variation of l_θ, $l_{\dot{\theta}}$ with M – wing G ($A = 3$ version)

---

1. *The Research Project.*

More than a decade ago the Flutter and Vibration Committee of the then Ministry of Supply, being much concerned with the inadequacy of methods of flutter prediction at that time, launched an ambitious research programme[1, 2] on oscillatory aerodynamic derivatives involving both government research establishments and industrial organisations. The objective was to develop theoretical methods of prediction for linearised potential flow (three-dimensional lifting surface theory) for all subsonic and supersonic flow regimes, and then to test these methods by experimental comparisons for a wide range of parameter variations (planform, Mach number, reduced frequency, mode of oscillation). Full details of the original programme are given in Ref. 2. Seven* planforms were selected (*see* Table 1) and the investigation was limited in the main to the derivatives for heave, pitch and control-surface rotation.

A few years later the experimental part of this research programme developed into a combined Commonwealth exercise under the influence of the Commonwealth Advisory Aeronautical Research Council (CAARC) with Australia and Canada taking an active part as well as the U.K. Further experiments were added to the programme. The aim of this extension was the comparison of different methods of determining experimentally the rigid body derivatives.

Both these projects have now been completed, apart from the experimental determination of the control surface derivatives, and several papers[6-17] have been issued on various portions of them. An interim statement on the progress of the original research programme was issued some years ago[3] but, bearing in mind that it will be some time before the control-surface derivative measurements are available and also that the CAARC exercise is now completed, the time is now ripe for an up-to-date thorough survey of all that has been done.

2. *Theoretical Investigations.*

2.1. *Subsonic Low-Frequency Calculations.*

Calculations of the limiting values of the rigid body derivatives**, as the frequency tends to zero, were made by Hornsby[6] in 1957, using a digital computer programme of Garner's adaptation[18] of Multhopp's steady flow lifting-surface theory[19]. This is a collocation solution of the integral equation giving the downwash in terms of the loading. It is assumed that terms involving powers of the frequency greater than the first can be neglected. Recently Garner[20] has shown that the method of spanwise integration that he and Multhopp used is not always accurate enough for collocation points near the wing leading or trailing edges. The inaccuracy is greater near the leading edge and gets worse with increase of aspect ratio. The more chordwise collocation points one uses and the greater the wing aspect ratio the more important it is that an improved method of spanwise integration should be used. Garner has developed a suitable method[21] which has been applied to one of the planforms (wing E) of this research programme. These results (Table 2, part (a)) indicate the order of error that may be present in Hornsby's results. With this example the differences are never greater than 3 per cent.

Also included in Table 2 (part (b)) are derivatives obtained by first determining the forces on the wing in reverse flow and then using the reverse flow theorem[22]. The differences between the two sets give some indication of the accuracy with which the integral equation has been solved in the two cases; for, if a good approximation had been obtained to the solution for the wing in direct flow and in reverse flow,

---

*A further planform was later added.

**The derivatives are defined in the Appendix.

there would be negligible differences between the two sets of derivatives. The converse does not however hold. Negligible differences do not necessarily imply that a good approximation to the true solution has been obtained.

One can conclude therefore that Hornsby's[6] results are of reasonable accuracy, sufficient for theoretical experimental comparisons which are the subject of this Report. More accurate values could have been obtained by using more collocation points (Hornsby[6] used 15 spanwise × 4 chordwise) and a more accurate method of spanwise integration. The complete set of results from Ref. 6 are given as the $\nu = 0$ (i.e. zero frequency parameter) entries in Tables 3 to 8 and 23 to 26. These include control surface derivatives which were obtained using the equivalent slope and displacement method due to Richardson[23]. For a two-dimensional wing a discontinuous chordwise upwash distribution can be replaced by an equivalent smooth distribution which gives the same overall forces on the whole wing; and for a slender wing a discontinuous spanwise upwash distribution can be similarly replaced by a smooth distribution. These two smooth distributions are combined by Richardson[23] to form an equivalent smooth upwash distribution for a three-dimensional wing.

2.2. *Subsonic Calculations for General Frequency.*

A Multhopp-type collocation method due to Davies[24] was used for the subsonic calculations at non-zero frequency. This uses the same method of spanwise integration as in the original Multhopp-Garner method[18] and so the remarks made in Section 2.1 about resulting inaccuracies still apply. The number of collocation points used by Woodcock[8] was 12 spanwise × 4 chordwise compared with 15 × 4 for the low frequency case[6]. Further work by Woodcock[25], in which he examined numerically, for several planforms, the relationship between the calculated values of the derivatives and the numbers of collocation points, indicated that, for the planforms and modes considered in the present Report, the best accuracy would be obtained with about twice as many spanwise as chordwise collocation points. One of the planforms used in that Report[25] was wing E of the present series. Some of the results obtained are reproduced in Table 2 section (d). Examination of all the results showed that the difference in derivative values obtained from calculations with 12 × 4 points and those with 12 × 6 points are, in general, less than 5 per cent and often much less. The exceptions are in the vicinity of a zero of a derivative and so are not significant. This confirms a similar conclusion obtained in Ref. 8 from one calculation for wing A at zero Mach number.

The equivalent slope and displacement method[23], used by Hornsby[6], was also used by Woodcock[8] when determining the control-surface derivatives. Since his results were issued an improved treatment of control surfaces has been suggested[24] but no results are yet available to show the magnitude of the improvement. The relevant derivative values from Ref. 8 are reproduced in Tables 3 to 10 and 23 to 35.

2.3. *Supersonic Collocation Solutions.*

For the calculations at low supersonic speeds – that is for cases where the wing leading edge was subsonic – a collocation method developed by Harris[26, 27] at the Royal Aircraft Establishment (RAE) was chosen. This is a refinement of the method originally proposed by Richardson[28]. The solution is a function not only of the number of collocation points but also of the number of stations used in the numerical integration over the wing section of the forward Mach cone from a collocation point. The results given in Ref. 10, and reproduced here in Tables 11 to 16, were obtained using 10 spanwise × 5 chordwise collocation points and 11 spanwise × 5 chordwise integration points in each Mach cone. Experience suggested that this arrangement would be adequate. However further confirmation was sought by comparison with the results of steady flow calculations by methods[29, 30, 31] of known good accuracy. In each case, for all the Mach numbers considered in the unsteady calculations, the results obtained by Harris's method at zero frequency were little different from those given by the other methods – the greatest discrepancy being less than 4 per cent (*see* Ref. 10). The calculations made by this method have so far been limited to the main surface derivatives.

2.4. *Box Method Calculations for High Supersonic Speeds.*

All the above mentioned calculations (Sections 2.1, 2.2 and 2.3) are solutions of the integral equation expressing the prescribed downwash at the wing surface in terms of the loading distribution. In 1952

Stewartson[32] obtained an equation applicable to a wing whose leading edge is supersonic in the vicinity of the wing apex, expressing the velocity potential at a point as the sum of an integral of the prescribed downwash, over part of the wing surface inside the forward Mach cone, and an integral of the velocity potential, over the remainder of the wing surface inside the forward Mach cone. Hunt[33] and Barnes[34] developed a method for evaluating the velocity potential, and hence the leading distribution, from this equation using an integration lattice formed by uniformly spaced intersecting Mach lines.

This method was applied by Barnes[7] to determine the rigid body and control-surface derivatives for wings A, B, D, E and G ($A = 3$ version) in a number of cases when the leading edge was supersonic. The lattice size used was such that there was 8 to 16 lattice points along the mean chord. This was predicted[34] to give results accurate to within 4 per cent. The derivative values calculated by Barnes[7] are given in Tables 17 to 21. It will be seen (cf. also Ref. 10 and Figs. 6 to 9, 12 to 15) that they form an acceptable continuation of the derivative – Mach number curves for lower supersonic speeds given by Harris's calculations[10]. Some values for the planform G (A = 3 version) are compared with Lehrian's results[12] in Figs. 51 to 54, and other comparisons are made in Ref. 12.

2.5. *Supersonic Low Frequency Calculations.*

A method due to Malvestuto[35,36,37] *et al*, was used by Orlik-Rüchemann[17] to determine the limiting values of the rigid body derivatives, as the frequency tended to zero, for the subsonic leading edge supersonic flow cases. Malvestuto obtained closed form expressions for the derivatives. In doing so he used a slightly different approximation for the loading in the wing tip region from that used by Jones and Cohen[29]. However the difference is certainly insignificant as regards the stiffness derivatives for the cases considered here. Comparison between Orlik-Rückemann's[17] values and the values obtained by Harris[10] using the method of Ref. 29 (and given in Ref. 10) showed very good agreement particularly for the wings D, E, and F.

For the case of supersonic leading edges Orlik-Rückemann[17] used design charts [38,39] obtained by a similar method. These results are probably slightly less accurate, because of the interpolation involved, than those for the lower Mach numbers. The complete set of theoretical results from Ref. 17 are given in Tables 11 to 20.

2.6. *Miscellaneous Calculations.*

A number of miscellaneous derivative calculations have been made for one or more of the planforms of this research programme. In nearly every case they were made primarily for some other reason. The results of these calculations will not in general be given here; but the following survey summarises what has been done.

In 1960 Adams[9] issued the results of calculations by Richardson's method[28] of the derivatives for wing B. The cases considered were $M = 1{\cdot}25$ using 11 spanwise $\times$ 5 chordwise collocation points, and $M = 1{\cdot}41$ using 11 $\times$ 4 collocation points. In both cases the frequency was assumed to be vanishingly small. The results obtained were disappointing. For example the value found for l_θ at $M = 1{\cdot}41$ was 1·26 compared with 1·37 given by steady flow theory[10]. This suggested, as had been suspected, that the method of spanwise integration used in Ref. 28 was inadequate. Adams was not able to continue with this work, which had been part of the original research programme; and as a consequence it was taken over by Harris (*see* Section 2.3) who used an improved method of spanwise integration which has proved to be adequate.

Lehrian in Ref. 40 obtained a closed form solution, exact to first order in frequency, for the linearised potential flow problem of an hexagonal wing oscillating in supersonic flow. She evaluated her solution, which is limited to wings with sonic or supersonic leading and trailing edges and non-interacting tip regions, for the two versions of wing G. The results are given in Refs. 11 and 12, and are reproduced in Tables 21 and 22. In addition comparisons are made in these papers with derivatives obtained from 2-dimensional strip theory and with the experimental values measured by Hall and Osborne[15].

As part of a separate research project Garvey[41] made some further calculations for the two slenderest wings (C and F) using a box method due to Allen and Sadler[42]. This method is based on the integral equation which gives the downwash in terms of the velocity potential. This is solved approximately using a lattice formed by intersecting Mach lines. The mesh size used by Garvey was such that there were

4 to 5 boxes on the semi span and between 16 and 30 boxes along the root chord. In Ref. 10 Harris showed that there were satisfactory agreement between his results and Garvey's though a direct quantitative comparison was not possible because the two calculations were made for different values of the frequency. The comparisons were for Mach numbers of 1·077 and 1·2806. Garvey[41] made calculations in addition for wing C at $M = 1{\cdot}0440$ and 1·1662.

The wing E has attracted particular attention as a suitable guinea pig for theoretical research. It has been used by Lehrian and Garner[13,22] in assessing different methods of determining control surface derivatives, by Woodcock[25] in an investigation already mentioned (Section 2.2), and is also involved in a current AGARD research project. The values calculated by Garner which are given in Table 2 form part of the latter item.

Also to be mentioned briefly are some evaluations[10,17] of the deriatives for triangular wings which are close approximations to the cropped delta wings A, B and C. The method[43,44] used was the series solution in the frequency parameter, originally due to Watkins. These calculations provided an initial estimate of the effect of frequency on the derivatives which was later confirmed by the collocation solutions due to Harris[10].

3. *Experimental Investigations.*

3.1. *Tunnel Measurements – Free Oscillation Technique.*

One can by measuring and analysing the decaying free oscillations of a rigid wing, free to rotate about a fixed axis against an elastic constraint, both in the wind stream and in vacuum, deduce what the air-forces are. This requires an assumption as to the form of the equation of motion. Presuming it is a second order differential equation with constant coefficients* one obtains expressions for the pitching derivatives as functions of the frequency and rate of decay for the two conditions and the stiffness of the elastic constraint. This was the method used by Orlik-Rückemann[17] to determine the pitching derivatives for two or more axes of rotation for each of the set of planforms apart from the wings G. The free oscillations were instigated by exciting the wing at its natural frequency, using a feedback system to control the frequency, and then cutting off the excitation when the motion had reached a preset amplitude. This procedure should minimise motion at the other natural frequencies and also ensure that the wake is fully established. The ensuing decaying oscillation was then analysed on a dampometer[57]. The derivatives were then obtained from the measured frequency and rate of decay, assuming that the latter was small enough for powers of it higher than the first to be neglected.

The measurements were made in the National Aeronautical Establishment (N.A.E.) 16 in. × 30 in. intermittent suction wind tunnel (*see* Table 27). The models were half-span models mounted to one side wall of the tunnel. Details are given in Table 28. Each model was separated from the tunnel wall by a reflector plate placed $\frac{1}{2}$ in. away from the actual wall in order to minimise the effect of the boundary layer at the tunnel wall. Small end plates were also fitted to the root chord of the models in order to reduce the effects of the small gap (0·01 in.) between the root and the reflector plate. Details of the measuring technique are given in Ref. 50. For each set of experimental conditions at least 10 wind-on readings, in one tunnel run, and 10 wind-off readings in vacuum (as well as readings at atmospheric pressure) were made, which were averaged to give one pair of data points (i.e. values of $-m_\theta$ and $-m_{\dot\theta}$ for a chosen axis position). In most cases a further tunnel run was made to give a second pair of data points for the same set of conditions.

These measured derivatives will, amongst other things, be functions of the axis position, Mach number, frequency, and rate of decay. However, provided the rates of decay are always small, it is assumed that they are good approximations to the derivatives appropriate to maintained sinusoidal oscillations of infinite duration. In general at each Mach number, for each wing, measurements were made for two axis positions and at two frequencies (obtained by using two different elastic constraints). For wings B and E measurements were also made at a third frequency. The results obtained showed a rather larger effect of frequency than one would expect. This was so for all the planforms, at all the Mach numbers investigated, without exception. Typical results are shown in Figs. 2 to 5. The theoretical predictions always gave little variation in value over the range of frequencies of the tunnel tests. No explanation

*This is an approximation to the integro-differential equation given by current theory.

of this discrepancy has yet been found. We will return to this point later (Section 4.2).

Since only the pitching derivatives, $(-m_\theta)$, $(-m_{\dot\theta})$, were obtained, and only two axis positions were used for each wing, it is not in general possible to deduce the derivatives appropriate to a further axis. However, in the limit when the frequency tends to zero, theory concludes that the stiffness derivatives due to heaving (l_z and $-m_z$) are zero; and that the damping derivatives due to heaving ($l_{\dot z}$ and $-m_{\dot z}$) are equal to the corresponding stiffness derivatives due to pitching (l_θ and $-m_\theta$ respectively). Thus in this case a complete set of derivatives for any axis position can be derived. The derivatives for maintained oscillation at $\nu = 0$ (zero frequency) were obtained by extrapolation from the measured values assuming that $-m_\theta$ and $-m_{\dot\theta}$ (with a small correction* to account for the non-zero decay rate of the actual motion) varied linearly with ν^2. This assumption agreed well with the measured values at 3 frequencies obtained for wings B and E.

Derivatives thus obtained, for $\nu = 0$, referred to an axis through the wing apex are given in Tables 29 to 46. The pitching derivatives $(-m_\theta)$, $(-m_{\dot\theta})$ are plotted in Figs. 6 to 17. It was not possible to analyse similarly the transonic results since they were made for only one frequency. The frequency varied little over the whole range of M and so the results are given, in Figs. 18 to 25, as curves of derivatives against Mach number for approximately constant frequency (i.e. constant νM).

A number of possible sources of inaccuracy were considered during the tests and where possible tests made to assess their importance. Approximate measurements of the lowest natural frequency of each model, clamped at its attachment to the elastic constraint, indicated that flexibility effects should be negligible at the test frequencies. The effects of aerodynamic drag, and of a cavity behind the reflection plate, were also investigated and found to be small. Experience in the United Kingdom, mainly at the National Physical Laboratory (N.P.L.) has indicated that tunnel interference effects may be large in tunnels with slotted walls. The arrangement used by Orlik-Rückemann[17] was however different from that for which large effects were discovered – in effect a full-span horizontally mounted model in a tunnel with solid roof and floor and slotted side walls in contradistinction to the slotted roof and floor and solid side walls used at the N.P.L. In fact Garner's theoretical treatment[46] of the subsonic case does suggest that the former arrangement will nearly always produce less interference. For the N.A.E. tunnel (*see* Table 27) the two most significant interference parameters used in Ref. 46 (δ_0 and δ'_0) are much smaller than those for tunnels where large interference effects have been reported[46]. Approximate values for comparison are

	δ_0	δ'_0
N.A.E. 16 in. × 30 in.	0·02	0·03
N.P.L. 14 in. × 36 in.	−0·11	0·07
N.P.L. 20 in. × 25 in.	−0·25	0·15
H.S.D. 20 in. × 22 in.	−0·24	0·14
H.S.D. 20 in. × 22 in. (slots closed)	0·13	−0·01

These relate to small half models. The last three tunnels have slotted roofs and floors. The H.S.D. (Hawker Siddeley Dynamics Ltd.) one is that used for the experiment described later in Section 3.2, and the two N.P.L. tunnels are ones where measured values of oscillatory derivatives have been shown to be considerably modified by tunnel interference[46]. In the tests in the H.S.D. tunnel diffusion screens were fitted behind the slots and so the conditions approximated more closely to be slots closed than the slots open condition.

The effect of fixing boundary-layer transition was investigated for wing A using a transition strip applied close to the leading edge. Repeat measurements were made for the three supersonic Mach

*The relationships used were obtained by writing the aerodynamic pitching moment for the actual decaying moment as

$$M_\theta\,\theta + M_{\dot\theta}\,\dot\theta + M_{\ddot\theta}\,\ddot\theta + M_{\dddot\theta}\,\dddot\theta$$

and then neglecting certain terms (*see* Ref. 17).

numbers and in some cases appreciable differences in the measured values were found. Typical points are shown on Figs. 26 and 27. The greatest difference was in the value of $-m_{\dot{\theta}}$ for the aftmost axis ($0{\cdot}759\,c_0$), at $M = 1{\cdot}56$ and $\nu = 0{\cdot}066$, where addition of the transition strip produced about 13 per cent increase in the value of the derivative (*see* Fig. 26). The magnitude of this effect is disturbing. It suggests that the measured values may sometimes be a rather poor approximation to the derivatives for high Reynolds numbers; and that it may have been better to have fixed transition in every case. Such a difference, at a Mach number well above 1, makes one wonder also whether there would not have been far larger differences for the transonic measurements with wings B and E. Removal of the root fences produced changes of the same order in the derivatives while the effect of transition peristed undiminished. It is interesting to note that the variation of derivatives with frequency parameter was even greater in general with the fences removed than in the normal condition (*see* e.g. Figs. 26 and 27). A possible explanation of the unexpected size of the rate of change with respect to frequency of the measured derivatives for all the wings is that it is a product of the flow conditions at the root.

An attempt to correct for half-model effects was made by applying a factor of 1·17 to all the zero frequency stiffness derivatives ($-m_\theta$) for the test axes and leaving the damping derivatives for the same axes unmodified*. This factor was based on comparisons between the values of derivatives for full span models measured by Tobak[47] and the values obtained by Orlik-Rückemann[17] with half-span models. The planforms used by Tobak** were not the same as those of the present investigation. The results used in deriving the factor were for delta wings of aspect ratios 2 and 3 mounted on a central body and of course some allowance had to be made for the difference in planform and the effect of the body. As the authors remark[17] this is a tentative correction procedure based on little evidence and this correction will require subsequent refinement. The derivative values given in Tables 29 to 58 and Figs. 6 to 17, 34 to 40 have been corrected in this way but those given in Figs. 2 to 5, 18 to 28 include no correction for half-model effects.

The variation of the derivatives with amplitude was also investigated for wing A at a Mach number of 1·56. The results for the aftmost axis are shown in Fig. 28, where the range of amplitude of oscillation for each case is noted. The stiffness derivative ($-m_\theta$) is little affected by change of amplitude but large changes occur in the value of ($-m_{\dot{\theta}}$). These are similar in magnitude to the changes produced by the root fence or the transition strip (*see* Fig. 26).

In considering the dependence of the derivatives on various parameters one should also bear in mind the repeatability of the measured values under supposedly the same conditions. As mentioned above each data point was obtained as the mean of at least 10 readings taken in immediate succession, and each derivative value quoted in this Report is nearly always obtained from the mean of two data points. The variation between the individual measurements of the frequency was always very small, but up to about 15 per cent difference was found between individual values of the logarithmic decrement. These differences are reflected in the differences between the values of two 'data-point' values of a derivative for the same condition. Differences in ($-m_\theta$) were always small but differences in ($-m_{\dot{\theta}}$) were often between 5 and 10 per cent.

3.2. *Tunnel Measurements – Forced Oscillation Technique.*

The method used by Hall and Osborne[15] to determine the derivatives, was an 'inexorable forcing' technique of the internal rigid drive type[49]. Briefly the wing was mounted on a mechanism which oscillated it continuously in pitch with constant amplitude about a chosen axis and the resulting reactions between the rig and the earth were measured. The differences between the measured reactions wind-off and wind-on, for the same frequency of excitation then enabled one to deduce the values of the aerodynamic forces (lift pitching moment and rolling moment) acting on the model. A system of balancing was used which virtually eliminated contributions to the reactions arising from the rig and model inertia; and hence

*All the derivatives, for any other axis, obtained using the axis transfer relationships, will therefore be modified.

**Though Tobaks paper[47] is, as the title implies, mainly concerned with measurements of ($-m_{\dot{\theta}}$), it does include some values of ($-m_\theta$) as well.

avoided the errors which would arise otherwise when the airforces were given by the small differences, of two large quantities. It was necessary to make measurements wind-off for some residual rig generated oscillatory forces remain after balancing, but this meant that the final result was the difference between the airforces wind-on and in still air and not the total airforces. It would have been preferable to have had the second test in vacuum. However the still air airforces should be relatively small at the test frequencies. A full description of the rig is given in Ref. 48.

The measurements were made in the H.S.D. 20 in. × 20 in. continuous wind tunnel at Coventry, (*see* Table 27). Details of the models are given in Table 28. They were half-span models mounted to the rig at one side wall of the tunnel. Each model was mounted in the model support disc of the rig which formed part of the tunnel wall. The gap between the model root and the tunnel wall was always kept small – between 0·004 in. and 0·008 in., and the root chord of the models in each case was a little greater than the diameter of the support disc. The measurements of rolling moment would of course include a contribution from the air pressure on the support disc in addition to that from the model wing itself. The position of the model attachment to the support disc was so arranged that the model could be oscillated in pitch about the mid-point of the root chord and (by 'turning over' the rig) about an axis through the root chord trailing edge.

For each Mach number measurements were made for pitching oscillations, about the above two axes, at three different frequencies and also at zero frequency*. This provided values of the derivatives due to pitch (i.e. the suffix θ and suffix $\dot{\theta}$ derivatives) for the two test axes; and from these, using the axis transfer relationships, the complete set of heave and pitch derivatives and also those derivatives giving the rolling moment on the half-wing due to heave or pitch, referred to an axis through the apex, were derived. Sufficient information was obtained for the test axes to permit axis transfer at any frequency and so no use was made of the theoretical relationship between certain damping and stiffness derivatives at zero frequency.

The three frequencies used were such that the frequency parameter range covered in each case was roughly 0 to 0·1. Values of the supersonic heave and pitch derivatives, for wings A → F, referred to the axis through the apex, for the different frequencies, are given in Tables 29 to 46 for three Mach numbers. It will be seen that the measured variation with frequency is often quite different from what one would expect. Consequently the complete set of derivatives from Ref. 15 have not been reproduced. Instead tables of mean values of the heave and pitch derivatives for $\nu = 0 \rightarrow 0{\cdot}1$ at all the measured Mach numbers for all the planforms are given in Tables 59 to 65. Where a value was measured at zero frequency this has been listed, otherwise the mean of the values at the other frequencies has been taken as the appropriate approximation. Values which appeared to be hopelessly wrong have been omitted from such averaging but it is of course difficult to decide where to draw the line.

The accuracy of the rolling moment derivatives (to be precise the generalised force coefficients for a mode of linear symmetric flexure) is, as mentioned above, very doubtful. Little point is served in giving them in detail. In every case these were considerably different from the theoretical values particularly for the slenderest wings. A few of the better examples are shown in Figs. 29 to 32 illustrate the sort of results that were obtained.

At the subsonic and transonic Mach numbers (up to $M = 1{\cdot}3$) the tunnel used had slotted liners applied to the roof and floor (*see* Table 27). Perforated sheet diffusion screens were fitted behind the slots for practically all the tests. A few measurements for wing A at a Mach number of 0·9 with both the slots open and the slots sealed did however show that the normal running conditions corresponded more closely to the slots closed state. It follows from the values of the interference parameters, δ_0, δ'_0, for this tunnel, quoted in Section 3.1, that the measured values of the derivatives may be significantly affected by tunnel interference at subsonic speeds. Corrected values, based on the theory of Garner *et alia*[4-6], have therefore been determined and these are given in Table 66. An approximate formula from Ref. 46, eqn. (70), was used which involved only the measured derivative values. It will be noticed that corrections have been obtained assuming both slots open and slots sealed. The assumption of open slots always

*Only the stiffness derivatives were of course obtained at zero frequency.

makes the free stream value greater than the tunnel value by an amount varying from about 2 per cent for the two slender wings up to about 20 per cent for wing G (A = 3 version); while the assumption of closed slots always makes the free stream values less than the tunnel value by half these amounts. The actual state probably corresponds to something intermediate and closer to the latter condition than the former. It may well be, therefore, that the required corrections are always fairly small, and certainly they should be smaller than the corrections given by the closed slots assumption. An alternative approach to the correction of the experimental results to give free stream values is to estimate theoretically the derivatives for the model in the tunnel. This has been done by Garner for two cases which are roughly the extremes as regards the amount of correction. He used the full theory of Ref. 46 in conjunction with the lifting-surface theory of Ref. 21. These results are also quoted in Table 66 for the same two assumed slot conditions. The amount of correction is, on the whole, similar to that estimated using the experimental derivative values though it varies more between the different derivatives and sometimes it is rather greater. A further doubt arises from the fact the ratio of the planform area to tunnel cross sectional area for the three wings A, D and G (ratios 0·141, 0·188 and0·218) is rather high for the tunnel interference theory to apply. In view of these uncertainties the uncorrected measured values have always been used elsewhere as experimental estimates of the free stream values.

The unexpected, and often large variation of derivatives with frequency, mentioned above, has been attributed[15] to tunnel interference. The authors of Ref. 46 conclude however from the evidence of some tests in other tunnels with slots open and sealed, and from their theory for low frequency, that there is little effect of frequency on the subsonic interference until the frequency parameter is of order unity.

In an attempt to explain the apparent tunnel interference effects Hall and Claridge[51] carried out some further tests in their 10 in. × 8 in. intermittent induction tunnel[45] using a smaller model of wing D. The arrangement was similar to that of the main tests: slotted roof and floor (though normally without diffusion screens), model mounted to side wall, ratio of wing plan area to tunnel cross sectional area 0·26 (cf. 0·19 in. main tests). Approximate values of the tunnel interference parameters δ_0, δ'_0 are $-0{\cdot}33$ and 0·20 respectively compared with $-0{\cdot}24$ and 0·14 for the 20 in. × 22 in. tunnel with open slots and 0·13 and $-0{\cdot}01$ for the latter tunnel with closed slots. The tests were to investigate the possibility of disturbances from the oscillating model propagating upstream *via* the plenum chamber. It was found, by making upwash measurements ahead of the wing with slots both closed and open, that this did indeed happen to a significant extent even at supersonic speeds as high as $M = 1{\cdot}14$. However the introduction of diffusion screens behind the open slots greatly reduced the effect and so it is doubtful if this mechanism leads to any noticeable errors in the derivative values measured in the 20 in. × 20 in. tunnel. A few measurements of $-m_\theta$ at subsonic speeds are also reported in Ref. 51. There were obtained by a free oscillation technique with the slots both open and sealed. Differences of the order of 20 per cent between the derivatives, for the two wall conditions, were found. This confirms to some extent the estimated corrections, assuming open slots (Table 66) to the 20 in. × 22 in. tunnel measurements.*

For one of the wings – wing G – it was found that there was some distortion of the wing-root mounting block structure under the conditions of measurement. This was predominantly pitch and roll of the wing relative to the mounting block. Corrections to the measured values of the derivatives were therefore made based on measured structural stiffnesses, and the tabulated values include these corrections. The corrections were always small the largest being $3\frac{1}{2}$ per cent.

As with the free oscillation tests one would expect there to be some inaccuracy due to half-model effects. In this case it will probably be mainly due to the tunnel-wall boundary layer. The small gap, 0·004 in., between the wing root and tunnel wall should have a rather smaller effect since it lies entirely within the tunnel-wall boundary layer. A rough estimate[15] suggested a correction factor of 1·05 compared with the 1·17 used by the authors of Ref. 17. This factor has not been applied to the measured values.

One or two tests at supersonic speeds with and without fixed boundary-layer transition showed no observable effect on the measured derivative values. The remainder of the supersonic tests were made therefore without boundary-layer transition forcing strips. For the transonic tests however, where one would expect larger effects, transition forcing strips were always used (*see* Table 28).

*The closed slot corrections are however considered to be more appropriate to the test conditions.

The chief sources of inaccuracy, were however indigenous to the internal rigid drive type of rig that was used. The inertia balancing used means that there are much larger forces generated in the rig than those actually measured at the supports; and this suggests that the measured forces may be very sensitive to imperfections of the rig such as backlash or deformation. In addition the use of mechanical excitation sets quite a low limit on the maximum attainable frequency and consequently the phases of the reactions relative to the excitation are very small. This places stringent demands on the instrumentation which could not be met. In fact an estimate of the possible errors in the measured derivatives due to instrument inaccuracies, given in Ref. 15, does suggest that there could be very large errors in the measured values of the damping derivatives and smaller, though still undesirably large, errors in the stiffness derivatives. Confirmation of this, to some extent, is given by the lack of repeatability that was sometimes found when tests were repeated. Differences up to about 50 per cent in the damping derivatives and 10 per cent in the stiffness derivatives were found. These figures cover in addition errors due to noise from the rig and the tunnel. They do not imply that the average error will be so large.

3.3. *Free flight measurements.*

A free oscillation technique was used for the derivative measurements made at the Weapons Research Establishment (W.R.E.) range, Woomera, Australia using ground-launched rocket-boosted test vehicles. Details of the Koorigal test vehicle, designed for this purpose, are given in detail in Ref. 16. Briefly it consists of a long cylindrical body with a parabolic nose cone and a cruciform tail assembly, the overall length of the vehicle being 18 ft. The rocket motor formed the rear half of the body. The test wings were mounted on the cylindrical part of the forebody well away from the nose. At this point the body diameter was 10·25 in. and so was not greatly different from the root chord dimension of most of the test wings (*see* Table 28). Break up between the forebody and the rocket motor was initiated after 65 sec of flight, and the forebody which contained all the instrumentation was saved using a parachute recovery system. Typical performance curves are shown in Fig. 33. For the conditions when measurements were taken the value of the Reynolds number/ft varied between about 4 and 12 $\times$ 10^6.

The test wings, one half on each side of the forebody, were free to oscillate in pitch about a diameter of the body against an elastic constraint. In flight free oscillations were repeatedly induced by displacing the wing, holding it still for a moment, and then releasing it cleanly. Each time the frequency and decay of the resulting oscillations was measured. From these measurements, and similar measurements on the stationary vehicle on the ground, values of the derivatives $-m_\theta$, $-m_{\dot\theta}$, appropriate to the axis of pitch, were obtained in the same way as was used for the free oscillation tunnel tests (Section 3.1). Thus each test flight provided a series of values of the derivatives over a range of Mach numbers 0·9 $\rightarrow$ 2·0. For each planform measurements were made for three different axes of pitch (plus an additional one for wing A). In the wind-tunnel experiments (Sections 3.1 and 3.2) the axes of pitch used always consisted of one about mid-root chord, and one about $\frac{3}{4}$ root chord or at the root trailing edge. In contrast in these free flight experiments they were, apart from the fourth axis for wing A, in each case forward of $\frac{1}{4}$ root chord. A slot in the body wall was provided for connection of the wing to its mounting. In each case it extended over more than half the wing root chord. Different slots were provided for the different wings, and to suit the different axes of pitch. For the foremost two axes of pitch the slots were of constant width between 2 and 3 times the maximum wing thickness. The slots, for the other two axes, varied in width to accommodate the wing motion from about 2 to 4 times the maximum wing thickness. The gap between the wing root and the body surface was 0·02 in. and no root fence was provided.

With these conditions at the wing root – relatively large hole in the body wall, no root fence and a rather larger gap between the root and the body than the root-tunnel wall gap of the tunnel tests – one would expect that their effect on the measured derivatives to be at least as large as in the other tests. The estimation of such errors cannot yet be made with any accuracy. The authors of Ref. 16 made a rough estimate of a correction factor of 1·05 to be applied to all the derivatives, though this factor has not been included in any of the values quoted here. This factor compares with the factor 1·17 used by Orlik-Rückemann and Laberge[17] to correct their tunnel measured values of the stiffness derivatives for the test axes for half-model effect (*see* Section 3.1).

From their measured values of the pitching derivatives for three axes of pitch Baines and Rockliff[16]

attempted to derive a complete set of heave and pitch derivatives for some reference axis. Three methods were tried. The first used the axis transfer relationships to give the direct derivatives (l_z, $-m_\theta$, $l_{\dot{z}}$, $-m_{\dot{\theta}}$) and the sums of the cross derivatives ($l_\theta + \{-m_z\}$, $l_{\dot{\theta}} + \{-m_{\dot{z}}\}$) for a reference axis. The whole set could then be obtained using two assumed relationships between the derivatives. This method failed because the accuracy of measurement was not sufficient with the three axes of pitch used. The second method was similar, and failed probably for the same reason. Since what was measured was the difference between the derivatives in flight and the still air derivatives (neglecting the effect of different air density) and as the frequency was small, one could reasonably assume that the zero frequency relationships ($l_z = -m_z = 0$, $l_\theta = l_{\dot{z}}$, $-m_\theta = -m_{\dot{z}}$) hold. This was in effect* what was done and there being now a superfluity of information (6 equations, 4 unknowns) a least squares method was used. The failure of this method was manifested by the unexpected values of $(-m_\theta)/l_\theta$ that were obtained (*see* Ref. 16). The third method assumed in addition values of the ratios $(-m_\theta)/l_\theta$, $(-m_{\dot{\theta}})/l_{\dot{\theta}}$ appropriate to the reference axis. Then from the measured values, for one axis of pitch of $(-m_\theta)$ and $(-m_{\dot{\theta}})$, the complete set of derivatives referred to the reference axis can be obtained. Mean values of the results thus obtained by this method using in turn the measured pitching derivatives for each axis of pitch were therefore taken as the best estimation and are given in detail in Ref. 16 for a reference axis though the leading edge of the wing mean chord. Comparison was made with the theoretical results of Refs. 7 and 11 but agreement was not good**.

In view of this experience it was therefore thought best to consider in the main the measured values of $(-m_\theta)$ and $(-m_{\dot{\theta}})$ for the test axes and make comparisons with the corresponding theoretical values. Some derivative values referred to an axis through the wing apex have however, been included in Tables 29 to 46. These were obtained from the curves of Ref. 16 using the second method described above (without the v^2 terms mentioned in the footnote) giving equal weight to all the measured b_{33} and c_{33}.

The measured values of the damping and stiffness moment coefficients, b_{33} and c_{33} for the test axes, are plotted in Figs. 34 to 47. These are the coefficients used by Baines and Rockliff[16] and are proportional to the derivatives $m_{\dot{\theta}}$ and m_θ respectively.

4. *Comparisons.*

4.1. *Subsonic Investigations.*

As one would hope, and would expect from two methods which are very similar, the two sets of calculations[6, 8] yielded results which conform excellently with each other. This can be seen by examining the entries in Tables 3 to 8 and 25 to 28 for $\nu = 0$ and $\nu = 0{\cdot}1$ and noting the variation with frequency parameter (ν) indicated by the other values. No unexpected features are brought to light by these calculations. All the derivatives have a peak or trough near $M = 1$. Sometimes this peak is very sharp, as, for example, with $-m_{\dot{\theta}}$ for the two G wings (Tables 9 and 10), but such is the exception rather than the rule. Nor is this peak (or trough) always at a Mach number very close to unity. It can occur at a Mach number as low as 0·8. Such an instance is shown in the plots of $l_{\dot{\theta}}$ for wing A in Fig. 48. One general trend that is illustrated by the results is that the damping derivatives for the higher aspect-ratio wings show a marked increase in variation with frequency parameter (ν) as the Mach number approaches unity.

The only direct comparisons between the different wind-tunnel experimental results that we have made are those shown in Figs. 18 to 25 where the pitching moment derivatives $(-m_\theta)$, $(-m_{\dot{\theta}})$ from the two sets of tests are compared. In the subsonic free oscillation tests[17] insufficient measurements were made to enable a complete set of pitching derivatives to be determined or any axis transfer relationships to be used (*see* Section 3.1). The comparisons have therefore been made for the two axes of pitch used in these tunnel tests. These are for the two wings of aspect ratio 2 (B and E). The agreement between the two sets of results is not at all good. In each case there is fair agreement between the measured values of

*Actually some rather doubtful terms proportional to ν^2 were added to these relationships but their effect should be small.

**The wing G ($A = 3$ version) derivatives from Ref. 7 at $M = 1{\cdot}875$ were however little different from the wing G ($A = 4$ version) experimental results; and values obtained at the same time for an $A = 4{\cdot}3$ rectangular wing showed good agreement with theory above $M = 1{\cdot}4$.

$(-m_\theta)$ – Fig. 22 is the best example – but there are always big differences between the values of the damping derivative $(-m_{\dot{\theta}})$. The forced oscillation tests made by Hall and Osborne[15] nearly always give much the smaller value – usually somewhere about half the value for Ref. 17.

It is convenient here to note how these results compare with the theoretical values. For the aftmost axis for each wing the values of $(-m_\theta)$ do not agree. The values of this derivative for the forward axes are however all in fair agreement; particularly for wing E (Fig. 22) where there is good agreement between Olik-Rückemann's results[17] and theory. The damping derivatives $(-m_{\dot{\theta}})$ obtained by the free oscillation technique[17] are also all in fair to good agreement with Woodcock's theoretical values[8]; it being particularly good in this case for the aftmost axes (Figs. 21 and 25).

We have pointed out in Section 3.3 that no axis transfer procedure could be satisfactorily applied to free flight results obtained in Australia[16]. Comparisons have therefore again to be made for the pitching moment derivatives appropriate to the test axes. The axes used by the Australians[16] were in every case well away from those used by the Canadians[17]. No comparison could therefore be made between these two sets of results. A similar comparison to that described above, and illustrated in Figs. 18 to 25, can however be made between the British wind-tunnel results[15] and Baines and Rockliff's results[16]. These comparisons have been made for the aftmost axis of pitch, which is nevertheless well forward, in each case, of either axis used in the tests of Ref. 17. Figs. 41 to 46 show the comparative values of the damping and stiffness moment coefficients, used by Baines and Rockliff[16]. These coefficients b_{33} and c_{33} are proportional to the damping and stiffness derivatives $(-m_{\dot{\theta}})$, $(-m_\theta)$ respectively. The agreement between the two sets of results is always very poor apart from $(-m_{\dot{\theta}})$ for wing F (Fig. 46) and occasional good agreement at or very close to $M = 1$ (*see* e.g. Fig. 42 (c_{33}), Fig. 44 (b_{33} and c_{33}) etc.).

In addition the free-flight results[16] are always in poor agreement with the theory for each axis of pitch (*see* Figs. 41 to 47). These figures incidentally show that the theoretical values of $(-m_{\dot{\theta}})$ are nearly always in good agreement with Hall and Osborned experimental results[15] for the one axis shown. The agreement is particularly good for the two slenderest wings C and F (Figs. 43 and 46) and it is interesting to note that it extends very close to $M = 1$. As regards the damping derivative $(-m_{\dot{\theta}})$ however the theoretical values are always much larger than those measured by Hall and Osborne[15].

Some further experiment-theory comparison are given in Tables 47 to 58, this time for the direct pitching derivatives $\{(-m_{\dot{\theta}})$ and $(-m_\theta)\}$ appropriate to an axis through the wing apex. Similar agreement, or disagreement, between the theoretical values and the experimental ones of Ref. 15 to that noted above, is indicated.

To sum up then it can be stated that:

(i) The three different experimental methods have failed in general to give a convincing indication of what are the correct values of the derivatives since they disagree so much between themselves. An exception may be the stiffness derivative $(-m_\theta)$ for axes of pitch in the forward half of the wing where the two sets of tunnel measurements[15,17] give answers which are fairly similar.

(ii) The free flight experimental results[16] appear to be not at all reliable since they have negligible confirmation from the other experiments, since they sometimes show big differences in values according to whether the Mach number is increasing or decreasing (*see* e.g. Fig. 44), and since they often have unexpectedly violent variation with Mach number (*see* e.g. Fig. 44).

(iii) The large differences between the values of the damping derivatives from the two types of tunnel experiments are probably largely due to the inaccuracies of the forced oscillation technique in particular the difficulty in measuring the quadrature forces with sufficient accuracy.

(iv) In view of (i), (ii) and (iii) it seems that the most reliable values of the damping derivatives are those given by the free oscillation tunnel tests[17], and of the stiffness derivatives those given by either type of tunnel test[15, 17]. These confirm the theoretical results to some extent and where there are appreciable differences there is no good reason for saying one is correct and the other is wrong. The free oscillation tests[17] have particular doubts because of the effect of fixed transition, and half-model effects (*see* Section 3.1); the forced oscillation test[15] results are suspect especially because of instrument inaccuracies and also because of half-model effects and tunnel interference (*see* Section 3.2); and the theoretical values are of course based on the usual assumption of linearised potential flow past an infinitesimally thin plate. It is interesting to note that Hall and Osborne's results[15] (forced oscillation wind tunnel tests) agree

best with theory (as regards $-m_\theta$) for the slenderest wings, for which one would expect tunnel interference effects to be smallest but half-model effects to be largest. Does this indicate that half-model effects were always small for these tests? And perhaps also that Orlik-Rückemann and Laberge's estimate of half-model effects in their free oscillation tunnel tests[17] is rather too large?

If one takes the tunnel measured values of $(-m_\theta)$ to be approximately correct then the disagreement with theory for aftward axes suggests, as indeed can be seen by examination of the appropriate tables (3 to 10, 59 to 65), that the theoretical values of l_θ are rather high. The difference is of the order of 10 per cent. This confirms similar findings from previous investigations (*see* Ref. 53).

The damping in pitch derivative $(-m_\dot{\theta})$ for isolated lifting surfaces has apparently usually been largely overestimated by theory if we are to believe the evidence of previous investigations (Refs. 52 and 53). The most reliable of the results discussed here (i.e. Orlik-Rückemann and Laberges[17] values, *see* Figs. 20, 21, 24 and 25) do not confirm this except possibly for Mach numbers very close to 1. Some recent results due to Garner, which are briefly referred to in Ref. 54, also show fairly good agreement between theory and experiment. The explanation may well be that poor agreement in the past has been largely due to experimental inaccuracies. The tunnel tests of Ref. 15 – using a forced oscillation technique with reactions being measured – certainly appear to have greater inaccuracy and scatter in the damping derivatives than is found in the free oscillation tunnel measurements of Ref. 17 (*see* Section 3.1). The results of Ref. 52 – Fig. 9 were obtained by a different type of forced oscillation method[55] in which the derivatives are deduced from measured values of the response and the excitation force for a full-span sting-mounted model. With this rig the scatter in the measured values of the cross damping derivatives, l_θ and $(-m_{\dot{z}})$, is large and this is reflected in values of $(-m_\dot{\theta})$ for axes not close to the axis of pitch of the predominantly pitching mode excited in the test. The values plotted in Ref. 52 are of doubtful accuracy for this reason.

The other damping derivatives $l_\dot{\theta}$ etc. were determined experimentally only by Hall and Osborne[15]. In nearly every case they are smaller than the theoretical values and sometimes quite a lot smaller. Three examples are shown in Figs. 48 to 50. Little value can be placed on these comparisons for, as already indicated, the experimental errors quite possibly will be large.

Also to be mentioned briefly are the rolling-moment derivatives of which the best results are plotted in Figs. 29 to 32. The agreement between theory and experiment is poor but since the accuracy of the experimental results is extremely doubtful (*see* Section 3.2) no weight can be given to these comparisons.

4.2. *Supersonic Investigations.*

In Ref. 10 Harris showed that his theoretical values of the derivatives were consistent with those obtained by Barnes[7] and Garvey[41]. Garvey's results have not been reproduced here. The results of Harris[10] and Barnes[7] provide a good coverage of the supersonic range of the tests for the planforms A → F. A similar coverage for zero ν only, is provided by Orlik-Rückemann's theoretical results[17]. These two sets of results are reproduced in full in Tables 11 to 20. The agreement between them is nearly always very good. Differences greater than 5 per cent only occur in one or two isolated instances either for Mach numbers very near one, or for cases where the wing leading edge is supersonic. Apparent instances of the former type occur for the two largest aspect-ratio wings A and D at $M = 1{\cdot}054$ (Tables 11 and 14). The values of $(-m_\dot{\theta})$ from Ref. 17 are considerably smaller than the $\nu = 0$ values, extrapolated from Harris's results[10], which are given in Tables 48 and 54. These differences however may well be the fault of the extrapolation. Differences of the latter type between Barnes[7] and Orlik-Rückemann's[17] theoretical results are not unexpected since some design chart interpolation was involved in the second case. These differences are never very great, in the worst case being about 10 per cent (*see* e.g. Table 17).

For the other two wings – the wings G – the only theoretical comparison is for the aspect ratio 3 version (Table 23) for which calculations have been made by the box method used by Barnes[7] and by the low frequency theory of Lehrian[12]. The agreement is fairly good, Lehrian's values being consistently the largest by about 5 per cent.

Thus for the whole set of planforms we have a convincing statement of the true theoretical values over the whole range of the supersonic experiments. A little doubt may remain in respect of frequency effects. Here we rely almost entirely on one theoretical solution for the subsonic leading-edge case (Harris's collocation solution[26]) and one for the supersonic leading-edge case (Hunt's method[33] as applied by

Barnes[34]). Some confirmation of Harris's results are given by the comparison with Garvey's results[41], mentioned above, for the two wings C and F – and also by the comparisons with Watkins's series solution for triangular wings[43, 44] referred to in Section 2.6. The only confirmation of Barnes's results[7] for varying frequency parameter ν is that, for the sonic leading edge case, they are an acceptable extrapolation of Harris's results[10] at lower Mach numbers.

It is this point – the variation of the derivatives with frequency parameter ν – that is one of the most puzzling features of the experimental-theoretical comparison. In Hall and Osborne's experimental results[15] the actual dependence on ν is obscured by experimental inaccuracies; but the other wind-tunnel results[17] do give a consistent picture. It is a picture which shows consistently a much larger variation with frequency parameter than that predicted by theory. For the two planforms, B and E, for which measurements were made at three frequencies the direct pitching-moment derivatives for the test axes are shown in Figs. 2 to 5 where they are compared with Harris's theoretical results[10]. Barnes's theoretical results[7] at a higher Mach number show a similar negligible variation with ν compared with the experimental results. The fact that removal of the root fence produced a change in the rate of change of the derivatives with respect to ν of the same order as the measured variation (*see* Figs. 26 and 27) does suggest that the flow conditions at the root are an important factor. This appears to be the only explanation, if indeed one is required. However, in the absence of any similar experimental evidence from any other tests, there is little reason for considering these measured effects of frequency to be anything other than spurious.

Comparisons between the different experimental results are best seen by the examination of Tables 29 to 46, where all the derivatives are compared at certain Mach numbers for an apex reference axis, and Figs. 34 to 40, where the pitching-moment coefficients are compared for the axes of pitch used in the free flight tests. The agreement between the different experimental results is on the whole not at all good. The Tables show that the free-flight results are not accurate enough for any axis transfer to be made. For the test axes the stiffness derivative $(-m_\theta)$ is nearly always a lot different from the tunnel results. The damping derivative shows rather better agreement – Fig. 38 for wing E is a good example – but even so there are some instances of large differences (*see* Figs. 34 and 37). The two sets of tunnel results agree with each other rather better but here again there can be some large discrepancies particularly in the damping derivatives (*see* e.g. Fig. 37 and Table 38).

In addition to these Tables and Figures comparisons of the direct pitching derivatives for an apex axis are made for the whole range of Mach numbers covered by the tests in Tables 47 to 58 and plotted in Figs. 6 to 17. These cover the six wings A to F. A similar comparison for the aspect ratio 3 version of wing G is made in Figs. 51 to 52, and the derivatives l_θ, $l_{\dot{\theta}}$ for the same wing are compared with theory – Figs. 53 to 54. All these comparisons are made at zero ν. However for the two wings B and E comparisons at a constant value of νM are made for the direct pitching derivatives, though this time they have to be referred to the axes used in the free oscillation tunnel tests because of axis transfer difficulties. The free flight results have not been included in any of the comparisons mentioned in this paragraph for the same reason.

All these presentations show a common tendency for theory to give higher values of the derivatives than the experimental results. The agreement rarely deserves to be called anything better than fair. The two unswept wings – the aspect ratio 3 and aspect ratio 4 versions of wing G – show probably the best agreement. At Mach numbers above about 1.2 it is on the whole fairly good (*see* Figs. 40, 51 to 54), and Lehrian has shown[12], for the aspect ratio 3 version, that agreement can be improved by including thickness effects in the theory. For this wing the experimental values of l_z are in poor agreement with the theoretical values; and also with the experimental values of l_θ which one would expect to be little different at the low frequency parameter value of the tests. This produces poor agreement in the theoretical and experimental values of $(-m_{\dot{\theta}})$ for axes well away from the apex. With the aspect ratio 4 version of wing G the comparisons (Fig. 40) have perforce to be made for the axes of pitch used in the free-flight experiments[16] (*see* Section 3.3). These three axes were all forward of the wing apex and the measure of agreement was similar in each case. One would of course expect the best agreement for these two planforms since they both have supersonic leading and trailing edges at all the supersonic test points and previous experience has shown that theory usually predicts the experimental values better in this case than at

lower supersonic speeds.

The change from subsonic to supersonic leading edge is not however shown by the present results to be an approximate boundary between poor and good experimental-theoretical agreement. For the two planforms just mentioned the leading edges are well supersonic before the agreement becomes fairly good. In contrast Fig. 6 shows, for wing A, for $(-m_\theta)$, such a changeover at a Mach number well below that at which the wing edge conditions change. Furthermore there is another example (Fig. 8, $(-m_\theta)$ for wing B) for which the agreement is similar over the whole range of supersonic tests covering both types of leading-edge condition.

Above a Mach number of about 1·4, for the cropped delta and tapered swept back wings (A to F), the tunnel results[15-17] are practically never in poor agreement with theory, and, Orlik-Rückemann has shown[17] that in this range the addition of a thickness correction to the theoretical values generally improves the agreement. The free flight results[16] for these planforms (Figs. 34 to 39) are generally much different from the theoretical predictions particularly in respect of the stiffness derivatives; and because of their lack of agreement with the other experimental results they can be discounted. At lower supersonic Mach numbers, for these six planforms (A to F), there is the expected large difference between theory and experiment and also between the different experiments (*see* Figs. 21, 36 for example).

5. *Conclusions.*

The numerical results of this exercise are somewhat disappointing in that the agreement obtained between experimental and theoretical values of the derivatives is on the whole only fair. However, the accuracy of the experimental results is not of sufficient certainty for one to conclude that the theoretical treatment is generally inadequate. All the tests were made with half-span models and the results indicate that root effects can have a significant, though as yet unpredictable, effect on the measured values. Other significant errors* resulted in some cases from failure to fix transition, amplitude dependence and tunnel interference. The experimental results from the three techniques also provided little confidence in the accuracy of any set of results because of their usual lack of agreement among themselves. Nevertheless there is sufficient evidence to conclude that theoretical values of the derivatives given by linearised potential flow theory are usually not very good estimates of the true physical values at near sonic and low supersonic speeds. To establish empirical methods of correcting the theoretical values in such cases one requires better experimental values than those reported here.

Of the three experimental techniques used the free oscillation wind tunnel method[50] of measurement looks easily the best as regards accuracy, efficiency and simplicity. The free flight version [5, 16] of this technique obviously needs appreciable development before it is of much use for low aspect-ratio wings. Here there is certainly room for improvement in the root arrangements to make the flow more similar to that of the full-span wing without fuselage. The internal rigid drive type of inexorable forcing technique[48] used in the other tunnel tests is also of inadequate accuracy. Careful design and development did not eliminate a severe demand on instrumentation accuracy which could not be satisfactorily met. As a result the damping derivatives, particularly, as determined by this method, are of uncertain accuracy**. The obvious conclusion is that a free oscillation technique using sting mounted full-span wings is the most promising method of derivative measurement especially in supersonic flow. Such a method precludes the determination of the cross derivatives, other than in combinations such as $\{l_\theta+(-m_{\dot{z}})\}$, except when the frequency tends to zero. It is also necessary to ensure that the motion is only in the one

*It is assumed that the object of the experiments was to determine the derivatives for a full-scale wing, undergoing infinitesimally small sinusoidal oscillations.

**It is interesting to note that other experimenters using forced oscillation techniques have found the same difficulty. For example in respect of a very recently developed testing system we read in Ref. 58. 'It is apparent that the rate-dependent aerodynamic terms cannot be measured accurately at low oscillation frequencies . . . The phase angle . . . cannot be measured with sufficient accuracy . . .'.

desired degree of freedom. This may be more difficult with sting-mounted than with wall-mounted models.

Following from these conclusions we have therefore the following two recommendations.

(i) The possibility of improving the accuracy of derivative measurement at transonic and supersonic speeds, by the use of a free oscillation technique with a full-span sting mounted model, should be considered.

(ii) The improvement of theoretical predictions of the oscillatory airforces at near sonic and low supersonic speeds, either by a more adequate representation of the physical system or by the development of satisfactory empirical methods of correction, requires urgent consideration.

6. *Acknowledgements.*

The reported work was carried out under the auspices of the, now, Ministry of Technology Flutter and Vibration Committee, and of the Commonwealth Advisory Aeronautical Research Council. Contributions were made by the Weapons Research Establishment, Australia, the National Aeronautical Establishment, Canada, De Havilland Aircraft Ltd., Hawker Aircraft Ltd., Hawker Siddeley Dynamics Ltd., the National Physical Laboratory, and the Royal Aircraft Establishment.

LIST OF SYMBOLS

A	Aspect ratio
M	Mach number
S	Total wing area (tip to tip)
V	Airspeed
b_{33}	Damping-moment coefficient used in analysis of free-flight results, proportional to $(-m_{\dot{\theta}})$
c_0	Root chord
c_1	Tip chord
c_{0f}	Control-surface root chord
c_{1f}	Control-surface tip chord
c_{33}	Stiffness-moment coefficient used in analysis of free-flight results, proportional to $(-m_{\theta})$
$\bar{c}$	First mean chord $= S/2s$
g	Distance of axis of pitch aft of apex $\div \bar{c}$
$h_z, h_{\dot{z}}, h_\theta, h_{\dot{\theta}}, h_\beta, h_{\dot{\beta}}, h_\phi, h_{\dot{\phi}}, h_\psi, h_{\dot{\psi}}$	Hinge-moment derivatives (*see* Appendix)
$l_z, l_{\dot{z}}, l_\theta, l_{\dot{\theta}}, l_\beta, l_{\dot{\beta}}, l_\phi, l_{\dot{\phi}}$	Lift derivatives (*see* Appendix)
m	Number of spanwise collocation points
$\overline{m}$	Number of spanwise integration stations in subsonic collocation method
$m_z, m_{\dot{z}}, m_\theta, m_{\dot{\theta}}, m_\beta, m_{\dot{\beta}}, m_\phi, m_{\dot{\phi}}$	Pitching-moment derivative (*see* Appendix)
n	Number of chordwise collocation points

$n_z, n_{\dot{z}}, n_\theta, n_{\dot{\theta}}, n_\beta, n_{\dot{\beta}}, n_\phi, n_{\dot{\phi}}$		Derivatives expressing forces in mode of linear flexure symmetric (*see* Appendix)
$r_\theta, r_{\dot{\theta}}, r_\beta, r_{\dot{\beta}}$		Rolling moment derivatives (*see* Appendix)
s		Semi-span
z		Downward displacement in heave
Λ_0		Sweepback angle of leading edge
Λ_1		Sweepback angle of trailing edge
Λ_H		Sweepback angle of control-surface leading edge
θ		Angle of pitch (nose up)
β		Incidence of control surface relative to wing
ψ		Angle of roll $\times$ $s/\bar{c}$ – starboard wing down
ν	=	$\omega\,\bar{c}/V$ frequency parameter
ρ		Air density
ϕ		Downward displacement of tip ($\div\bar{c}$) in mode of linear symmetric flexure
ω		Angular frequency

REFERENCES

The research programme

No.	*Author*	*Title, etc.*
1	H. Templeton	Proposals for a flutter research programme by Industry. Unpublished M.O.S. Report, (1954).
2	H. Templeton	Research programme on aerodynamic flutter derivatives. Unpublished M.O.S. Report, (1954). (Reproduced as Appendix 1 of Ref. 3).
3	W. G. Molyneux	Summary of the present position on flutter and derivative programme. Unpublished M.O.S. Report, (1958).
4	R. J. Rockliff	A programme of unsteady aerodynamic wing force derivative measurements using ground launched, rocket boosted test vehicles. Unpublished Weapons Research Establishment Report (1958).
5	R. J. Rockliff	A detailed programme of measurements of unsteady aerodynamic wing force derivatives using a free oscillation technique with ground launched rocket boosted test vehicles. Unpublished Weapons Research Establishment Report (1958).

REFERENCES—*continued*

No.	*Author*	*Title, etc.*
	Theoretical investigations (*see* also Ref. 17)	
6	J. S. Hornsby	Subsonic flutter derivatives for the R.A.E. research programme calculated using the Multhopp-Garner theory. Hawker Aircraft Ltd. DDR 1226 (1957). (Reproduced as Appendix 2 of Ref. 3).
7	P. G. Barnes	Flutter derivatives for five planforms: Hunt's method. De Havilland Aircraft Ltd. Report Maths/Aero/PGB/GEN/14(1), (1959).
8	D. L. Woodcock	Subsonic flutter derivatives for the planforms of the Ministry of Aviation Flutter and Vibration Committee first research programme. Unpublished M.O.A. Report and Addendum (1962, 1963).
9	V. E. Adams	Calculation of aerodynamic flutter derivatives for the Ministry of Supply derivative research programme. Fairey Aviation Ltd. T.O. Report 328 (1960).
10	G. Z. Harris	Supersonic flutter derivatives for a series of swept and cropped delta wings. A.R.C. C.P.920. January 1966.
11	Doris E. Lehrian and Gillian Smart	Theoretical stability derivatives for a symmetrically tapered wing at low supersonic speeds. A.R.C. C.P.736, April 1963.
12	Doris E. Lehrian	Theoretical stability derivatives for a symmetrically tapered wing of aspect ratio 3 at supersonic speeds. A.R.C. C.P.855, April 1964.
13	Doris E. Lehrian	Calculation of subsonic flutter derivatives for an arrowhead wing with control surfaces. A.R.C. R. & M. 3561 (1967).
	Experimental investigations	
14	G. Q. Hall and L. A. Osborne	Supersonic derivative measurements on the planforms of the Ministry of Aviation Flutter and Vibration Committee's first research programme. Hawker Siddeley Aviation Ltd. Report ARL 63/10, A.R.C. 25604, (1963).
15	G. Q. Hall and L. A. Osborne	Transonic and supersonic derivative measurements on the planforms of the Ministry of Aviation Flutter and Vibration Committee's first research programme. Hawker Siddeley Dynamics Ltd. Report ARL 64/9, A.R.C. 26016, (1964).
16	D. J. Baines and R. J. Rockliff	Results of a programme of unsteady aerodynamic wing force derivative measurement using ground launched rocket boosted test vehicles. Unpublished Weapons Research Establishment Report (1964).

No.	*Author*	*Title, etc.*
17	K. J. Orlik-Rückemann and J. G. Laberge	Static and dynamic longitudinal stability characteristics of a series of delta and sweptback wings at supersonic speeds. National Aeronautical Establishment Report N.R.C. 8980, A.R.C. 28435 (1966).
Other references		
18	H. C. Garner	Multhopp's subsonic lifting-surface theory of wings in slow pitching oscillations. R. & M. 2885, July 1952.
19	H. Multhopp	Methods for calculating the lift distribution of wings (subsonic lifting-surface theory). R. & M. 2884, January 1950.
20	H. C. Garner	Accuracy of downwash evaluation by Multhopp's lifting-surface theory. A.R.C. R. & M. 3431, July 1964.
21	H. C. Garner and D. A. Fox	Algol 60 programme for Multhopp's low-frequency subsonic lifting-surface theory. A.R.C. R. & M. 3517, April 1966.
22	Doris E. Lehrian and H. C. Garner	Comparative numerical applications of the reverse-flow theorem to oscillating wings and control surfaces. A.R.C. R. & M. 3488, August 1965.
23	J. R. Richardson	The application of the Multhopp-Garner theory to the calculation of control surface derivatives. Fairey Aviation Co. Tech. Off. Dept. Report 135 (1954).
24	D. E. Davies	Calculation of unsteady generalised airforces on a thin wing oscillating harmonically in subsonic flow. A.R.C. R. & M. 3409, August 1963.
25	D. L. Woodcock	On the accuracy of collocation solutions of the integral equation of linearised subsonic flow past an oscillating aerofoil. *Proceedings of the International Symposium on Analogue and Digital Techniques applied to Aeronautics, Liege 1963* pp. 173–202 (1964).
26	G. Z. Harris	The calculation of generalised forces on oscillating wings in supersonic flow by lifting surface theory. A.R.C. R. & M. 3453, April 1965.
27	G. Z. Harris	Mercury programmes for lifting surface theory calculations on wings oscillating in supersonic flow. A.R.C. C.P.851, November 1964.
28	J. R. Richardson	A method for calculating the lifting forces on wings (unsteady subsonic and supersonic lifting-surface theory). A.R.C. R. & M. 3157, April 1955.

No.	*Author*	*Title, etc.*
29	R. T. Jones and Doris Cohen	Aerodynamics of wings at high speeds – Part A of *Aerodynamic components of aircraft at high speeds* pp. 206, 207. Oxford Un. Press (1957).
30	Doris Cohen	The theoretical lift of flat sweptback wings at supersonic speeds. NACA Technical Note 1555 (1948).
31	J. H. B. Smith, J. A. Beasley and A. Stevens ..	Calculations of lift slope and aerodynamic centre of cropped delta wings at supersonic speeds. A.R.C. Current Paper 562, July 1960.
32	K. Stewartson	On the linearised potential theory of unsteady supersonic motion. *Quart. J. Mech. and Appl. Math. Vol V, Pt 2* (1952).
33	P. M. Hunt	A methof for the calculation of three-dimensional supersonic flutter derivatives, Part II. Ferranti Ltd., List CS 41 (1955).
34	P. G. Barnes	A programme for the calculation of three-dimensional supersonic flutter, derivatives on a digital computer. De Havilland Maths Aero/PGB/Gen 14 (1959).
35	F. S. Malvestuto Jr., K. Margolis and H. S. Ribner	Theoretical lift and damping in roll at supersonic speeds of thin sweptback tapered wings with streamwise tips, subsonic leading edges, and supersonic trailing edges. NACA Report 970 (1950).
36	F. S. Malvestuto Jr. and D. M. Hoover ..	Lift and pitching derivatives of thin sweptback tapered wings with streamwise tips and subsonic leading edges at supersonic speeds. NACA Technical Note 2294 (1951).
37	F. S. Malvestuto Jr. and D. M. Hoover ..	Supersonic lift and pitching moment of thin sweptback tapered wings produced by constant vertical acceleration. Subsonic leading edges and supersonic trailing edges. NACA Technical Note 2315 (1951).
38	J. C. Martin, K. Margolis and I Jeffreys	Calculation of lift and pitching moments due to angle of attack and steady pitching velocity at supersonic speeds for thin sweptback tapered wings with streamwise tips and supersonic leading and trailing edges. NACA Technical Note 2699 (1952).
39	I. J. Cole and K. Margolis ..	Lift and pitching moment at supersonic speeds due to constant vertical acceleration for thin sweptback tapered wings with streamwise tips. Supersonic leading and trailing edges. NACA Technical Note 3196 (1954).
40	Doris E. Lehrian	Calculation of stability derivatives for tapered wings of hexagonal planform oscillating in a supersonic stream. A.R.C. R. & M. 3298, September 1960.

REFERENCES—*continued*

No.	*Author*	*Title, etc.*
41	S. J. Garvey	Calculation of supersonic aerodynamic derivatives. Vickers Ltd. (Engineering Group) BT/11/MS/TECH R/1–16 (1964–66).
42	D. J. Allen and D. S. Sadler ..	Oscillatory aerodynamic forces in linearised supersonic flow for arbitrary frequencies, planforms and Mach numbers. A.R.C. R. & M. 3415, January 1963.
43	C. E. Watkins and J. H. Berman	Airfroces and moments on triangular and related wings with subsonic leading edges oscillating in supersonic potential flow. NACA Report 1099 (1952).
44	D. E. Davies	The velocity potential on triangular and related wings with subsonic leading edges oscillating harmonically in supersonic flow. A.R.C. R. & M. 3229, February 1959.
45	C. A. K. Irwin	Characteristics of high speed wind tunnels in the United Kingdom relevant to aero-elastic-model tests. A.R.C. C.P.876, July 1965.
46	H. C. Garner, A. W. Moore and K. C. Wight ..	The theory of interference effects on dynamic measurements in slotted-wall tunnels at subsonic speeds and comparisons with experiment. A.R.C. R. & M. 3500, September 1966.
47	M. Tobak	Damping in pitch of low-aspect-ratio wings at subsonic and supersonic speeds. NACA R.M. A52L04a, (1953).
48	G. Q. Hall and L. A. Osborne	Description of the H.S.D./Cov. half model oscillating derivative measurement rig. H.S.D./Cov. ARL Report 64/10, (1964).
49	J. B. Bratt	Wind tunnel techniques for the measurement of oscillatory derivatives. *AGARD Manual on Aeroelasticity* Part IV, Chapter 5.
50	K. J. Orlik-Rückemann ..	Measurement of aerodynamic damping and stiffness derivatives in free oscillation with automatically recycled feedback excitation. N.R.C. Aeronautical Report LR–246, (1959).
51	G. Q. Hall and J. S. Claridge	Measurements of flow disturbances caused by an oscillating wing in a slotted wall tunnel. H.S.D./Cov. ARL Report 66/4, A.R.C. 28447, (1966).
52	H. H. B. M. Thomas, J. Weber and K. G. Winter	Aerodynamic data for loading action studies. R.A.E. Technical Report 66321 (also reproduced in R.A.E. Technical Report 67166), (1966). A.R.C. 29491.
53	W. E. A. Acum	The comparison of theory and experiment for oscillating wings. *AGARD Manual on Aeroelasticity* Part II, Chapter 10.

No.	*Author*	*Title, etc.*
54	D. L. Woodcock	Research on aeroelasticity in the United Kingdom 1966–7. Unpublished Mintech Report (1967)
55	J. S. Thompson and R. A. Fail	Measurements of oscillatory derivatives at Mach numbers up to 2·6 on a model of a supersonic transport design study (Bristol Type 198). A.R.C. C.P. 815, November 1964.
56	K. E. Brazier	Comparison between theoretical and experimental flutter derivatives. B.A.C. (Weybridge) VTO/D/M/61 (1965).
57	C. O. Olssen and K. J. Orlik-Rückemann	An electronic apparatus for automatic recording of the logarithmic decrement and frequency of oscillations in the audio and subaudio frequency range. F.F.A. Report 52, (1954).
58	I. C. Statler	The development and evaluation of the CAL/Air Force dynamic wind-tunnel testing system. Part II – dynamic tests of an F 104 model. A.F.F.D.L. Technical Report 66–153, (1967).

APPENDIX

Derivative Definition

We use a frame of reference Oxy where the origin 0 is $g\bar{c}$ aft of the wing apex, Ox is aft and Oy to starboard. Motion of the form $e^{i\omega t}$ is assumed. This factor is omitted in the following definitions:

(i) Symmetric motion

If the downward displacement of a point (x, y) is, with H the unit step function, and $x = {}_H$ the control leading edge,

$$z_0 = z + x\theta + (x - x_H)\, H\,(x - x_H)\, H\left(|y| - \frac{s}{2}\right)\beta + \frac{\bar{c}}{s}|y|\,\phi \qquad \text{(A.1)}$$

(the control surface in each case extending from mid semi-span to the wing tip) then we write

$$L = \rho V^2 S \left\{ (l_z + ivl_{\dot{z}}) \frac{z}{\bar{c}} + (l_\theta + ivl_{\dot{\theta}})\,\theta + (l_\beta + ivl_{\dot{\beta}})\,\beta \right.$$
$$\left. + (l_\phi + ivl_{\dot{\phi}})\,\phi \right\} \tag{A.2}$$

$$\mathscr{M} = \rho V^2 S\bar{c} \left\{ (m_z + ivm_{\dot{z}}) \frac{z}{\bar{c}} + (m_\theta + ivm_{\dot{\theta}})\,\theta + (m_\beta + ivm_{\dot{\beta}})\,\beta \right.$$
$$\left. + (m_\phi + ivm_{\dot{\phi}})\,\phi \right\} \tag{A.3}$$

$$\mathscr{H} = \rho V^2 S\bar{c} \left\{ (h_z + ivh_{\dot{z}}) \frac{z}{\bar{c}} + (h_\theta + ivh_{\dot{\theta}})\,\theta + (h_\beta + ivh_{\dot{\beta}})\,\beta \right.$$
$$\left. + (h_\phi + ivh_{\dot{\phi}})\,\phi \right\} \tag{A.4}$$

$$N = \rho V^2 S\bar{c} \left\{ (n_z + ivn_{\dot{z}}) \frac{z}{\bar{c}} + (n_\theta + ivn_{\dot{\theta}})\,\theta + (n_\beta + ivn_{\dot{\beta}})\,\beta \right.$$
$$\left. + (n_\phi + ivn_{\dot{\phi}})\,\phi \right\} \tag{A.5}$$

where L is the lift on the wing (including the control surface)

$\mathscr{M}$ is the pitching moment (nose up) on the wing (including the control surface)

$\mathscr{H}$ is the control surface hinge moment* (nose up)

N is the generalised force for the mode of linear symmetric flexure.

(ii) Antisymmetric motion
If the downward displacement of a point (x, y) is

$$z_0 = \frac{\bar{c}}{s}\psi + sgn(y)\,(x - x_H)\,H\,(x - x_H)\,H\left(|y| - \frac{s}{2}\right)\beta \tag{A.6}$$

where

$$sgn(y) = H(y) - H(-y) = 2H(y) - 1 \tag{A.7}$$

then we write

$$R = \rho V^2 S\bar{c}\,\{(r_\psi + ivr_{\dot{\psi}})\,\psi + (r_\beta + ivr_{\dot{\beta}})\,\beta\} \tag{A.8}$$

$$\mathscr{H} = \rho V^2 S\bar{c}\,\{(h_\psi + ivh_{\dot{\psi}})\,\psi + (h_\beta + ivh_{\dot{\beta}})\,\beta\} \tag{A.9}$$

where $sR/\bar{c}$ is the rolling moment, starboard wing up, and $\mathscr{H}$ is the generalised force for the control surface rotation mode.

---

*What is described as a hinge moment is not strictly a hinge moment because of the hinge sweep, but the generalised force when the control surface displacement is measured not by its angle of rotation about the hinge but by the 'projection' β of this angle in the vertical plane of symmetry of the wing (*see* e.g. equation (A.1)). It is the force on both control surfaces.

TABLE 1

Details of Planforms.

Wing	A	A tan Λ_o	A tan Λ_1	A tan Λ_H	Λ_o	Λ_1	Λ_H	c_1/c_o	c_{1_f}/c_{o_f}	sec Λ_o*
A	3	3.464	0	0.464	49.1°	0	8.8°	0.0718	0.536	1.528
B	2	3.464	0	0.464	60°	0	13.07°	0.0718	0.536	2
C	1.25	3.464	0	0.464	70.13°	0	20.39°	0.0718	0.536	2.946
D	3	3.464	1	1.5	49.1°	18.43°	26.57°	0.238	0.5	1.528
E	2	3.464	1	1.5	60°	26.57°	36.87°	0.238	0.5	2
F	1.25	3.464	1	1.5	70.13°	38.67°	50.2°	0.238	0.5	2.946
G	4	0.75	-0.75	-	10.62°	-10.62°	--	5/11	-	1.017
	3	0.75	-0.75	-0.375	14.04°	-14.04°	-7.13°	5/11	5/8	1.031

A = aspect ratio

Λ_0 = sweepback angle of leading edge

Λ_1 = sweepback angle of trailing edge

Λ_H = sweepback angle of control-surface leading edge

c_1 = tip chord, c_{1_f} = control-surface tip chord

c_0 = root chord, c_{0_f} = control-surface inboard chord

The control surface on each wing runs from half span to the tip, has an inboard chord equal to 1/4 wing mean chord, and is hinged along its leading edge.

*The wing leading edge is sonic when M = sec Λ_0

TABLE 2

Comparison of Subsonic Low Frequency Derivatives for Wing E Obtained by Different Procedures.

$M = 0{\cdot}7806$, $\nu = 0$, axis at apex ($g = 0$).

m, n, $\bar{m}$	ℓ_θ	$-m_\theta$	$\ell_{\dot{\theta}}$	$-m_{\dot{\theta}}$	
(a) By method of Ref.21.					
15, 3, 15	1.281	1.381	2.323	2.927	
15, 3, 31	1.261	1.377	2.347	2.963	
15, 3, 63	1.265	1.377	2.370	2.987	
15, 3, 95	1.264	1.377	2.371	2.989	
15, 3, 127	1.264	1.377	2.372	2.990	
31, 3, 63	1.273	1.376	2.315	2.917	(m = 15 rounding)*
(b) By method of Ref.21 for wing in reversed-flow followed by application of reversed-flow theorem[22].					
15, 3, 15	1.280	1.359	2.332	2.910	
15, 3, 31	1.281	1.367	2.295	2.882	
15, 3, 63	1.279	1.370	2.280	2.871	
15, 3, 95	1.279	1.368	2.282	2.871	
15, 3, 127	1.280	1.367	2.283	2.872	
31, 3, 63	1.273	1.377	2.298	2.898	(m = 15 rounding)*
(c) By method of Ref.18 - i.e. Hornsby's[6] results.					
15, 4, 15	1.291	1.358	2.378	2.964	
(d) By method of Ref.24 - Woodcock's[25] results.					
4, 8, 4	1.290	1.331	2.395	2.955	
8, 6, 8	1.291	1.351	2.383	2.960	
8, 8, 8	1.288	1.352	2.364	2.938	
12, 4, 12	1.291	1.352	2.401	2.987	
16, 2, 16	1.263	1.374	2.268	2.840	
20, 4, 20	1.287	1.371	2.357	2.955	

*This refers to the rounding at the central kink (*see* Ref. 21). Thus the same rounded planform is considered in the calculations with $m = 15$ and with $m = 31$.

TABLE 3

Subsonic Theoretical Derivatives.

Wing A, Symmetric, Axis at Apex ($g = 0$).

M	0				0.745				0.909				0.968			
ν	0*	0.1	0.25	0.5	0*	0.1	0.25	0.5	0*	0.1	0.25	0.5	0*	0.1	0.25	0.5
ℓ_z	0	−0.003	−0.021	−0.109	0	−0.001	−0.010	−0.073	0	0.003	0.012	0.029		0.008	0.046	0.090
ℓ_θ	1.506	1.492	1.449	1.306	1.754	1.747	1.731	1.697	1.979	1.981	2.018	2.152		2.159	2.229	2.243
ℓ_β	0.366	0.358	0.352	0.341	0.460	0.453	0.442	0.421	0.566	0.557	0.522	0.413		0.651	0.519	0.366
ℓ_ϕ											0.016				0.034	
$-m_z$	0	−0.004	−0.028	−0.136	0	−0.003	−0.026	−0.138	0	−0.002	−0.015	−0.052		0.001	0.024	0.054
$-m_\theta$	1.536	1.519	1.464	1.278	1.825	1.807	1.771	1.670	2.105	2.090	2.128	2.322		2.334	2.494	2.586
$-m_\beta$	0.530	0.519	0.513	0.499	0.683	0.674	0.665	0.649	0.869	0.860	0.837	0.720		1.054	0.897	0.625
$-m_\phi$											0.007				0.032	
$-h_z$	0	−0	−0.0001	−0.0005	0	−0	−0.0002	−0.0010	0	−0.0001	−0.0005	−0.0021		−0.0002	−0.0010	−0.0027
$-h_\theta$	0.0034	0.0031	0.0029	0.0022	0.0040	0.0037	0.0033	0.0020	0.0045	0.0042	0.0036	0.0021		0.0039	0.0050	0.0061
$-h_\beta$	0.0057	0.0054	0.0054	0.0054	0.0077	0.0075	0.0075	0.0075	0.0102	0.0101	0.0103	0.0108		0.0132	0.0144	0.0145
$-h_\phi$											−0.0003				−0.0005	
n_z											0.013				0.027	
n_θ											0.854				0.941	
n_β											0.301				0.307	
n_ϕ											0.007				0.014	
$\ell_{\dot{z}}$	1.506	1.493	1.465	1.408	1.754	1.743	1.715	1.682	1.979	1.966	1.936	1.879		2.130	2.055	1.861
$\ell_{\dot{\theta}}$	2.673	2.685	2.704	2.704	2.896	2.940	2.982	3.032	2.962	3.031	3.036	2.868		2.914	2.674	2.460
$\ell_{\dot{\beta}}$	−0.027	−0.017	−0.003	0.016	−0.189	−0.172	−0.148	−0.118	−0.537	−0.511	−0.470	−0.349		−1.118	−0.894	−0.318
$\ell_{\dot{\phi}}$											0.779				0.820	
$-m_{\dot{z}}$	1.536	1.522	1.491	1.428	1.825	1.806	1.778	1.752	2.105	2.082	2.081	2.107		2.312	2.315	2.131
$-m_{\dot{\theta}}$	3.119	3.122	3.143	3.141	3.642	3.679	3.732	3.816	4.139	4.212	4.254	4.109		4.582	4.106	3.542
$-m_{\dot{\beta}}$	0.004	0.012	0.027	0.048	−0.158	−0.141	−0.118	−0.090	−0.544	−0.523	−0.523	−0.483		−1.360	−1.337	−0.543
$-m_{\dot{\phi}}$											0.953				1.055	
$-h_{\dot{z}}$	0.0034	0.0032	0.0031	0.0029	0.0040	0.0038	0.0037	0.0036	0.0045	0.0043	0.0045	0.0052		0.0052	0.0065	0.0089
$-h_{\dot{\theta}}$	0.0093	0.0089	0.0090	0.0090	0.0135	0.0132	0.0133	0.0136	0.0208	0.0208	0.0215	0.0232		0.0338	0.0359	0.0341
$-h_{\dot{\beta}}$	0.0025	0.0024	0.0024	0.0025	0.0043	0.0041	0.0042	0.0042	0.0077	0.0076	0.0075	0.0067		0.0138	0.0098	0.0069
$-h_{\dot{\phi}}$											0.0026				0.0038	
$n_{\dot{z}}$											0.813				0.863	
$n_{\dot{\theta}}$											1.155				1.014	
$n_{\dot{\beta}}$											−0.180				−0.346	
$n_{\dot{\phi}}$											0.380				0.398	

*The $\nu = 0$ values are from Ref. 6 (Hornsby); the remainder from Ref. 8 (Woodcock).

TABLE 4

Subsonic Theoretical Derivatives.

Wing B, Symmetric, Axis at Apex ($g = 0$).

M	0				0.781				0.927			
ν	0*	0.1	0.25	0.5	0*	0.1	0.25	0.5	0*	0.1	0.25	0.5
ℓ_z	0	-0.004	-0.027	-0.119	0	-0.004	-0.026	-0.113		-0.003	-0.020	-0.077
ℓ_θ	1.169	1.161	1.125	0.999	1.320	1.315	1.296	1.239		1.430	1.442	1.504
ℓ_β	0.306	0.303	0.301	0.295	0.378	0.376	0.373	0.367		0.448	0.438	0.392
$-m_z$	0	-0.005	-0.034	-0.147	0	-0.006	-0.040	-0.171		-0.007	-0.042	-0.152
$-m_\theta$	1.217	1.201	1.154	1.487	1.404	1.384	1.348	1.229		1.530	1.535	1.598
$-m_\beta$	0.455	0.451	0.447	0.441	0.580	0.576	0.575	0.574		0.711	0.709	0.666
$-h_z$	0	-0	-0.0001	-0.0006	0	-0	-0.0003	-0.0011		-0.0001	-0.0005	-0.0021
$-h_\theta$	0.0027	0.0025	0.0023	0.0015	0.0030	0.0028	0.0024	0.0010		0.0032	0.0025	0.0006
$-h_\beta$	0.0051	0.0050	0.0050	0.0049	0.0068	0.0067	0.0067	0.0067		0.0086	0.0088	0.0094
$\ell_{\dot{z}}$	1.169	1.165	1.154	1.129	1.320	1.317	1.312	1.317		1.428	1.434	1.461
$\ell_{\dot{\theta}}$	2.327	2.337	2.342	2.336	2.581	2.607	2.627	2.665		2.789	2.800	2.764
$\ell_{\dot{\beta}}$	0.022	0.025	0.031	0.039	-0.071	-0.065	-0.057	-0.049		-0.238	-0.237	-0.220
$-m_{\dot{z}}$	1.217	1.207	1.194	1.166	1.404	1.390	1.386	1.396		1.533	1.556	1.634
$-m_{\dot{\theta}}$	2.774	2.775	2.780	2.772	3.273	3.291	3.319	3.384		3.756	3.794	3.804
$-m_{\dot{\beta}}$	0.056	0.059	0.065	0.074	-0.036	-0.029	-0.022	-0.017		-0.232	-0.256	-0.293
$-h_{\dot{z}}$	0.0027	0.0025	0.0025	0.0024	0.0030	0.0029	0.0029	0.0028		0.0033	0.0034	0.0040
$-h_{\dot{\theta}}$	0.0089	0.0086	0.0086	0.0086	0.0127	0.0125	0.0126	0.0129		0.0184	0.0189	0.0208
$-h_{\dot{\beta}}$	0.0027	0.0026	0.0026	0.0026	0.0043	0.0043	0.0043	0.0043		0.0071	0.0069	0.0062

*The $\nu = 0$ values are from Ref. 6 (Hornsby); the remainder from Ref. 8 (Woodcock).

TABLE 5

Subsonic Theoretical Derivatives.
Wing C, Symmetric, Axis at Apex ($g = 0$).

M	0				0.8				0.9165				0.9798			
ν	0*	0.1	0.25	0.5	0*	0.1	0.25	0.5	0*	0.1	0.25	0.5	0*	0.1	0.25	0.5
ℓ_z	0	-0.004	-0.026	-0.107		-0.004	-0.028	-0.115		-0.005		-0.114		-0.005		-0.105
ℓ_θ	0.825	0.818	0.789	0.684		0.888	0.865	0.783		0.924		0.856		0.961		0.947
ℓ_β	0.236	0.235	0.234	0.232		0.281	0.281	0.282		0.314		0.312		0.359		0.326
ℓ_ϕ			-0.008				-0.008									
$-m_z$	0	-0.005	-0.033	-0.134		-0.006	-0.039	-0.160		-0.007		-0.170		-0.007		-0.161
$-m_\theta$	0.877	0.862	0.822	0.681		0.949	0.911	0.777		0.997		0.868		1.051		1.018
$-m_\beta$	0.362	0.360	0.359	0.356		0.444	0.445	0.449		0.506		0.515		0.594		0.556
$-m_\phi$			-0.011				-0.012									
$-h_z$	0	-0	-0.0001	-0.0006		-0	-0.0002	-0.0009		-0.0001		-0.0013		-0.0001		-0.0018
$-h_\theta$	0.0019	0.0018	0.0016	0.0008		0.0020	0.0017	0.0004		0.0023		0.0001		0.0029		0.0013
$-h_\beta$	0.0042	0.0042	0.0042	0.0041		0.0054	0.0054	0.0054		0.0063		0.0066		0.0079		0.0088
$-h_\phi$			-0.0001				-0.0001									
n_z			-0.007				-0.008									
n_θ			0.338				0.370									
n_β			0.133				0.154									
n_ϕ			-0.003				-0.003									
$\ell_{\dot{z}}$	0.825	0.823	0.820	0.812		0.893	0.894	0.903		0.928		0.956		0.964		1.005
$\ell_{\dot{\theta}}$	1.797	1.806	1.807	1.803		1.990	1.999	2.024		2.093		2.139		2.193		2.192
$\ell_{\dot{\beta}}$	0.043	0.045	0.047	0.049		0.009	0.010	0.011		-0.035		-0.041		-0.136		-0.133
$\ell_{\dot{\phi}}$			0.333				0.369									
$-m_{\dot{z}}$	0.877	0.869	0.865	0.855		0.957	0.958	0.969		1.004		1.050		1.058		1.136
$-m_{\dot{\theta}}$	2.201	2.201	2.202	2.197		2.536	2.549	2.587		2.746		2.835		2.983		2.986
$-m_{\dot{\beta}}$	0.077	0.079	0.081	0.083		0.047	0.048	0.048		-0.002		-0.027		-0.147		-0.199
$-m_{\dot{\phi}}$			0.398				0.448									
$-h_{\dot{z}}$	0.0019	0.0018	0.0018	0.0018		0.0021	0.0021	0.0020		0.0024		0.0025		0.0031		0.0041
$-h_{\dot{\theta}}$	0.0076	0.0074	0.0074	0.0074		0.0103	0.0103	0.0104		0.0129		0.0137		0.0180		0.0199
$-h_{\dot{\beta}}$	0.0025	0.0024	0.0024	0.0024		0.0036	0.0037	0.0037		0.0048		0.0047		0.0069		0.0040
$-h_{\dot{\phi}}$			0.0010				0.0012									
$n_{\dot{z}}$			0.347				0.378									
$n_{\dot{\theta}}$			0.709				0.787									
$n_{\dot{\beta}}$			0.027				0.014									
$n_{\dot{\phi}}$			0.163				0.178									

*The $\nu = 0$ values are from Ref. 6 (Hornsby); the remainder from Ref. 8 (Woodcock).

TABLE 6

Subsonic Theoretical Derivatives

Wing D, Symmetrics, Axis at Apex ($g = 0$)

M	0				0.745				0.909				0.968			
ν	0*	0.1	0.25	0.5	0*	0.1	0.25	0.5	0*	0.1	0.25	0.5	0*	0.1	0.25	0.5
ℓ_z	0	-0.002	-0.017	-0.091	0	+0	-0.005	-0.053	0	0.004	0.018	0.038		0.009	0.049	0.078
ℓ_θ	1.498	1.485	1.445	1.314	1.729	1.723	1.707	1.672	1.936	1.937	1.960	2.037		2.096	2.116	2.085
ℓ_β	0.334	0.329	0.323	0.314	0.398	0.394	0.384	0.365	0.455	0.450	0.415	0.329		0.473	0.374	0.324
ℓ_ϕ											0.015				0.032	
$-m_z$	0	-0.003	-0.022	-0.113	0	-0.002	-0.018	-0.108	0	-0	-0.005	-0.034		0.004	0.030	0.030
$-m_\theta$	1.535	1.520	1.469	1.300	1.794	1.780	1.746	1.651	2.036	2.027	2.049	2.153		2.231	2.305	2.296
$-m_\beta$	0.511	0.502	0.496	0.485	0.624	0.618	0.610	0.594	0.736	0.732	0.703	0.600		0.804	0.772	0.580
$-m_\phi$											0.006				0.028	
$-h_z$	0	-0	-0.0001	-0.0005	0	-0	-0.0002	-0.0010	0	-0.0001	-0.0005	-0.0018		-0.0001	-0.0007	-0.0025
$-h_\theta$	0.0021	0.0020	0.0018	0.0010	0.0022	0.0021	0.0017	0.0004	0.0020	0.0018	0.0012	-0.0008		0.0013	0.0007	0.0009
$-h_\beta$	0.0055	0.0053	0.0053	0.0052	0.0074	0.0073	0.0073	0.0073	0.0096	0.0096	0.0097	0.0101		0.0116	0.0122	0.0127
$-h_\phi$											-0.0003				-0.0004	
n_z											0.012				0.024	
n_θ											0.840				0.905	
n_β											0.264				0.259	
n_ϕ											0.005				0.011	
$\ell_{\dot{z}}$	1.498	1.486	1.457	1.397	1.729	1.718	1.687	1.642	1.936	1.922	1.879	1.792		2.066	1.961	1.774
$\ell_{\dot{\theta}}$	2.522	2.540	2.561	2.563	2.686	2.738	2.778	2.818	2.661	2.743	2.749	2.622		2.488	2.355	2.329
$\ell_{\dot{\beta}}$	-0.014	-0.006	0.007	0.023	-0.152	-0.137	-0.117	-0.089	-0.421	-0.400	-0.347	-0.207		-0.787	-0.467	-0.132
$\ell_{\dot{\phi}}$											0.756				0.777	
$-m_{\dot{z}}$	1.535	1.522	1.490	1.423	1.794	1.778	1.746	1.705	2.036	2.017	1.998	1.969		2.209	2.152	1.973
$-m_{\dot{\theta}}$	2.937	2.951	2.972	2.974	3.352	3.403	3.451	3.517	3.671	3.768	3.794	3.672		3.858	3.523	3.312
$-m_{\dot{\beta}}$	0.022	0.029	0.043	0.060	-0.118	-0.104	-0.083	-0.058	-0.431	-0.415	-0.391	-0.283		-0.990	-0.698	-0.199
$-m_{\dot{\phi}}$											0.918				0.979	
$-h_{\dot{z}}$	0.0021	0.0021	0.0020	0.0019	0.0022	0.0022	0.0021	0.0021	0.0020	0.0019	0.0020	0.0024		0.0016	0.0021	0.0032
$-h_{\dot{\theta}}$	0.0077	0.0075	0.0075	0.0075	0.0106	0.0106	0.0107	0.0109	0.0145	0.0149	0.0153	0.0162		0.0200	0.0210	0.0220
$-h_{\dot{\beta}}$	0.0026	0.0024	0.0024	0.0025	0.0040	0.0039	0.0039	0.0039	0.0061	0.0061	0.0059	0.0055		0.0085	0.0068	0.0053
$-h_{\dot{\phi}}$											0.0011				0.0013	
$n_{\dot{z}}$											0.804				0.841	
$n_{\dot{\theta}}$											1.146				1.016	
$n_{\dot{\beta}}$											-0.131				-0.191	
$n_{\dot{\phi}}$											0.378				0.390	

*The $\nu = 0$ values are from Ref. 6 (Hornsby); the remainder from Ref. 8 (Woodcock).

TABLE 7

Subsonic Theoretical Derivatives.

Wing E, Symmetric, Axis at Apex ($g = 0$).

M	0				0.781				0.927			
ν	0*	0.1	0.25	0.5	0*	0.1	0.25	0.5	0*	0.1	0.25	0.5
ℓ_z	0	-0.004	-0.024	-0.104	0	-0.003	-0.021	-0.094		-0.002	-0.013	-0.057
ℓ_θ	1.153	1.146	1.113	1.000	1.291	1.287	1.271	1.220		1.393	1.402	1.435
ℓ_β	0.265	0.264	0.262	0.257	0.303	0.304	0.301	0.294		0.330	0.317	0.276
$-m_z$	0	-0.004	-0.029	-0.127	0	-0.005	-0.032	-0.141		-0.005	-0.031	-0.115
$-m_\theta$	1.196	1.184	1.141	0.993	1.358	1.344	1.313	1.209		1.471	1.472	1.494
$-m_\beta$	0.416	0.413	0.411	0.405	0.491	0.491	0.489	0.485		0.550	0.539	0.488
$-h_z$	0	-0	-0.0001	-0.0006	0	-0	-0.0002	-0.0009		-0.0001	-0.0003	-0.0014
$-h_\theta$	0.0015	0.0014	0.0012	0.0004	0.0013	0.0012	0.0008	-0.0004		0.0009	0.0004	-0.0014
$-h_\beta$	0.0050	0.0048	0.0048	0.0048	0.0064	0.0064	0.0064	0.0064		0.0077	0.0078	0.0080
$\ell_{\dot{z}}$	1.153	1.150	1.138	1.112	1.291	1.288	1.281	1.278		1.391	1.388	1.387
$\ell_{\dot{\theta}}$	2.185	2.201	2.206	2.201	2.378	2.414	2.431	2.457		2.515	2.517	2.472
$\ell_{\dot{\beta}}$	0.025	0.028	0.033	0.039	-0.054	-0.049	-0.042	-0.035		-0.179	-0.165	-0.118
$-m_{\dot{z}}$	1.196	1.189	1.176	1.146	1.358	1.349	1.342	1.342		1.472	1.482	1.513
$-m_{\dot{\theta}}$	2.581	2.593	2.598	2.591	2.964	3.002	3.024	3.070		3.310	3.325	3.297
$-m_{\dot{\beta}}$	0.061	0.065	0.070	0.077	0.022	-0.016	-0.010	-0.004		-0.180	-0.183	-0.151
$-h_{\dot{z}}$	0.0015	0.0014	0.0014	0.0014	0.0013	0.0012	0.0012	0.0012		0.0010	0.0010	0.0012
$-h_{\dot{\theta}}$	0.0067	0.0067	0.0067	0.0067	0.0085	0.0087	0.0087	0.0088		0.0106	0.0107	0.0114
$-h_{\dot{\beta}}$	0.0025	0.0024	0.0024	0.0025	0.0036	0.0036	0.0036	0.0036		0.0047	0.0047	0.0044

*The $\nu = 0$ values are from Ref. 6 (Hornsby); the remainder from Ref. 8 (Woodcock).

TABLE 8

Subsonic Theoretical Derivatives.

Wing F, Symmetric, Axis at Apex ($g = 0$)

M	0				0.6		0.8			0.9165				0.9539		0.9798				0.9902	
ν	0*	0.1	0.25	0.5	0.1	0.5	0.1	0.25	0.5	0.03	0.1	0.3	0.5	0.1	0.5	0.03	0.1	0.3	0.5	0.1	0.5
ℓ_z	0	-0.004	-0.023	-0.095	-0.004	-0.098	-0.004	-0.024	-0.098	-0	-0.004	-0.033	-0.093	-0.004	-0.088	-0	-0.003	-0.030	-0.084	-0.003	-0.082
ℓ_θ	0.807	0.802	0.775	0.683	0.833	0.725	0.867	0.847	0.777	0.903	0.900	0.880	0.842	0.916	0.874	0.932	0.931	0.920	0.895	0.938	0.901
ℓ_β	0.190	0.190	0.190	0.188	0.200	0.198	0.208	0.208	0.207	0.216	0.215	0.212	0.206	0.218	0.199	0.220	0.218	0.205	0.193	0.217	0.192
ℓ_ϕ			-0.008					-0.007													
$-m_z$	0	-0.004	-0.028	-0.117	-0.005	-0.125	-0.005	-0.032	-0.132	-0	-0.005	-0.048	-0.134	-0.005	-0.129	-0	-0.005	-0.045	-0.124	-0.005	-0.122
$-m_\theta$	0.849	0.838	0.803	0.680	0.875	0.720	0.914	0.882	0.771	0.959	0.954	0.917	0.850	0.974	0.895	0.995	0.993	0.973	0.925	1.003	0.936
$-m_\beta$	0.307	0.307	0.307	0.304	0.326	0.325	0.345	0.344	0.345	0.362	0.362	0.360	0.353	0.368	0.346	0.374	0.372	0.355	0.338	0.371	0.335
$-m_\phi$			-0.011					-0.012													
$-h_z$	0	-0	-0.0001	-0.0005	-0	-0.0006	-0	-0.0002	-0.0007	-0	-0	-0.0003	-0.0008	-0	-0.0008	-0	-0	-0.0003	-0.0009	-0	-0.0009
$-h_\theta$	0.0008	0.0007	0.0006	-0.0001	0.0007	-0.0003	0.0006	0.0003	-0.0006	0.0005	0.0005	-0	-0.0009	0.0004	-0.0011	0.0004	0.0004	-0.0002	-0.0012	0.0003	-0.0011
$-h_\beta$	0.0040	0.0040	0.0040	0.0040	0.0044	0.0044	0.0048	0.0048	0.0048	0.0052	0.0052	0.0052	0.0053	0.0054	0.0055	0.0055	0.0055	0.0057	0.0057	0.0056	0.0058
$-h_\phi$			-0.0001					-0.0001													
n_z			-0.007					-0.007													
n_θ			0.336					0.365													
n_β			0.117					0.128													
n_ϕ			-0.003					-0.003													
ℓ_z	0.807	0.806	0.802	0.794	0.837	0.833	0.870	0.870	0.875	0.903	0.903	0.907	0.918	0.919	0.934	0.932	0.932	0.935	0.942	0.938	0.944
ℓ_θ	1.670	1.685	1.686	1.683	1.756	1.767	1.826	1.833	1.850	1.884	1.888	1.898	1.910	1.909	1.915	1.914	1.914	1.908	1.906	1.902	1.900
ℓ_β	0.036	0.038	0.039	0.041	0.025	0.028	0.004	0.005	0.007	-0.031	-0.030	-0.028	-0.025	-0.056	-0.034	-0.094	-0.089	-0.058	-0.033	-0.106	-0.032
ℓ_ϕ			0.326					0.357													
$-m_z$	0.849	0.843	0.839	0.829	0.881	0.879	0.920	0.920	0.926	0.959	0.960	0.968	0.986	0.979	1.011	0.995	0.998	1.008	1.023	1.006	1.027
$-m_\theta$	2.010	2.023	2.024	2.019	2.144	2.156	2.272	2.282	2.307	2.398	2.403	2.422	2.447	2.461	2.477	2.504	2.496	2.477	2.478	2.489	2.476
$-m_\beta$	0.068	0.070	0.072	0.074	0.057	0.061	0.033	0.034	0.035	-0.012	-0.011	-0.014	-0.015	-0.049	-0.035	-0.102	-0.105	-0.071	-0.038	-0.137	-0.037
$-m_\phi$			0.387					0.428													
$-h_z$	0.0008	0.0008	0.0008	0.0008	0.0007	0.0007	0.0006	0.0006	0.0006	0.0005	0.0005	0.0005	0.0005	0.0005	0.0005	0.0004	0.0004	0.0005	0.0006	0.0004	0.0006
$-h_\theta$	0.0050	0.0050	0.0050	0.0050	0.0054	0.0054	0.0058	0.0058	0.0058	0.0061	0.0061	0.0062	0.0063	0.0064	0.0067	0.0067	0.0067	0.0069	0.0072	0.0070	0.0074
$-h_\beta$	0.0021	0.0021	0.0021	0.0021	0.0023	0.0023	0.0026	0.0026	0.0026	0.0030	0.0030	0.0029	0.0029	0.0031	0.0029	0.0034	0.0034	0.0030	0.0028	0.0034	0.0028
$-h_\phi$			0.0004					0.0004													
n_z			0.345					0.373													
n_θ			0.696					0.758													
n_β			0.025					0.013													
n_ϕ			0.163					0.176													

*The $\nu = 0$ values are from Ref. 6 (Hornsby); the remainder from Ref. 8 (Woodcock).

TABLE 9

Subsonic Theoretical Derivatives.

Wing G (A = 3 Version), Symmetric, Axis at Apex (g = 0).

M	0.8	0.9	0.95	0.99
ν	0.01	0.01	0.01	0.01
ℓ_z	+0	+0	+0	+0
ℓ_θ	1.939	2.100	2.215	2.331
ℓ_β	0.538	0.615	0.686	0.810
ℓ_ϕ	+0	+0	+0	+0
$-m_z$	-0	-0	-0	-0
$-m_\theta$	0.736	0.755	0.748	0.682
$-m_\beta$	0.393	0.469	0.546	0.697
$-m_\phi$	-0	-0	-0	-0
$-h_z$	-0	-0	-0	-0
$-h_\theta$	0.0020	0.0019	0.0015	0.0005
$-h_\beta$	0.0078	0.0090	0.0100	0.0120
$-h_\phi$	-0	-0	-0	-0
n_z	+0	+0	+0	+0
n_θ	0.820	0.888	0.937	0.989
n_β	0.298	0.334	0.366	0.422
n_ϕ	+0	+0	+0	+0
$\ell_z^\bullet$	1.939	2.100	2.215	2.331
$\ell_\theta^\bullet$	1.773	1.834	1.958	2.504
$\ell_\beta^\bullet$	-0.281	-0.522	-0.843	-1.788
$\ell_\phi^\bullet$	0.820	0.888	0.937	0.988
$-m_z^\bullet$	0.737	0.755	0.748	0.682
$-m_\theta^\bullet$	1.483	1.915	2.532	4.406
$-m_\beta^\bullet$	-0.034	-0.082	-0.137	-0.272
$-m_\phi^\bullet$	0.330	0.341	0.342	0.320
$-h_z^\bullet$	0.0020	0.0019	0.0015	0.0005
$-h_\theta^\bullet$	0.0130	0.0189	0.0265	0.0426
$-h_\beta^\bullet$	0.0059	0.0096	0.0155	0.0456
$-h_\phi^\bullet$	0.0009	0.0008	0.0007	0.0002
$n_z^\bullet$	0.820	0.888	0.937	0.988
$n_\theta^\bullet$	0.692	0.701	0.735	0.939
$n_\beta^\bullet$	-0.104	-0.209	-0.350	-0.798
$n_\phi^\bullet$	0.399	0.428	0.450	0.472

TABLE 10

Subsonic Theoretical Derivatives

Wing G ($A = 4$ Version), Symmetric, Axis at Apex ($g = 0$)

M	0.8	0.9	0.95	0.99
ν	0.01	0.01	0.01	0.01
ℓ_z	+0	+0	+0	+0
ℓ_θ	2.336	2.609	2.825	3.077
ℓ_ϕ	+0	+0	+0	+0
$-m_z$	-0	-0	-0	-0
$-m_\theta$	0.925	0.986	1.008	0.944
$-m_\phi$	-0	-0	-0	-0
n_z	+0	+0	+0	+0
n_θ	0.989	1.104	1.195	1.304
n_ϕ	+0	+0	+0	+0
$\ell_z^\bullet$	2.336	2.609	2.825	3.077
$\ell_\theta^\bullet$	1.272	0.963	0.709	1.033
$\ell_\phi^\bullet$	0.988	1.103	1.195	1.304
$-m_z^\bullet$	0.925	0.989	1.008	0.944
$-m_\theta^\bullet$	1.374	1.826	2.643	6.132
$-m_\phi^\bullet$	0.412	0.442	0.456	0.439
$n_z^\bullet$	0.989	1.103	1.195	1.304
$n_\theta^\bullet$	0.480	0.327	0.187	0.251
$n_\phi^\bullet$	0.488	0.537	0.576	0.623

TABLE 11

Supersonic Theoretical Derivatives

Wing A, Symmetric, Subsonic Leading Edge, Axis at Apex ($g = 0$)

M	1.054				1.118				1.202				1.302				1.414			
ν	0*	0.1	0.25	0.5	0*	0.1	0.25	0.5	0*	0.1	0.25	0.5	0*	0.1	0.25	0.5	0*	0.1	0.25	0.5
ℓ_z	0	0.03	0.08	0.14	0	0.02	0.08	0.15	0	0.02	0.08	0.15	0	0.01	0.06	0.16	0	0.01	0.05	0.15
ℓ_θ	2.37 (2.388)	2.29	2.19	2.16	2.23 (2.241)	2.20	2.11	2.07	2.08 (2.087)	2.07	2.02	1.95	1.94 (1.939)	1.93	1.90	1.84	1.82 (1.801)	1.81	1.79	1.74
$-m_z$	0	0.03	0.10	0.14	0	0.03	0.10	0.15	0	0.02	0.09	0.17	0	0.01	0.08	0.18	0	0.01	0.07	0.19
$-m_\theta$	2.83 (2.903)	2.72	2.61	2.58	2.67 (2.733)	2.63	2.52	2.49	2.51 (2.550)	2.49	2.42	2.34	2.33 (2.372)	2.33	2.29	2.21	2.18 (2.205)	2.18	2.15	2.08
$\ell_z^\bullet$	2.37	2.24	1.99	1.78	2.23	2.17	1.95	1.73	2.08	2.05	1.90	1.65	1.94	1.92	1.82	1.60	1.82	1.80	1.73	1.55
$\ell_{\dot\theta}$	(0.336)	1.13	1.82	2.08	(1.108)	1.33	1.67	1.95	(1.380)	1.45	1.57	1.78	(1.440)	1.46	1.51	1.62	(1.408)	1.38	1.40	1.48
$-m_z^\bullet$	2.83	2.64	2.33	2.08	2.67	2.58	2.29	2.03	2.51	2.46	2.25	1.93	2.33	2.31	2.17	1.87	2.18	2.16	2.07	1.82
$-m_{\dot\theta}^\bullet$	(0.496)	1.73	2.67	2.97	(1.557)	1.96	2.44	2.80	(1.931)	2.08	2.25	2.55	(2.012)	2.08	2.15	2.31	(1.966)	1.96	2.00	2.11

*The $\nu = 0$ values in brackets are from Ref. 17 (Orlik-Rückemann *et al*); the remainder are from Ref. 10 (Harris).

TABLE 12

Supersonic Theoretical Derivatives

Wing B, Symmetric, Subsonic Leading Edge, Axis at Apex ($g = 0$)

M	1.118				1.25				1.414				1.601				1.803			
ν	0*	0.1	0.25	0.5	0*	0.1	0.25	0.5	0*	0.1	0.25	0.5	0*	0.1	0.25	0.5	0*	0.1	0.25	0.5
ℓ_z	0	0.00	0.02	0.02	0	0.00	0.02	0.03	0	0.00	0.02	0.04	0	0.00	0.01	0.04	0	0.00	0.01	0.05
ℓ_θ	1.58 (1.592)	1.57	1.56	1.59	1.49 (1.494)	1.49	1.49	1.49	1.39 (1.392)	1.39	1.39	1.40	1.29 (1.293)	1.29	1.29	1.30	1.21 (1.201)	1.21	1.21	1.21
$-m_z$	0	0.01	0.02	0.00	0	0.00	0.02	0.02	0	0.00	0.02	0.04	0	0.00	0.02	0.05	0	0.00	0.02	0.05
$-m_\theta$	1.89 (1.935)	1.88	1.87	1.91	1.78 (1.822)	1.78	1.78	1.80	1.67 (1.700)	1.67	1.67	1.68	1.56 (1.581)	1.56	1.56	1.57	1.46 (1.470)	1.46	1.46	1.46
ℓ_z^*	1.58	1.56	1.50	1.43	1.49	1.48	1.44	1.37	1.39	1.38	1.36	1.30	1.29	1.29	1.27	1.22	1.21	1.21	1.19	1.15
ℓ_θ^*	(1.944)	2.09	2.15	2.16	(1.856)	1.92	1.92	1.93	(1.677)	1.70	1.70	1.70	(1.491)	1.50	1.50	1.50	(1.322)	1.31	1.31	1.31
$-m_z^*$	1.89	1.86	1.78	1.70	1.78	1.77	1.72	1.63	1.67	1.66	1.63	1.55	1.56	1.55	1.53	1.46	1.46	1.45	1.43	1.38
$-m_\theta^*$	(2.702)	2.92	3.00	3.01	(2.581)	2.68	2.69	2.70	(2.334)	2.38	2.38	2.37	(2.076)	2.10	2.10	2.09	(1.842)	1.84	1.84	1.84

*The $v = 0$ values in brackets are from Ref. 17 (Orlik Rückemann *et al*); the remainder from Ref. 10 (Harris).

TABLE 13

Supersonic Theoretical Derivatives.

Wing C, Symmetric, Subsonic/Sonic Leading Edge, Axis at Apex ($g = 0$).

M	1.281				1.562				1.887				2.236	2.600	2.946
ν	0*	0.1	0.25	0.5	0*	0.1	0.25	0.5	0*	0.1	0.25	0.5	0*	0*	0*
ℓ_z	0	0.00	-0.01	-0.05	0	0.00	-0.01	-0.03	0	0.00	0.00	-0.01			
ℓ_θ	0.99 (0.995)	0.98	0.98	0.98	0.93 (0.934)	0.93	0.93	0.93	0.87 (0.870)	0.87	0.87	0.87	(0.808)	(0.751)	(0.702)
$-m_z$	0	0.00	-0.02	-0.08	0	0.00	-0.01	-0.05	0	0.00	-0.01	-0.03			
$-m_\theta$	1.18 (1.210)	1.18	1.17	1.17	1.11 (1.139)	1.11	1.11	1.12	1.04 (1.063)	1.05	1.05	1.05	(0.988)	(0.919)	(0.860)
$\ell_{\dot{z}}$	0.99	0.98	0.98	0.99	0.93	0.93	0.93	0.93	0.87	0.87	0.87	0.87			
$\ell_{\dot{\theta}}$	(1.739)	1.78	1.78	1.78	(1.500)	1.53	1.53	1.52	(1.279)	1.29	1.29	1.29	(1.093)	(0.943)	(0.830)
$-m_{\dot{z}}$	1.18	1.18	1.17	1.18	1.11	1.11	1.11	1.12	1.04	1.04	1.06	1.05			
$-m_{\dot{\theta}}$	(2.412)	2.47	2.47	2.46	(2.083)	2.12	2.12	2.11	(1.778)	1.80	1.80	1.79	(1.521)	(1.313)	(1.157)

*The $\nu = 0$ values in brackets are from Ref. 17 (Orlik-Rückemann *et al*); the remainder from Ref. 10 (Harris).

TABLE 14

Supersonic Theoretical Derivatives

Wing D, Symmetric, Subsonic Leading Edge, Axis at Apex ($g = 0$)

M	1.054				1.118				1.202				1.302				1.414			
ν	0*	0.1	0.25	0.5	0*	0.1	0.25	0.5	0*	0.1	0.25	0.5	0*	0.1	0.25	0.5	0*	0.1	0.25	0.5
ℓ_z	0	0.2	0.8	0.13	0	0.02	0.08	0.14	0	0.02	0.08	0.15	0	0.01	0.06	0.16	0	0.01	0.06	0.16
ℓ_θ	2.28 (2.313)	2.21	2.12	2.10	2.19 (2.186)	2.16	2.07	2.02	2.06 (2.047)	2.05	1.99	1.91	1.92 (1.910)	1.92	1.89	1.82	1.81 (1.782)	1.81	1.79	1.74
$-m_z$	0	0.03	0.08	0.11	0	0.02	0.09	0.14	0	0.02	0.10	0.17	0	0.02	0.08	0.19	0	0.01	0.07	0.19
$-m_\theta$	2.67 (2.774	2.58	2.48	2.47	2.58 (2.640)	2.54	2.43	2.39	2.47 (2.486)	2.45	2.37	2.27	2.32 (2.329)	2.31	2.27	2.18	2.18 (2.178)	2.18	2.15	2.08
$\ell_{\dot{z}}$	2.28	2.16	1.94	1.75	2.19	2.12	1.91	1.69	2.06	2.03	1.88	1.62	1.92	1.90	1.81	1.58	1.81	1.80	1.73	1.55
$\ell_{\dot{\theta}}$	(0.357)	1.18	1.82	2.06	(1.090)	1.27	1.61	1.90	(1.348)	1.36	1.49	1.71	(1.403)	1.41	1.45	1.57	(1.371)	1.34	1.36	1.43
$-m_{\dot{z}}$	2.67	2.51	2.24	2.04	2.58	2.50	2.22	1.98	2.47	2.42	2.21	1.89	2.32	2.29	2.15	1.85	2.18	2.16	2.06	1.81
$-m_{\dot{\theta}}$	(0.551)	1.86	2.70	2 .96	(1.545)	1.91	2.39	2.75	(1.892)	1.96	2.14	2.46	(1.966)	2.00	2.07	2.23	(1.920)	1.91	1.94	2.04

*The $\nu = 0$ values in brackets are from Ref. 17 (Orlik-Rückemann *et al*); the remainder from Ref. 10 (Harris).

TABLE 15

Supersonic Theoretical Derivatives

Wing E, Symmetric, Subsonic Leading Edge, Axis at Apex ($g = 0$)

M	1.118				1.250				1.414				1.601				1.803			
ν	0*	0.1	0.25	0.5	0*	0.1	0.25	0.5	0*	0.1	0.25	0.5	0*	0.1	0.25	0.5	0*	0.1	0.25	0.5
ℓ_z	0	0.00	0.02	0.01	0	0.00	0.02	0.03	0	0.00	0.02	0.05	0	0.00	0.02	0.05	0	0.00	0.02	0.05
ℓ_θ	1.52 (1.542)	1.51	1.51	1.52	1.46 (1.457)	1.46	1.45	1.46	1.37 (1.365)	1.37	1.37	1.38	1.28 (1.274)	1.28	1.28	1.29	1.21 (1.188)	1.21	1.21	1.21
$-m_z$	0	0.00	0.01	0.01	0	0.00	0.02	0.02	0	0.00	0.02	0.05	0	0.00	0.02	0.05	0	0.00	0.02	0.06
$-m_\theta$	1.78 (1.849)	1.77	1.76	1.79	1.72 (1.760)	1.72	1.72	1.72	1.65 (1.657)	1.65	1.65	1.65	1.54 (1.552)	1.54	1.55	1.55	1.45 (1.452)	1.45	1.45	1.45
$\ell_{\dot{z}}$	1.52	1.50	1.45	1.39	1.46	1.45	1.41	1.33	1.37	1.37	1.34	1.27	1.28	1.28	1.26	1.21	1.21	1.21	1.19	1.15
$\ell_{\dot{\theta}}$	(1.873)	2.02	2.08	2.10	(1.795)	1.84	1.85	1.86	(1.627)	1.64	1.64	1.64	(1.450)	1.46	1.46	1.45	(1.288)	1.28	1.28	1.28
$-m_{\dot{z}}$	1.78	1.76	1.69	1.63	1.72	1.71	1.66	1.57	1.65	1.64	1.60	1.51	1.54	1.54	1.52	1.45	1.45	1.45	1.43	1.37
$-m_{\dot{\theta}}$	(2.594)	2.81	2.89	2.91	(2.492)	2.57	2.59	2.60	(2.263)	2.28	2.28	2.28	(2.020)	2.04	2.03	2.03	(1.797)	1.80	1.80	1.79

*The $\nu = 0$ values in brackets are from Ref. 17 (Orlik-Rückemann *et al*); the remainder from Ref. 10 (Harris).

TABLE 16

Supersonic Theoretical Derivatives

Wing F, Symmetric, Subsonic/Sonic Leading Edge, Axis at Apex ($g = 0$)

M	1.281				1.562				1.887				2.236	2.600	2.946
ν	0*	0.1	0.25	0.5	0*	0.1	0.25	0.5	0*	0.1	0.25	0.5	0*	0*	0*
ℓ_z		0.00	-0.01	-0.05		0.00	-0.01	-0.03		0.00	0.00	-0.01			
ℓ_θ	0.95 (0.964)	0.95	0.95	0.94	0.91 (0.911)	0.91	0.91	0.91	0.86 (0.853)	0.86	0.86	0.86	(0.796)	(0.742)	(0.696)
$-m_z$		0.00	-0.02	-0.08		0.00	-0.01	-0.05		0.00	0.00	-0.02			
$-m_\theta$	1.11 (1.156)	1.11	1.11	1.10	1.08 (1.100)	1.08	1.08	1.07	1.03 (1.036)	1.03	1.03	1.03	(0.970)	(0.908)	(0.854)
$\ell_{\dot{z}}$		0.95	0.95	0.95		0.91	0.91	0.91		0.86	0.86	0.85			
$\ell_{\dot{\theta}}$	(1.669)	1.71	1.71	1.70	(1.448)	1.47	1.47	1.47	(1.239)	1.25	1.25	1.24	(1.063)	(0.919)	(0.810)
$-m_{\dot{z}}$		1.11	1.11	1.12		1.08	1.08	1.08		1.03	1.03	1.02			
$-m_{\dot{\theta}}$	(2.300)	2.34	2.34	2.34	(2.003)	2.03	2.03	2.02	(1.719)	1.73	1.73	1.72	(1.478)	(1.280)	(1.130)

*The $\nu = 0$ values in brackets are from Ref. 17 (Orlik-Rückemann *et al*); the remainder from Ref. 10 (Harris).

TABLE 17

Supersonic Theoretical Derivatives

Wing A, Symmetric, Sonic/Supersonic Leading Edge, Axis at Apex ($g = 0$)

M	1.53				1.67	1.95	2.0				2.53			
ν	0*	0.1	0.25	0.5	0*	0*	0*	0.1	0.25	0.5	0*	0.1	0.25	0.5
ℓ_z	0	0.028	0.041		0	0	0	0.008	0.011	0.039	0	0.001	0.008	0.028
ℓ_θ	1.685	1.645	1.635	1.608	1.47	1.20		1.064	1.064	1.063		0.884	0.879	0.872
ℓ_β		0.157	0.157	0.157				0.103	0.103	0.103		0.077	0.077	0.077
$-m_z$	0	0.009	0.055		0	0	0	0.002	0.014	0.082	0	0.002	0.011	0.041
$-m_\theta$	2.064	1.969	1.954	1.927	1.79	1.46		1.286	1.286	1.284		1.132	1.120	1.114
$-m_\beta$		0.024	0.024	0.024				0.016	0.016	0.016		0.012	0.012	0.012
$-h_z$	0	0.0002	0.0006		0	0	0	0.0002	0.0008	0.0139	0		0.0001	
$-h_\theta$		0.0145	0.0144					0.0218	0.0219	0.0221			0.0018	
$-h_\beta$		0.0146	0.0146	0.0146				0.0104	0.0104	0.0104		0.0080	0.0080	0.0080
$\ell_{\dot{z}}$	1.685	1.638	1.595	1.515	1.47	1.20		1.062	1.053	1.024		0.877	0.872	0.855
$\ell_{\dot{\theta}}$	1.343	1.308	1.317	1.335	1.26	1.21		1.135	1.134	1.134		0.97	0.967	0.966
$\ell_{\dot{\beta}}$		0.004	0.004	0.004				0.006	0.006	0.006		0.006	0.006	0.006
$-m_{\dot{z}}$	2.064	1.954	1.897	1.790	1.79	1.46		1.288	1.271	1.245		1.116	1.109	1.083
$-m_{\dot{\theta}}$	1.876	1.798	1.813	1.842	1.83	1.65		1.576	1.575	1.575		1.376	1.371	1.368
$-m_{\dot{\beta}}$		0.001	0.001	0.001				0.001	0.001	0.001		0.001	0.001	0.001
$-h_{\dot{z}}$		0.0144	0.0136					0.0266	0.0211			0.0019	0.0019	0.0020
$-h_{\dot{\theta}}$		0.0134	0.0136					0.0172	0.0171	0.0170			0.0093	
$-h_{\dot{\beta}}$		0.0007	0.0007	0.0007				0.0010	0.0010	0.0010		0.0009	0.0009	0.0009

*The $\nu = 0$ values are from Ref. 17 (Orlik-Rückemann *et al*); the remainder are from Ref. 7 (Barnes).

TABLE 18

Supersonic Theoretical Derivatives.

Wing B, Symmetric, Sonic/Supersonic Leading Edge. Axis at Apex ($g = 0$).

M	2.0				2.46			2.69		
ν	0*	0.1	0.25	0.5	0.1	0.25	0.5	0.1	0.25	0.5
ℓ_z	0	0.002	0.011	0.038	0.001	0.007	0.025	0.001	0.003	0.011
ℓ_θ	1.123	1.080	1.080	1.079	0.893	0.894	0.899	0.738	0.739	0.741
ℓ_β		0.101	0.101	0.101	0.077	0.077	0.077	0.068	0.068	0.068
$-m_z$	0	0.002	0.013	0.102	0.002	0.010	0.058	0.001	0.004	0.050
$-m_\theta$	1.376	1.280	1.279	1.277	1.124	1.127	1.134	0.899	0.900	0.902
$-m_\beta$		0.016	0.016	0.016	0.013	0.013	0.013	0.011	0.011	0.011
$-h_z$		0	0	0.0065			0.0043	0.0001	0.0005	0.0019
$-h_\theta$		0.0049	0.0049	0.0048				0.0166	0.0165	0.0168
$-h_\beta$		0.0088	0.0088	0.0087	0.0081	0.0081	0.0081	0.0071	0.0071	0.0071
$\ell_{\dot{z}}$	1.123	1.078	1.069	1.040	0.892	0.887	0.872	0.738	0.736	0.728
$\ell_{\dot{\theta}}$	1.187	1.143	1.143	1.143	1.004	1.003	1.001	0.872	0.872	0.871
$\ell_{\dot{\beta}}$		0.006	0.006	0.006	0.006	0.006	0.006	0.005	0.005	0.005
$-m_{\dot{z}}$	1.376	1.278	1.265	1.246	1.122	1.153	1.102	0.899	0.895	0.884
$-m_{\dot{\theta}}$	1.654	1.564	1.564	1.563	1.415	1.414	1.410	1.212	1.211	1.211
$-m_{\dot{\beta}}$		0.001	0.001	0.001	0.001	0.001	0.001	0.001	0.001	0.001
$-h_{\dot{z}}$		0.0049	0.0048	0.2640					0.0162	0.0034
$-h_{\dot{\theta}}$		0.0104	0.0104	0.0104	0.0100	0.0101	0.0102	0.0150	0.0150	0.0149
$-h_{\dot{\beta}}$		0.0009	0.0009	0.0009	0.0009	0.0009	0.0009	0.0009	0.0009	0.0009

*The $\nu = 0$ values are from Ref. 17 (Orlik-Rückemann *et al*); the remainder are from Ref. 7 (Barnes).

TABLE 19

Supersonic Theoretical Derivatives

Wing D, Symmetric, Sonic/Supersonic Leading Edge, Axis at Apex ($g = 0$)

M	1.53				1.67	1.95	2.0				2.53			
ν	0*	0.1	0.25	0.5	0*	0*	0*	0.1	0.25	0.5	0*	0.1	0.25	0.5
ℓ_z	0	0.008	0.045		0	0		0.003	0.017	0.060		0.001	0.007	0.028
ℓ_θ	1.671	1.686	1.687	1.687	1.49	1.24		1.132	1.132	1.132		0.852	0.856	0.858
ℓ_β		0.144	0.144	0.144				0.092	0.092	0.092		0.068	0.068	0.068
$-m_z$	0	0.010	0.069		0	0		0.004	0.025	0.139		0.002	0.011	0.082
$-m_\theta$	2.048	2.052	2.057	2.060	1.82	1.50		1.430	1.430	1.428		1.076	1.082	1.084
$-m_\beta$		0.039	0.038	0.038				0.025	0.025	0.025		0.018	0.018	0.018
$-h_z$		0.0001	0.0047					0.0001	0.0009	0.0227			0.0001	
$-h_\theta$		0.0131	0.0130					0.0209	0.0210	0.0210			0.0006	
$-h_\beta$		0.0113	0.0112	0.0112				0.0085	0.0085	0.0085		0.0063	0.0063	0.0063
$\ell_z^\bullet$	1.671	1.690	1.644	1.571	1.49	1.24		1.129	1.117	1.076		0.854	0.849	0.834
$\ell_\theta^\bullet$	1.309	1.322	1.331	1.346	1.20	1.16		1.109	1.108	1.106		0.93	0.930	0.93
$\ell_\beta^\bullet$		0.002	0.002	0.002				0.005	0.005	0.005		0.005	0.005	0.005
$-m_z^\bullet$	2.048	2.062	2.056	2.039	1.82	1.50		1.427	1.407	1.380		1.079	1.072	1.050
$-m_\theta^\bullet$	1.832	1.846	1.859	1.880	1.70	1.51		1.543	1.542	1.539		1.316	1.315	1.312
$-m_\beta^\bullet$		+0	+0	+0				0.001	0.001	0.001		0.001	0.001	0.001
$-h_z^\bullet$		0.0130						0.0208	0.2017	0.5471		0.0002	0.0002	0.0002
$-h_\theta^\bullet$		0.0173	0.0174					0.0161	0.0161	0.0160			0.0053	
$-h_\beta^\bullet$		0.0004	0.0004	0.0004				0.0006	0.0006	0.0006		0.0006	0.0006	0.0006

*The $\nu = 0$ values are from Ref. 17 (Orlik-Rückemann *et al*); the remainder are from Ref. 7 (Barnes).

TABLE 20

Supersonic Theoretical Derivatives

Wing E, Symmetric, Sonic/Supersonic Leading Edge, Axis at Apex ($g = 0$)

M	2.0				2.46			2.69		
ν	0*	0.1	0.25	0.5	0.1	0.25	0.5	0.1	0.25	0.5
ℓ_z	0	0.002	0.012	0.042	0.001	0.006	0.021		0.004	0.015
ℓ_θ	1.114	1.101	1.101	1.101	0.820	0.820	0.818	0.748	0.746	0.744
ℓ_β		0.086	0.086	0.086	0.065	0.065	0.065	0.056	0.056	0.056
$-m_z$	0	0.003	0.016	0.125	0.001	0.009	0.069		0.006	0.049
$-m_\theta$	1.366	1.344	1.344	1.343	1.004	1.003	0.998	0.925	0.924	0.924
$-m_\beta$		0.023	0.023	0.023	0.018	0.018	0.018	0.015	0.015	0.015
$-h_z$				0.0207			0.0052			
$-h_\theta$		0.0060	0.0060	0.0059						
$-h_\beta$		0.0062	0.0062	0.0062	0.0053	0.0053	0.0053	0.0046	0.0046	0.0046
$\ell_{\dot{z}}$	1.114	1.099	1.089	1.057	0.819	0.815	0.800	0.748	0.746	0.736
$\ell_{\dot{\theta}}$	1.157	1.168	1.167	1.165	0.909	0.909	0.909	0.86	0.86	0.858
$\ell_{\dot{\beta}}$		0.005	0.005	0.005	0.004	0.004	0.004	0.004	0.004	0.004
$-m_{\dot{z}}$	1.366	1.341	1.326	1.299	1.003	0.996	0.993	0.925	0.920	0.910
$-m_{\dot{\theta}}$	1.616	1.639	1.638	1.633	1.249	1.249	1.249	1.192	1.192	1.192
$-m_{\dot{\beta}}$		0.001	0.001	0.001	0.001	0.001	0.001	0.001	0.001	0.001
$-h_{\dot{z}}$		0.0060	0.0059							
$-h_{\dot{\theta}}$		0.0157	0.0157	0.0156	0.0050	0.0051	0.0053			
$-h_{\dot{\beta}}$		0.0006	0.0006	0.0006	0.0005	0.0005	0.0005	0.0005	0.0005	0.0005

*The $\nu = 0$ values are from Ref. 17 (Orlik-Rückemann *et al*); the remainder are from Ref. 7 (Barnes).

TABLE 21

Supersonic Theoretical Derivatives

Wing G (A = 3 Version), Symmetric, Axis at Apex (g = 0)

M	1.031	1.100	1.202	1.25				1.414	1.875				2.5			
ν	0*	0*	0*	0*	0.1	0.25	0.5	0*	0*	0.1	0.25	0.5	0*	0.1	0.25	0.5
ℓ_z	0	0	0	0	0.015	0.082		0	0	0.002	0.013	0.048		0.001	0.005	0.019
ℓ_θ	2.780	2.788	2.377	2.205	2.049	1.976		1.773	1.184	1.141	1.139	1.129		0.806	0.806	0.804
ℓ_β					0.270	0.269	0.266			0.122	0.122	0.122		0.083	0.083	0.083
$-m_z$	0	0	0	0	0.010	0.085		0	0	0.002	0.010	0.063		0.001	0.004	0.015
$-m_\theta$	0.986	1.569	1.502	1.420	1.188	1.127		1.174	0.800	0.766	0.763	0.754		0.557	0.556	0.555
$-m_\beta$					0.021	0.021	0.020			0.009	0.009	0.009		0.007	0.007	0.007
$-h_z$	0	0	0	0				0	0	0.0001	0.0054	0.0122	0	0.0000	0.0000	0.0000
$-h_\theta$										0.0262	0.0261	0.0258		0.0052	0.0052	0.0052
$-h_\beta$					0.0235	0.0234	0.0232			0.0125	0.0125	0.0125		0.0009	0.0009	0.0009
$\ell_{\dot{z}}$	2.780	2.788	2.377	2.205	2.041	1.929		1.773	1.184	1.156	1.148	1.105		0.806	0.803	0.794
$\ell_{\dot{\theta}}$	-3.838	-2.483	-0.529	-0.118				0.455	0.612	0.572	0.574	0.579		0.482	0.482	0.483
$\ell_{\dot{\beta}}$					-0.031	-0.030	-0.030			0.007	0.007	0.007		0.006	0.006	0.006
$-m_{\dot{z}}$	0.986	1.569	1.502	1.420	1.182			1.174	0.800	0.776	0.768			0.557	0.554	
$-m_{\dot{\theta}}$	1.252	-1.565	-0.403	-0.095				0.365	0.501	0.483	0.484	0.489		0.402	0.402	0.403
$-m_{\dot{\beta}}$					-0.005	-0.005	-0.005			0.001	0.001	0.001		0.001	0.001	0.001
$-h_{\dot{z}}$										0.0262	0.0173	0.0241		0.0052	0.0052	0.0051
$-h_{\dot{\theta}}$					0.0201	0.0207				0.0074	0.0074	0.0076		0.0069	0.0069	0.0069
$-h_{\dot{\beta}}$					-0.0021	-0.0021	-0.0020			0.0011	0.0011	0.0011		0.0010	0.0010	0.0010

*The $\nu = 0$ values are from Ref. 12 (Lehrian); the remainder from Ref. 7 (Barnes).

TABLE 22

Supersonic Theoretical Derivatives

Wing G (A = 4 Version) Symmetric Axis at Apex (g = 0)

M	1.017	1.057	1.118	1.250	1.505	1.803	2.125	2.462
ν	0	0	0	0	0	0	0	0
ℓ_z	0	0	0	0	0	0	0	0
ℓ_θ	3.707	3.718	3.169	2.363	1.661	1.273	1.030	0.864
$-m_z$	0	0	0	0	0	0	0	0
$-m_\theta$	1.315	2.093	2.003	1.566	1.121	0.865	0.703	0.590
$\ell_z^\bullet$	3.707	3.718	3.169	2.363	1.661	1.273	1.030	0.864
$\ell_\theta^\bullet$	-13.959	-8.957	-3.359	-0.323	0.528	0.612	0.573	0.517
$-m_z^\bullet$	1.315	2.093	2.003	1.566	1.121	0.865	0.703	0.590
$-m_\theta^\bullet$	-0.970	-6.292	-2.717	-0.302	0.418	0.497	0.469	0.423

All these values are from Ref. 11 (Lehrian).

TABLE 23

Subsonic Theoretical Derivatives

Wing A, Antisymmetric, Axis at Apex ($g = 0$)

M	0				0.745				0.909				0.968			
ν	0*	0.1	0.25	0.5	0*	0.1	0.25	0.5	0*	0.1	0.25	0.5	0*	0.1	0.25	0.5
r_ψ	0	-0.001	-0.004	-0.015	0	-0.001	-0.004	-0.016	0	-0.001	-0.005	-0.017		-0.001	-0.005	-0.013
r_β	0.190	0.191	0.191	0.189	0.227	0.231	0.231	0.232	0.264	0.271	0.273	0.279		0.305	0.312	0.308
$-h_\psi$	0	-0.0000	-0.0001	-0.0004	0	-0.0000	-0.0002	-0.0006	0	-0.0000	-0.0003	-0.0012		-0.0001	-0.0005	-0.0021
$-h_\beta$		0.0054	0.0054	0.0053		0.0073	0.0073	0.0074		0.0097	0.0098	0.0104		0.0121	0.0129	0.0169
r^*_ψ	0.229	0.234	0.234	0.232	0.255	0.262	0.262	0.263	0.275	0.283	0.285	0.294		0.296	0.302	0.319
r^*_β	0.031	0.029	0.029	0.030	0.017	0.014	0.015	0.015	-0.006	-0.011	-0.015	-0.027		-0.041	-0.062	-0.124
$-h^*_\psi$		0.0015	0.0015	0.0015		0.0017	0.0017	0.0017		0.0018	0.0018	0.0019		0.0020	0.0021	0.0032
$-h^*_\beta$		0.0025	0.0025	0.0026		0.0045	0.0045	0.0045		0.0083	0.0084	0.0085		0.0150	0.0154	0.0120

*The $\nu = 0$ values are from Ref. 6 (Hornsby); the remainder from Ref. 8 (Woodcock).

TABLE 24

Subsonic Theoretical Derivatives.

Wing B, Antisymmetric, Axis at Apex ($g = 0$)

M	0				0.781				0.927			
ν	0*	0.1	0.25	0.5	0*	0.1	0.25	0.5	0*	0.1	0.25	0.5
r_ψ	0	-0.001	-0.004	-0.014	0	-0.001	-0.004	-0.017		-0.001	-0.005	-0.019
r_β	0.152	0.151	0.151	0.150	0.176	0.176	0.177	0.178		0.197	0.199	0.204
$-h_\psi$	0	-0.0000	-0.0001	-0.0004	0	-0.0000	-0.0001	-0.0006		-0.0000	-0.0002	-0.0009
$-h_\beta$		0.0048	0.0048	0.0048		0.0064	0.0064	0.0064		0.0079	0.0079	0.0082
$r^\bullet_\psi$	0.170	0.170	0.170	0.170	0.183	0.183	0.183	0.184		0.191	0.192	0.195
$r^\bullet_\beta$	0.034	0.034	0.034	0.034	0.031	0.031	0.031	0.031		0.028	0.027	0.024
$-h^\bullet_\psi$		0.0011	0.0011	0.0011		0.0012	0.0012	0.0012		0.0013	0.0013	0.0013
$-h^\bullet_\beta$		0.0027	0.0027	0.0027		0.0044	0.0044	0.0044		0.0070	0.0071	0.0072

*The $\nu = 0$ values are from Ref. 6 (Hornsby); the remainder from Ref. 8 (Woodcock)

TABLE 25

Subsonic Theoretical Derivatives

Wing C, Antisymmetric, Axis at Apex ($g = 0$)

M	0				0.8			
ν	0*	0.1	0.25	0.5	0*	0.1	0.25	0.5
r_ψ	0	-0.000	-0.003	-0.012		-0.001	-0.003	-0.013
r_β	0.110	0.110	0.110	0.110		0.123	0.123	0.124
$-h_\psi$	0	-0.0000	-0.0001	-0.0003		-0.0000	-0.0001	-0.0004
$-h_\beta$		0.0040	0.0040	0.0039		0.0049	0.0049	0.0049
$r^\bullet_\psi$	0.114	0.114	0.114	0.114		0.119	0.119	0.120
$r^\bullet_\beta$	0.030	0.030	0.030	0.030		0.032	0.032	0.032
$-h^\bullet_\psi$		0.0007	0.0007	0.0007		0.0008	0.0008	0.0008
$-h^\bullet_\beta$		0.0024	0.0024	0.0024		0.0036	0.0036	0.0036

*The $\nu = 0$ values are from Ref. 6 (Hornsby); the remainder from Ref. 8 (Woodcock).

TABLE 26

Subsonic Theoretical Derivatives

Wings D, E, F, Antisymmetric, Axis at Apex ($g = 0$)

Wing	D			E		F
M	0	0.745	0.909	0	0.781	0
ν	0	0	0	0	0	0
r_{ψ}	0	0	0	0	0	0
r_{β}	0.186	0.217	0.245	0.144	0.163	0.102
$r^{\bullet}_{\psi}$	0.243	0.265	0.280	0.176	0.186	0.117
$r^{\bullet}_{\beta}$	0.034	0.019	-0.007	0.034	0.028	0.028

All these values are from Ref. 6 (Hornsby).

TABLE 27

Tunnel Details

Tunnel	N.A.E. 16 in. × 30 in. (Ottawa)	H.S.D. 20 in. × 22 in. (Coventry)*
Type	Intermittent suction (run duration about 15 sec)	10 000 hp continuous
Working section (breadth × height)	Not available	20 in. × 22 in. (transonic) reducing to $14\frac{1}{2}$ in. × 16 in. ($M = 2{\cdot}96$)
Mach numbers	$0{\cdot}5 \rightarrow 1{\cdot}1$ (slotted liner); discrete values $1{\cdot}2 \rightarrow 2{\cdot}0$ (fixed liner)	$0{\cdot}3 \rightarrow 1{\cdot}3$ (slotted liners); discrete values $1{\cdot}4 \rightarrow 2{\cdot}96$ (fixed liners)
Stagnation pressure	1 atmosphere approx.	$0{\cdot}25 \rightarrow 2{\cdot}8$ atmospheres
Reynolds number/ft	$2{\cdot}6 \rightarrow 4{\cdot}6 \times 10^6$	$2{\cdot}5 \rightarrow 8{\cdot}0 \times 10^6$ (for test conditions)
Model mounting	Half-model side wall with reflection plate $\frac{1}{2}$ in. away from the wall	Half-model from support disc forming part of tunnel side wall

**See* Ref. 45 for further details.

TABLE 28

Model Details

All the wing models have biconvex chordwise sections of 5 per cent thickness – chord ratio.

Tests	*N.A.E. and W.R.E.*	*H.S.D.*
Root chord		
Wing A	9·55 in.	12 in.
Wing B	10·93 in.	12 in.
Wing C	12·82 in.	12 in.
Wing D	8·56 in.	12 in.
Wing E	9·77 in.	12 in.
Wing F	11·41 in.	12 in.
Wing G (A = 3 version)	—	11 in.
Wing G (A = 4 version)	6·82 in.	—
Semi-span		
Wing A	7·71 in.	9·65 in.
Wing B	5·89 in.	6·43 in.
Wing C	4·30 in.	4·03 in.
Wing D	7·99 in.	11·14 in.
Wing E	6·09 in.	7·43 in.
Wing F	4·42 in.	4·64 in.
Wing G (A = 3 version)	—	12·00 in.
Wing G (A = 4 version)	9·91 in.	—
Material	Solid dural	Not recorded
Boundary-layer transition forcing strips	0·008 in. grain size Kyanite sand in 0·30 in. wide strip at 10 per cent chord approx.	Carborundum grit 0·25 in. wide at 10 per cent chord approx. roughness height 0·006 → 0·008 in.

TABLE 29

Wing A, $M \approx 1{\cdot}2$, Axis at Apex ($g = 0$)

	Experimental						Theoretical M = 1.20			
	Baines & Rockliff M = 1.2	Orlik-Rückemann & Laberge M = 1.22	Hall & Osborne M = 1.20				Harris		Harris* (Jones & Cohen)	Orlik-Rückemann & Laberge
ν	0	0	0	0.042	0.056	0.069	0	0.1	0	0
ℓ_z				-0.01	-0.02	-0.01		0.02		
ℓ_θ	1.4	1.86	1.75	1.71	1.68	1.67	2.08	2.07	2.05	2.09
$-m_z$				-0.02	-0.04	0.01		0.02		
$-m_\theta$	1.4	2.30	2.07	2.08	2.01	2.05	2.51	2.49	2.49	2.55
$\ell_{\dot{z}}$				1.98	1.74	1.68		2.05		
$\ell_{\dot{\theta}}$	0.5	1.28		1.88	1.09	0.74		1.45		1.38
$-m_{\dot{z}}$				1.82	2.17	2.19		2.46		
$-m_{\dot{\theta}}$	2.1	1.73		1.46	1.42	1.31		2.08		1.93

*These are values given by Harris in Ref. 10 which he obtained by the method of Ref. 29.

TABLE 30

Wing A, $M = 1{\cdot}5 \rightarrow 1{\cdot}6$, Axis at Apex ($g = 0$).

	Experimental						Theoretical M = 1.53	
	Baines & Rockliff M = 1.5	Orlik-Rückemann & Laberge M = 1.56	Hall & Osborne M = 1.56				Barnes	Orlik-Rückemann & Laberge
ν	0	0	0	0.034	0.046	0.057	0.1	0
ℓ_z				-0.01	-0.03	-0.01	0.03	
ℓ_θ	1.7	1.45	1.51	1.34	1.31	1.33	1.65	1.69
$-m_z$				0.02	-0.06	0.04	0.01	
$-m_\theta$	1.4	1.77	1.65	1.68	1.56	1.66	1.97	2.06
$\ell_{\dot{z}}$				1.63	1.65	1.62	1.64	
$\ell_{\dot{\theta}}$	0.6	1.25		1.42	1.52		1.31	1.34
$-m_{\dot{z}}$				1.83	1.93	1.91	1.95	
$-m_{\dot{\theta}}$	1.7	1.68		1.92	1.87	1.82	1.80	1.88

TABLE 31

Wing A, $M = 1{\cdot}9 \rightarrow 2{\cdot}0$, Axis at Apex ($g = 0$)

	Experimental						Theoretical	
	Baines & Rockliff M = 2.0	Orlik-Rückemann & Laberge M = 2.0	Hall & Osborne M = 1.90				Barnes M = 2.0	Orlik-Rückemann & Laberge M = 1.95
ν	0	0	0	0.030	0.041	0.051	0.1	0
ℓ_z				-0.05	-0.08	-0.07	0.01	
ℓ_θ	1.1	1.29	1.16	1.09	1.03	1.07	1.06	1.20
$-m_z$				-0.05	-0.08	-0.18	0.00	
$-m_\theta$	1.1	1.56	1.41	1.33	1.29	1.13	1.29	1.46
$\ell_{\dot{z}}$				1.28			1.06	
$\ell_{\dot{\theta}}$	0.4	1.32		0.98			1.13	1.21
$-m_{\dot{z}}$				1.63			1.29	
$-m_{\dot{\theta}}$	1.3	1.78		1.67			1.58	1.65

TABLE 32

Wing B, M = 1·2 → 1·25, Axis at Apex (g = 0)

	Experimental						Theoretical M = 1.25			
	Baines & Rockliff M = 1.2	Orlik-Rückemann & Laberge M = 1.22	Hall & Osborne M = 1.20				Harris		Harris (Jones & Cohen)	Orlik-Rückemann & Laberge
ν	0	0	0	0.042	0.056	0.069	0	0.1	0	0
ℓ_z				-0.02	-0.03	-0.08		0.00		
ℓ_θ	2.4	1.24	1.33	1.29	1.29	1.18	1.49	1.49	1.47	1.49
$-m_z$				-0.06	-0.11	-0.16		0.00		
$-m_\theta$	1.5	1.54	1.27	1.55	1.50	1.38	1.78	1.78	1.78	1.82
$\ell_{\dot{z}}$				1.49	1.46	1.22		1.48		
$\ell_{\dot{\theta}}$	1.2	1.83		1.95	1.77	1.31		1.92		1.86
$-m_{\dot{z}}$				1.78	1.80	1.04		1.77		
$-m_{\dot{\theta}}$	2.0	2.52		2.18	2.14	0.98		2.68		2.58

TABLE 33

Wing B, M = 1·55 → 1·6, Axis at Apex (g = 0)

	Experimental						Theoretical M = 1.60			
	Baines & Rockliff M = 1.5	Orlik-Rückemann & Laberge M = 1.56	Hall & Osborne M = 1.56				Harris		Harris (Jones & Cohen)	Orlik-Rückemann & Laberge
ν	0	0	0	0.034	0.046	0.057	0	0.1	0	0
ℓ_z				-0.03	-0.05	-0.05		0.00		
ℓ_θ	1.9	0.99	1.14	1.10	1.05	1.03	1.29	1.29	1.26	1.29
$-m_z$				-0.03	-0.11	-0.08		0.00		
$-m_\theta$	1.3	1.20	1.40	1.36	1.24	1.24	1.56	1.56	1.54	1.58
$\ell_{\dot{z}}$				1.19	1.19			1.29		
$\ell_{\dot{\theta}}$	1.0	1.32		1.31	1.38			1.50		1.49
$-m_{\dot{z}}$				1.38	1.63			1.55		
$-m_{\dot{\theta}}$	1.7	1.81		1.73	2.02			2.10		2.08

TABLE 34

Wing B, $M = 1{\cdot}9 \rightarrow 2{\cdot}0$, Axis at Apex ($g = 0$).

	Experimental						Theoretical M = 2.0	
	Baines & Rockliff M = 2.0	Orlik-Rückemann & Laberge M = 2.00	Hall & Osborne M = 1.90				Barnes	Orlik-Rückemann & Laberge
ν	0	0	0	0.030	0.041	0.051	0.1	0
ℓ_z				-0.03	-0.03	-0.01	0.00	
ℓ_θ	1.7	0.89	0.97	0.90	0.89	0.91	1.08	1.12
$-m_z$				-0.04	-0.05		0.00	
$-m_\theta$	1.1	1.05	1.17	1.09	1.07		1.28	1.38
$\ell_z^\bullet$				1.08	1.07		1.08	
$\ell_\theta^\bullet$	0.5	1.14		1.21	1.27		1.14	1.19
$-m_z^\bullet$				1.43	1.25		1.28	
$-m_\theta^\bullet$	1.2	1.52		1.73	1.53		1.56	1.65

TABLE 35

Wing C, $M = 1{\cdot}2 \rightarrow 1{\cdot}3$, Axis at Apex ($g = 0$)

	Experimental						Theoretical M = 1.28			
	Baines & Rockliff M = 1.2	Orlik-Rückemann & Laberge M = 1.22	Hall & Osborne M = 1.2				Harris		Harris (Jones & Cohen)	Orlik-Rückemann & Laberge
ν	0	0	0	0.042	0.056	0.069	0	0.1	0	0
ℓ_z				-0.04	-0.03	-0.06		0.00		
ℓ_θ	-1.1	1.03	0.97	0.89	0.89	0.85	0.99	0.98	0.99	1.00
$-m_z$				-0.07	-0.02	-0.09		0.00		
$-m_\theta$	0.1	1.31	1.17	1.09	1.12	1.00	1.18	1.18	1.19	1.21
$\ell_{\dot{z}}$				-1.34	1.34	1.44		0.98		
$\ell_{\dot{\theta}}$	0.5	1.58		2.09	2.00	2.06		1.78		1.74
$-m_{\dot{z}}$				1.22	1.72	1.88		1.18		
$-m_{\dot{\theta}}$	1.3	2.18		1.76	2.31	2.65		2.47		2.41

TABLE 36

Wing C, M = 1·56, Axis at Apex (g = 0).

	Experimental						Theoretical M = 1.56			
	Baines & Rockliff M = 1.5	Orlik-Rückemann & Laberge M = 1.56	Hall & Osborne M = 1.56				Harris		Harris (Jones & Cohen)	Orlik-Rückemann & Laberge
ν	0	0	0	0.034	0.046	0.057	0	0.1	0	0
ℓ_z				-0.05	-0.08	-0.01		0.00		
ℓ_θ	-1.1	0.83	0.83	0.78	0.72	0.83	0.93	0.93	0.92	0.93
$-m_z$				-0.02	-0.02	0.06		0.00		
$-m_\theta$	0.1	1.05	1.04	1.04	1.01	1.17	1.11	1.11	1.12	1.14
$\ell_{\dot{z}}$				0.78	0.91			0.93		
$\ell_{\dot{\theta}}$	1.0	1.25		1.05	1.17			1.53		1.50
$-m_{\dot{z}}$				1.14	1.26			1.11		
$-m_{\dot{\theta}}$	1.5	1.74		1.94	1.89			2.12		2.08

TABLE 37

Wing C, M = 1·89 → 2·0, Axis at Apex (g = 0)

	Experimental						Theoretical M = 1.89			
	Baines & Rockliff M = 2.0	Orlik-Rückemann & Laberge M = 2.00	Hall & Osborne M = 1.90				Harris		Harris (Jones & Cohen)	Orlik-Rückemann & Laberge
ν	0	0	0	0.030	0.041	0.051	0	0.1	0	0
ℓ_z				-0.01	0.01	-0.01		0.00		
ℓ_θ	-1.0	0.73	0.73	0.72	0.76	0.76	0.87	0.87	0.85	0.87
$-m_z$				-0.03	-0.01	-0.04		0.00		
$-m_\theta$	0.0	0.91	0.88	0.88	0.91	0.87	1.04	1.05	1.03	1.06
$\ell_{\dot{z}}$				0.82	0.84	0.82		0.87		
$\ell_{\dot{\theta}}$	1.1	1.13		1.14	1.15			1.29		1.28
$-m_{\dot{z}}$				1.06	0.79			1.04		
$-m_{\dot{\theta}}$	1.4	1.56		1.59	1.28			1.80		1.78

TABLE 38

Wing D, $M \approx 1{\cdot}2$, Axis at Apex ($g = 0$)

	Experimental						Theoretical M = 1.20			
	Baines & Rockliff M = 1.2	Orlik-Rückemann & Laberge M = 1.22	Hall & Osborne M = 1.20				Harris		Harris (Jones & Cohen)	Orlik-Rückemann & Laberge
ν	0	0	0	0.052	0.069	0.087	0	0.1	0	0
ℓ_z				-0.07	-0.04	0.00		0.02		
ℓ_θ	1.0	1.77	1.75	1.67	1.70	1.76	2.06	2.05	2.05	2.05
$-m_z$				-0.07	-0.02	0.12		0.02		
$-m_\theta$	1.3	2.23	2.13	2.06	2.10	2.28	2.47	2.45	2.49	2.49
$\ell_{\dot{z}}$				2.46	2.26	2.15		2.03		
$\ell_{\dot{\theta}}$	1.3	1.15		2.38	1.68	1.36		1.36		1.35
$-m_{\dot{z}}$				3.30	3.00	3.01		2.42		
$-m_{\dot{\theta}}$	2.1	1.46		3.36	2.49	2.21		1.96		1.89

TABLE 39

Wing D, $M = 1{\cdot}5 \rightarrow 1{\cdot}6$, Axis at Apex ($g = 0$).

	Experimental						Theoretical M = 1.53	
	Baines & Rockliff M = 1.5	Orlik-Rückemann & Laberge M = 1.56	Hall & Osborne M = 1.56				Barnes	Orlik-Rückemann & Laberge
ν	0	0	0	0.040	0.053	0.066	0.1	0
ℓ_z				-0.04	-0.01	-0.06	0.01	
ℓ_θ	1.7	1.37	1.36	1.31	1.33	1.31	1.69	1.67
$-m_z$				0.03	-0.03		0.01	
$-m_\theta$	1.5	1.68	1.63	1.69			2.05	2.05
$\ell_{\dot{z}}$				1.60	1.63	1.78	1.69	
$\ell_{\dot{\theta}}$	0.6	0.99		1.30	1.36	1.41	1.32	1.31
$-m_{\dot{z}}$				1.79	1.89	1.89	2.06	
$-m_{\dot{\theta}}$	1.5	1.41		1.60	1.72	1.62	1.85	1.83

TABLE 40

Wing D, $M = 1{\cdot}9 \rightarrow 2{\cdot}0$, Axis at Apex ($g = 0$)

	Experimental						Theoretical	
	Baines & Rockliff M = 2.0	Orlik-Rückemann & Laberge M = 2.00	Hall & Osborne M = 1.90				Barnes M = 2.0	Orlik-Rückemann & Laberge M = 1.95
ν	0	0	0	0.035	0.047	0.059	0.1	0
ℓ_z				-0.02	-0.01	0.00	0.00	
ℓ_θ	1.4	1.23	1.15	1.08	1.09	1.11	1.13	1.24
$-m_z$				0.01	0.03	0.09	0.00	
$-m_\theta$	1.3	1.52	1.41	1.35	1.37	1.45	1.43	1.50
$\ell_{\dot{z}}$				1.07	1.24	1.11	1.13	
$\ell_{\dot{\theta}}$	-0.3	1.04		1.00	1.20	1.00	1.11	1.16
$-m_{\dot{z}}$				1.17	1.46	1.24	1.43	
$-m_{\dot{\theta}}$	1.5	1.45		1.31	1.41	1.17	1.54	1.51

TABLE 41

Wing E, $M = 1{\cdot}2 \rightarrow 1{\cdot}25$ Axis at Apex ($g = 0$)

	Experimental						Theoretical M = 1.25			
	Baines & Rockliff M = 1.2	Orlik-Rückemann & Laberge M = 1.22	Hall & Osborne M = 1.20				Harris		Harris (Jones & Cohen)	Orlik-Rückemann & Laberge
ν	0	0	0	0.052	0.069	0.087	0	0.1	0	0
ℓ_z				-0.04	-0.02	0.00		0.00		
ℓ_θ	3.6	1.27	1.34	1.27	1.27	1.29	1.46	1.46	1.46	1.46
$-m_z$				-0.05	-0.02	0.05		0.00		
$-m_\theta$	1.9	1.60	1.36	1.54	1.56	1.64	1.72	1.72	1.76	1.76
$\ell_{\dot{z}}$				1.72	1.49	1.55		1.45		
$\ell_{\dot{\theta}}$	1.4	1.57		2.07	1.70	1.56		1.84		1.80
$-m_{\dot{z}}$				1.98	1.91	2.02		1.71		
$-m_{\dot{\theta}}$	1.9	2.24		2.62	2.27	2.11		2.57		2.49

TABLE 42

Wing E, M = 1·55 → 1·6, Axis at Apex (g = 0)

	Experimental						Theoretical M = 1.60			
	Baines & Rockliff M = 1.5	Orlik-Rückemann & Laberge M = 1.56	Hall & Osborne M = 1.56				Harris		Harris (Jones & Cohen)	Orlik-Rückemann & Laberge
ν	0	0	0	0.040	0.053	0.066	0	0.1	0	0
ℓ_z				-0.01	0.01	0.05		0.00		
ℓ_θ	3.9	1.10	1.14	1.13	1.14	1.20	1.28	1.28	1.27	1.27
$-m_z$				-0.03	0.05	0.00		0.00		
$-m_\theta$	2.0	1.37	1.42	1.38	1.45	1.38	1.54	1.54	1.55	1.55
$\ell_{\dot{z}}$				1.32	1.36	1.29		1.28		
$\ell_{\dot{\theta}}$	0.4	1.28		1.36	1.46			1.46		1.45
$-m_{\dot{z}}$				1.40	1.60			1.54		
$-m_{\dot{\theta}}$	1.4	1.78		1.69	2.03			2.04		2.02

TABLE 43

Wing E, $M = 1{\cdot}9 \rightarrow 2{\cdot}0$, Axis at Apex ($g = 0$).

	Experimental						Theoretical M = 2.0	
	Baines & Rockliff M = 2.0	Orlik-Rückemann & Laberge M = 2.00	Hall & Osborne M = 1.90				Barnes	Orlik-Rückemann & Laberge
ν	0	0	0	0.035	0.047	0.059	0.1	0
ℓ_z				-0.03	-0.02	-0.04	0.00	
ℓ_θ	3.5	1.03	1.00	0.91	0.93	0.91	1.10	1.11
$-m_z$				-0.03	-0.01	-0.01	0.00	
$-m_\theta$	1.7	1.27	1.24	1.13	1.15	1.14	1.34	1.37
$\ell_{\dot{z}}$				1.01	0.96		1.10	
$\ell_{\dot{\theta}}$	0.4	1.22		1.14	1.08		1.17	1.16
$-m_{\dot{z}}$				1.14	0.95	1.12	1.34	
$-m_{\dot{\theta}}$	1.0	1.66		1.45	1.10	1.60	1.64	1.62

TABLE 44

Wing F, $M = 1{\cdot}2 \rightarrow 1{\cdot}3$, Axis at Apex ($g = 0$)

	Experimental						Theoretical M = 1.28			
	Baines & Rockliff M = 1.2	Orlik-Rückemann & Laberge M = 1.22	Hall & Osborne M = 1.20				Harris		Harris (Jones & Cohen)	Orlik-Rückemann & Laberge
ν	0	0	0	0.052	0.069	0.087	0	0.1	0	0
ℓ_z				-0.03	0.01	0.02		0.00		
ℓ_θ	-0.8	0.97	0.94	0.87	0.92	0.93	0.95	0.95	0.96	0.96
$-m_z$				-0.04	0.03	0.00		0.00		
$-m_\theta$	0.2	1.18	1.10	1.03	1.12	1.09	1.11	1.11	1.15	1.16
$\ell_{\dot{z}}$				1.16	1.13	1.01		0.95		
$\ell_{\dot{\theta}}$	-0.2	1.47		1.73	1.65	1.43		1.71		1.67
$-m_{\dot{z}}$				1.21	0.75	1.63		1.11		
$-m_{\dot{\theta}}$	1.1	2.03		1.84	1.33	2.41		2.34		2.30

TABLE 45

Wing F, M = 1·56, Axis at Apex (g = 0).

	Experimental						Theoretical M = 1.56			
	Baines & Rockliff M = 1.5	Orlik-Rückemann & Laberge M = 1.56	Hall & Osborne M = 1.56				Harris		Harris (Jones & Cohen)	Orlik-Rückemann & Laberge
ν	0	0	0	0.040	0.053	0.066	0	0.1	0	0
ℓ_z				0.04	0.07	0.05		0.00		
ℓ_θ	-0.6	0.76	0.84	0.89	0.93	0.88	0.91	0.91	0.91	0.91
$-m_z$				0.07	0.03	0.11		0.00		
$-m_\theta$	0.2	0.96	1.04	1.13	1.05	1.14	1.08	1.08	1.10	1.10
$\ell_{\dot{z}}$				0.88	0.89			0.91		
$\ell_{\dot{\theta}}$	0.2	1.22		1.20	1.19			1.47		1.45
$-m_{\dot{z}}$				0.93	1.11	1.04		1.08		
$-m_{\dot{\theta}}$	1.2	1.74		1.52	1.75	1.61		2.03		2.00

TABLE 46

Wing F, M = 1·89 → 2·0, Axis at Apex (g = 0).

	Experimental						Theoretical M = 1.89			
	Baines & Rockliff M = 2.0	Orlik-Rückemann & Laberge M = 2.00	Hall & Osborne M = 1.90				Harris		Harris (Jones & Cohen)	Orlik-Rückemann & Laberge
ν	0	0	0	0.035	0.047	0.059	0	0.1	0	0
ℓ_z				0.01	0.00	-0.02		0.00		
ℓ_θ	-0.7	0.77	0.72	0.76	0.74	0.72	0.86	0.86	0.85	0.85
$-m_z$				-0.02	-0.03	-0.11		0.00		
$-m_\theta$	0.1	0.95		0.91	0.89	0.78	1.03	1.03	1.03	1.04
$\ell_{\dot{z}}$				0.81	0.86			0.86		
$\ell_{\dot{\theta}}$	0.1	1.13		1.07	1.17			1.25		1.24
$-m_{\dot{z}}$				0.71				1.03		
$-m_{\dot{\theta}}$	1.0	1.58		1.11				1.73		1.72

TABLE 47

$-m_\theta$, *Wing A*, $v = 0$, *Axis at Apex* ($g = 0$)

$A\sqrt{1-M^2}$ or $A\sqrt{M^2-1}$	M	Theoretical		Experimental	
		Woodcock Harris Barnes	Hornsby Orlik-Rückemann	Hall Osborne	Orlik-Rückemann Laberge
3.0	0	1.53	1.54		
2.0	0.745	1.82	1.82		
1.8	0.8			1.65	
1.31	0.9			1.85	
1.25	0.91	2.10	2.10		
0.75	0.97	2.18			
0	1.0			1.78	
1.0	1.05	2.83	2.90		
1.37	1.1			2.05	
1.5	1.12	2.67	2.73		
2	1.2	2.51	2.55	2.07	
2.09	1.22				2.30
2.5	1.30	2.33	2.37		
2.72	1.35				
3	1.41	2.18	2.21		
3.19	1.46				
3.464*	1.53	1.98	2.06		
3.59	1.56			1.65	1.77
4	1.67		1.79		
4.42	1.78				
4.85	1.90			1.41	
5.02	1.95		1.46		
5.20	2.0	1.29			1.56
6.87	2.5			1.00	
6.97	2.53	1.14			

*Leading edge sonic.

The horizontal lines in the theoretical columns of Tables 47 to 58 separate the results of different methods of calculation. Orlik-Rückemann[17] made calculations both by the method of Malvestuto[35,36,37], for the subsonic leading-edge case, and by the method of Martin[38] and Cole[39], for the supersonic leading-edge case.

TABLE 48

$-m_{\dot{\theta}}$, *Wing A*, $v = 0$, *Axis at Apex* ($g = 0$)

$A\sqrt{1-M^2}$ or $A\sqrt{M^2-1}$	M	Theoretical		Experimental	
		Woodcock Harris Barnes	Hornsby Orlik-Rückemann	Hall Osborne	Orlik-Rückemann Laberge
3.0	0	3.10	3.12		
2.0	0.745	3.64	3.64		
1.8	0.8			2.92	
1.31	0.9			2.93	
1.25	0.91	4.13	4.14		
0.75	0.97	4.96			
0	1.0			1.33	
1.0	1.05	0.79	0.50		
1.37	1.1			1.91	
1.5	1.12	1.53	1.56		
2	1.2	1.97	1.93	1.40	
2.09	1.22				1.73
2.5	1.30	2.04	2.01		
2.72	1.35				
3	1.41	1.94	1.97		
3.19	1.46				
3.464*	1.53	1.79	1.88		
3.59	1.56			1.87	1.68
4	1.67		1.83		
4.42	1.78				
4.85	1.90			1.67	
5.02	1.95		1.65		
5.20	2.0	1.58			1.78
6.87	2.5			1.48	
6.97	2.53	1.38			

*Leading edge sonic.

TABLE 49

$-m_\theta$, *Wing B*, $v = 0$, *Axis at Apex* ($g = 0$)

$A\sqrt{1-M^2}$ or $A\sqrt{M^2-1}$	M	Theoretical		Experimental	
		Woodcock Harris Barnes	Hornsby Orlik-Rückemann	Hall Osborne	Orlik-Rückemann Laberge
2.0	0	1.21	1.22		
	0.49				
	0.62				
	0.71				
1.25	0.78	1.39	1.40		
1.2	0.8			1.37	
	0.83				
	0.89				
0.87	0.9			1.42	
0.75	0.93	1.54			
	0.95				
	0.96				
	0.99				
0	1.0			0.98	
0.92	1.1			1.71	
1.0	1.12	1.89	1.94		
1.33	1.2			1.27	
1.4	1.22				1.54
1.5	1.25	1.78	1.82		
2.0	1.41	1.67	1.70		
2.4	1.56			1.40	1.20
2.5	1.6	1.56	1.58		
3.0	1.8	1.46	1.47		
3.23	1.9			1.17	
3.464*	2.0	1.28	1.38		1.05
4.5	2.46	1.12			
4.58	2.5			0.92	
5.0	2.69	0.90			

*Leading edge sonic.

TABLE 50

$-m_\phi$, *Wing B*, $v = 0$, *Axis at Apex* ($g = 0$)

$A\sqrt{1-M^2}$ or $A\sqrt{M^2-1}$	M	Theoretical		Experimental	
		Woodcock Harris Barnes	Hornsby Orlik-Rückemann	Hall Osborne	Orlik-Rückemann Laberge
2.0	0	2.27	2.27		
	0.49				
	0.62				
	0.71				
1.25	0.78	3.28	3.27		
1.2	0.8			2.12	
	0.83				
	0.89				
0.87	0.9			1.97	
0.75	0.93	3.72			
	0.95				
	0.96				
	0.99				
0	1.0			1.50	
0.92	1.1			1.80	
1.0	1.12	2.84	2.70		
1.33	1.2			1.77	
1.4	1.22				2.52
1.5	1.25	2.67	2.58		
2.0	1.41	2.38	2.33		
2.4	1.56			1.83	1.81
2.5	1.6	2.10	2.08		
3.0	1.8	1.84	1.84		
3.23	1.9			1.63	
3.464*	2.0	1.56	1.65		1.52
4.5	2.46	1.42			
4.58	2.5			1.70	
5.0	2.69	1.21			

*Leading edge sonic.

TABLE 51

$-m_\theta$, *Wing C*, $v = 0$, *Axis at Apex* ($g = 0$)

$A\sqrt{1-M^2}$ or $A\sqrt{M^2-1}$	M	Theoretical		Experimental	
		Woodcock Harris	Hornsby Orlik-Rückemann	Hall Osborne	Orlik-Rückemann Laberge
1.25	*0	0.87	0.88		
0.75	0.8	0.96		0.94	
0.55	0.9			0.93	
0.5	0.92	1.02			
0.25	0.98	1.06			
0	1.0			1.07	
0.57	1.1			1.17	
0.83	1.2			1.17	
0.87	1.22				1.31
1.0	1.28	1.18	1.21		
1.5	1.56	1.11	1.14	1.04	1.05
2.0	1.89	1.04	1.06		
2.02	1.9			0.88	
2.17	2.0				0.91
2.5	2.24		0.99		
2.86	2.5			0.84	
3.0	2.6		0.92		
3.464*	2.95		0.86		

*Leading edge sonic.

TABLE 52

$-m_{\dot{\theta}}$, *Wing C*, $v = 0$, *Axis at Apex* ($g = 0$).

$A\sqrt{1-M^2}$ or $A\sqrt{M^2-1}$	M	Theoretical		Experimental	
		Woodcock Harris	Hornsby Orlik-Rückemann	Hall Osborne	Orlik-Rückemann Laberge
1.25	0	2.20	2.20		
0.75	0.8	2.53		1.52	
0.55	0.9			1.51	
0.5	0.92	2.72			
0.25	0.98	2.98			
0	1.0			1.43	
0.57	1.1			2.07	
0.83	1.2			2.24	
0.87	1.22				2.18
1.0	1.28	2.47	2.41		
1.5	1.56	2.12	2.08	1.92	1.74
2.0	1.89	1.80	1.78		
2.02	1.9			1.44	
2.17	2.0				1.56
2.5	2.24		1.52		
2.86	2.5			1.04	
3.0	2.6		1.31		
3.464*	2.95		1.16		

*Leading edge sonic.

TABLE 53

$-m_\theta$, *Wing D*, $v = 0$, *Axis at Apex* ($g = 0$)

$A\sqrt{1-M^2}$ or $A\sqrt{M^2-1}$	M	Theoretical		Experimental	
		Woodcock Harris Barnes	Hornsby Orlik-Rückemann	Hall Osborne	Orlik-Rückemann Laberge
3.0	0	1.53	1.53		
2.0	0.745	1.79	1.79		
1.8	0.8			1.67	
1.31	0.9			1.81	
1.25	0.91	2.03	2.04		
0.75	0.97	2.15			
0	1.0			1.87	
1.0	1.05	2.67	2.77		
1.37	1.1			2.12	
1.5	1.12	2.58	2.64		
2.0	1.2	2.47	2.49	2.13	
2.09	1.22				2.23
2.5	1.30	2.32	2.33		
3.0	1.41	2.18	2.18		
3.464*	1.53	2.05	2.05		
3.59	1.56			1.63	1.68
4.0	1.67		1.82		
4.85	1.90			1.41	
5.02	1.95		1.50		
5.20	2.0	1.43			1.52
6.87	2.5			1.05	
6.97	2.53	1.07			

*Leading edge sonic.

TABLE 54

$-m_\theta$, *Wing D*, $v = 0$, *Axis at Apex* ($g = 0$)

$A\sqrt{1-M^2}$ or $A\sqrt{M^2-1}$	M	Theoretical		Experimental	
		Woodcock Harris Barnes	Hornsby Orlik-Rückemann	Hall Osborne	Orlik-Rückemann Laberge
3.0	0	2.93	2.94		
2.0	0.745	3.37	3.35		
1.8	0.8			2.85	
1.31	0.9			2.96	
1.25	0.91	3.71	3.67		
0.75	0.97	4.17			
0	1.0			2.21	
1.0	1.05	1.02	0.55		
1.37	1.1			2.38	
1.5	1.12	1.48	1.54		
2.0	1.2	1.85	1.89	2.69	
2.09	1.22				1.46
2.5	1.30	1.96	1.97		
3.0	1.41	1.90	1.92		
3.464*	1.53	1.84	1.83		
3.59	1.56			1.65	1.41
4.0	1.67		1.70		
4.85	1.90			1.30	
5.02	1.95		1.51		
5.20	2.0	1.54			1.45
6.87	2.5			0.75	
6.97	2.53	1.32			

*Leading edge sonic.

TABLE 55

$-m_\theta$, *Wing E*, $v = 0$, *Axis at Apex* ($g = 0$)

$A\sqrt{1-M^2}$ or $A\sqrt{M^2-1}$	M	Theoretical		Experimental	
		Woodcock Harris Barnes	Hornsby Orlik-Rückemann	Hall Osborne	Orlik-Rückemann Laberge
2.0	0	1.19	1.20		
	0.49				
	0.62				
	0.71				
1.25	0.78	1.35	1.36		
1.2	0.8			1.30	
	0.82				
	0.83				
	0.89				
0.87	0.9			1.39	
0.75	0.93	1.47			
	0.95				
	0.96				
	0.99				
0	1.0			1.53	
	1.04				
	1.07				
0.92	1.1			1.59	
1.0	1.12	1.78	1.85		
1.33	1.2			1.36	
1.4	1.22				1.60
1.5	1.25	1.72	1.76		
2.0	1.41	1.65	1.66		
2.4	1.56			1.42	1.37
2.5	1.6	1.54	1.55		
3.0	1.8	1.45	1.45		
3.23	1.9			1.24	
3.464*	2.0	1.34	1.37		1.27
4.50	2.46	1.00			
4.58	2.5			0.97	
5.0	2.69	0.93			

*Leading edge sonic.

TABLE 56

$-m_{\dot{\theta}}$, *Wing E, v = 0, Axis at Apex (g = 0)*

$A\sqrt{1-M^2}$ or $A\sqrt{M^2-1}$	M	Theoretical		Experimental	
		Woodcock Harris Barnes	Hornsby Orlik-Rückemann	Hall Osborne	Orlik-Rückemann Laberge
2.0	0	2.59	2.58		
	0.49				
	0.62				
	0.71				
1.25	0.78	2.99	2.96		
1.2	0.8			2.32	
	0.82				
	0.83				
	0.89				
0.87	0.9			2.17	
0.75	0.93	3.29			
	0.95				
	0.96				
	0.99				
0	1.0			2.25	
	1.04				
	1.07				
0.92	1.1			2.23	
1.0	1.12	2.73	2.59		
1.33	1.2			2.33	
1.4	1.22				2.24
1.5	1.25	2.55	2.49		
2.0	1.41	2.28	2.26		
2.4	1.56			1.86	1.78
2.5	1.6	2.04	2.02		
3.0	1.8	1.80	1.80		
3.23	1.9			1.38	
3.464*	2.0	1.64	1.62		1.66
4.50	2.46	1.25			
4.58	2.5			1.12	
5.0	2.69	1.19			

*Leading edge sonic.

TABLE 57

$-m_\theta$, *Wing F*, $v = 0$, *Axis at Apex* ($g = 0$)

$A\sqrt{1-M^2}$ or $A\sqrt{M^2-1}$	M	Theoretical		Experimental	
		Woodcock Harris	Hornsby Orlik-Rückemann	Hall Osborne	Orlik-Rückemann Laberge
1.25	0	0.84	0.85		
1.0	0.6	0.90			
0.75	0.8	0.92		0.94	
0.55	0.9			0.95	
0.5	0.92	0.96			
0.375	0.95	0.98			
0.25	0.98	0.99			
0.175	0.99	1.01			
0	1.0			1.05	
0.57	1.1			1.13	
0.83	1.2			1.10	
0.87	1.22				1.18
1.0	1.28	1.11	1.16		
1.5	1.56	1.08	1.10	1.04	0.96
2.0	1.89	1.03	1.04		
2.02	1.9			0.86	
2.17	2.0				0.95
2.5	2.24		0.97		
2.86	2.5			0.83	
3.0	2.6		0.91		
3.464*	2.95		0.85		

*Leading edge sonic.

TABLE 58

$-m_{\dot{\theta}}$, *Wing F*, $v = 0$, *Axis at Apex* ($g = 0$)

$A\sqrt{1-M^2}$ or $A\sqrt{M^2-1}$	M	Theoretical		Experimental	
		Woodcock Harris	Hornsby Orlik-Rückemann	Hall Osborne	Orlik-Rückemann Laberge
1.25	0	2.02	2.01		
1.0	0.6	2.14			
0.75	0.8	2.27		1.82	
0.55	0.9			1.86	
0.5	0.92	2.39			
0.375	0.95	2.45			
0.25	0.98	2.50			
0.175	0.99	2.49			
0	1.0			1.95	
0.57	1.1			1.85	
0.83	1.2			1.86	
0.87	1.22				2.03
1.0	1.28	2.34	2.30		
1.5	1.56	2.03	2.00	1.63	1.74
2.0	1.89	1.73	1.72		
2.02	1.9			1.11	
2.17	2.0				1.58
2.5	2.24		1.48		
2.86	2.5			1.36	
3.0	2.6		1.28		
3.464*	2.95		1.13		

*Leading edge sonic.

TABLE 59

Wing A, $v = 0 \rightarrow 0{\cdot}1$, Axis at Apex ($g = 0$) Hall and Osborne's[15] Experimental Results*

M	0.8	0.9	1.0	1.1	1.2	1.56	1.90	2.5
ℓ_z	0.02	-0.06	-0.02	-0.06	-0.01	-0.01	-0.07	0.00
ℓ_θ	1.59	1.72	1.65	1.76	1.75	1.51	1.16	0.82
$-m_z$	-0.04	-0.10	-0.01	-0.05	-0.02	0.00	-0.10	0.00
$-m_\theta$	1.65	1.85	1.78	2.05	2.07	1.65	1.41	1.00
$\ell_{\dot{z}}$	1.56	1.51	1.41	1.87	1.80	1.63	1.28	0.95
$\ell_{\dot{\theta}}$	2.46	2.14	1.16	1.68	1.24	1.42	0.98	1.02
$-m_{\dot{z}}$	1.55	1.61	1.61	1.97	2.06	1.89	1.63	1.29
$-m_{\dot{\theta}}$	2.92	2.93	1.33	1.91	1.40	1.87	1.67	1.48

*The values tabulated in Tables 59 to 65 are either values for $v = 0$ (where measured) or else the mean of up to three measured values for different v between 0 and 0·1.

TABLE 60

Wing B, $v = 0 \rightarrow 0{\cdot}1$, Axis at Apex ($g = 0$) Hall and Osborne's[15] Experimental Results

M	0.8	0.9	1.0	1.1	1.2	1.56	1.90	2.5
ℓ_z	0.03	0.01	-0.03	-0.08	-0.05	-0.04	-0.02	-0.03
ℓ_θ	1.27	1.31	1.18	1.41	1.33	1.14	0.97	0.77
$-m_z$	0.02	-0.03	-0.10	-0.16	-0.11	-0.07	-0.04	-0.04
$-m_\theta$	1.37	1.42	0.98	1.71	1.27	1.40	1.17	0.92
$\ell_{\dot{z}}$	1.02	0.99	1.06	1.38	1.39	1.16	1.08	0.81
$\ell_{\dot{\theta}}$	2.00	1.83	1.49	1.81	1.68	1.34	1.24	1.06
$-m_{\dot{z}}$	0.83	0.80	0.93	1.36	1.54	1.61	1.34	1.14
$-m_{\dot{\theta}}$	2.12	1.97	1.50	1.80	1.77	1.83	1.63	1.70

TABLE 61

Wing C, $v = 0 \rightarrow 0{\cdot}1$, Axis at Apex ($g = 0$) Hall and Osborne's[15] Experimental Results

M	0.8	0.9	1.0	1.1	1.2	1.56	1.90	2.5
ℓ_z	0.00	-0.02	-0.03	-0.02	-0.04	-0.05	0.00	-0.03
ℓ_θ	0.86	0.85	0.91	0.94	0.97	0.83	0.73	0.61
$-m_z$	-0.01	-0.04	-0.03	-0.02	-0.06	0.01	-0.03	-0.05
$-m_\theta$	0.94	0.93	1.07	1.17	1.17	1.04	0.88	0.84
$\ell_{\dot{z}}$	0.90	0.84	0.94	1.33	1.37	0.84	0.83	0.63
$\ell_{\dot{\theta}}$	1.64	1.61	1.63	2.04	2.05	1.11	1.14	0.76
$-m_{\dot{z}}$	0.59	0.55	0.64	1.38	1.61	1.20	0.93	0.86
$-m_{\dot{\theta}}$	1.52	1.51	1.43	2.07	2.24	1.92	1.44	1.04

TABLE 62

Wing D, $v = 0 \rightarrow 0{\cdot}1$, Axis at Apex ($g = 0$) Hall and Osborne's[15] Experimental Results

M	0.8	0.9	1.0	1.1	1.2	1.56	1.90	2.5
ℓ_z	-0.09	-0.06	-0.05	-0.06	-0.04	-0.04	-0.01	0.00
ℓ_θ	1.57	1.68	1.69	1.79	1.75	1.36	1.15	0.86
$-m_z$	-0.07	-0.03	-0.01	0.03	0.01	0.00	0.04	0.07
$-m_\theta$	1.67	1.81	1.87	2.12	2.13	1.63	1.41	1.05
$\ell_{\dot{z}}$	1.61	1.72	1.78	1.95	2.29	1.67	1.14	0.86
$\ell_{\dot{\theta}}$	2.37	2.26	1.74	1.81	1.81	1.36	1.07	0.82
$-m_{\dot{z}}$	1.68	1.94	2.02	2.28	3.10	1.86	1.29	0.90
$-m_{\dot{\theta}}$	2.85	2.96	2.21	2.38	2.69	1.65	1.30	0.75

TABLE 63

Wing E, $v = 0 \rightarrow 0{\cdot}1$, Axis at Apex ($g = 0$) Hall and Osborne's[15] Experimental Results

M	0.8	0.9	1.0	1.1	1.2	1.56	1.90	2.5
ℓ_z	-0.01	-0.03	0.01	-0.01	-0.02	0.02	-0.03	-0.02
ℓ_θ	1.20	1.27	1.34	1.35	1.34	1.14	1.00	0.78
$-m_z$	-0.02	-0.12	0.00	0.01	-0.01	0.01	-0.02	-0.01
$-m_\theta$	1.30	1.39	1.53	1.59	1.36	1.42	1.24	0.97
$\ell_{\dot{z}}$	1.02	1.15	1.33	1.40	1.59	1.32	0.99	0.91
$\ell_{\dot{\theta}}$	1.83	1.88	1.73	1.74	1.78	1.41	1.11	0.93
$-m_{\dot{z}}$	1.09	1.08	1.58	1.69	1.97	1.50	1.07	1.20
$-m_{\dot{\theta}}$	2.32	2.17	2.25	2.23	2.33	1.86	1.38	1.10

TABLE 64

Wing F, $v = 0 \rightarrow 0{\cdot}1$, Axis at Apex ($g = 0$) Hall and Osborne's[15] Experimental Results

M	0.8	0.9	1.0	1.1	1.2	1.56	1.90	2.50
ℓ_z	0.02	0.01	0.04	0.00	0.00	0.05	0.00	-0.03
ℓ_θ	0.86	0.85	0.90	0.98	0.94	0.84	0.74	0.62
$-m_z$	0.02	0.05	0.07	0.01	0.00	0.07	-0.05	-0.05
$-m_\theta$	0.94	0.95	1.05	1.13	1.10	1.04	0.86	0.83
$\ell_{\dot{z}}$	0.88	0.95	1.06	1.18	1.10	0.88	0.83	0.74
$\ell_{\dot{\theta}}$	1.60	1.64	1.67	1.75	1.60	1.20	1.12	0.95
$-m_{\dot{z}}$	0.85	0.97	1.19	1.16	1.20	1.03	0.71	1.26
$-m_{\dot{\theta}}$	1.82	1.86	1.95	1.85	1.86	1.63	1.11	1.36

TABLE 65

Wing G, ($A = 3$ Version), $v = 0 \rightarrow 0{\cdot}1$, Axis at Apex ($g = 0$) Hall and Osborne's[15] Experimental Results

M	0.8	0.9	1.0	1.1	1.2	1.56	1.90	2.50
ℓ_z	0.03	-0.03	-0.07	-0.04	0.18	-0.10	-0.04	0.00
ℓ_θ	1.65	1.78	1.87	2.09	2.20	1.53	1.17	0.77
$-m_z$	0.03	-0.02	-0.02	-0.05	0.07	-0.07	-0.02	0.00
$-m_\theta$	0.57	0.61	0.76	1.05	1.19	0.94	0.72	0.44
$\ell_{\dot{z}}$	1.95	2.06	1.87	2.91	1.84	2.04	1.58	0.71
$\ell_{\dot{\theta}}$	1.92	2.03	0.16	0.90	1.77	0.51	0.63	0.31
$-m_{\dot{z}}$	0.83	0.87	0.81	1.64	1.25	1.34	0.96	0.08
$-m_{\dot{\theta}}$	1.34	1.72	1.32	1.08	0.89	0.43	0.37	0.11

TABLE 66

Slotted Wall Interference, Corrected Vales for the H.S.D. 20 in. × 22 in. Tunnel, Axis at Apex ($g = 0$).

Wing	M	ℓ_θ			$-m_\theta$			ℓ_θ^*			$-m_\theta^*$		
Experimental*		Tunnel	Corrected open slots	Corrected closed slots	Tunnel	Corrected open slots	Corrected closed slots	Tunnel	Corrected open slots	Corrected closed slots	Tunnel	Corrected open slots	Corrected closed slots
A	0.8	1.59	1.78	1.50	1.65	1.85	1.56	2.46	2.78	2.33	2.92	3.30	2.76
	0.9	1.72	1.94	1.62	1.85	2.09	1.74	2.14	2.49	2.02	2.93	3.39	2.76
B	0.8	1.27	1.35	1.23	1.37	1.45	1.33	2.00	2.13	1.94	2.12	2.26	2.06
	0.9	1.31	1.39	1.27	1.42	1.51	1.38	1.83	1.96	1.77	1.97	2.11	1.91
C	0.8	0.86	0.88	0.85	0.94	0.96	0.93	1.64	1.68	1.62	1.52	1.56	1.50
	0.9	0.85	0.87	0.84	0.93	0.95	0.92	1.61	1.65	1.59	1.51	1.55	1.49
D	0.8	1.57	1.83	1.46	1.67	1.94	1.55	2.37	2.77	2.20	2.85	3.33	2.65
	0.9	1.68	1.98	1.55	1.81	2.13	1.67	2.26	2.69	2.09	2.96	3.51	2.74
E	0.8	1.20	1.29	1.16	1.30	1.40	1.25	1.83	1.97	1.76	2.32	2.50	2.23
	0.9	1.27	1.37	1.22	1.39	1.50	1.34	1.88	2.04	1.81	2.17	2.35	2.09
F	0.8	0.86	0.89	0.85	0.94	0.97	0.92	1.60	1.65	1.57	1.82	1.88	1.79
	0.9	0.85	0.88	0.84	0.95	0.97	0.92	1.64	1.69	1.61	1.86	1.92	1.83
G (A = 3 version)	0.8	1.65	1.99	1.51	0.57	0.69	0.52	1.92	2.32	1.76	1.34	1.62	1.23
	0.9	1.78	2.18	1.62	0.61	0.75	0.55	2.03	2.51	1.85	1.72	2.12	1.56
Theoretical**		Tunnel closed slots	Tunnel open slots	Free stream	Tunnel closed slots	Tunnel open slots	Free stream	Tunnel closed slots	Tunnel open slots	Free stream	Tunnel closed slots	Tunnel open slots	Free stream
C	0.8	0.91	0.86	0.89	1.03	0.96	1.00	2.05	2.03	2.02	2.67	2.63	2.63
D	0.8	2.01	1.42	1.74	2.21	1.50	1.88	2.80	2.95	2.69	3.68	3.71	3.50

*The experimental values are from Ref. 15. The corrected values have been obtained from Garner's approximate formula (eqn. (70) Ref. 46) assuming closed sides and either open roof and floor ('corrected open slots') or closed roof and floor ('corrected closed slots'). The values of the interference parameters were

$$(\delta_0, \delta_0') = -0{\cdot}2379, 0{\cdot}1446$$

and

$$= 0{\cdot}1285, -0{\cdot}0061 \text{ respectively.}$$

**The theoretical free-stream values were obtained by the method of Ref. 21. The tunnel corrections were obtained by the full theory of Ref. 46 using the following values of the interference parameters.

$$(\delta_0, \delta_1, \delta_0') = -0{\cdot}2380, -0{\cdot}3477, 0{\cdot}1447 \text{ (open)}$$

$$= 0{\cdot}1285, 0{\cdot}2706, -0{\cdot}0061 \text{ (closed).}$$

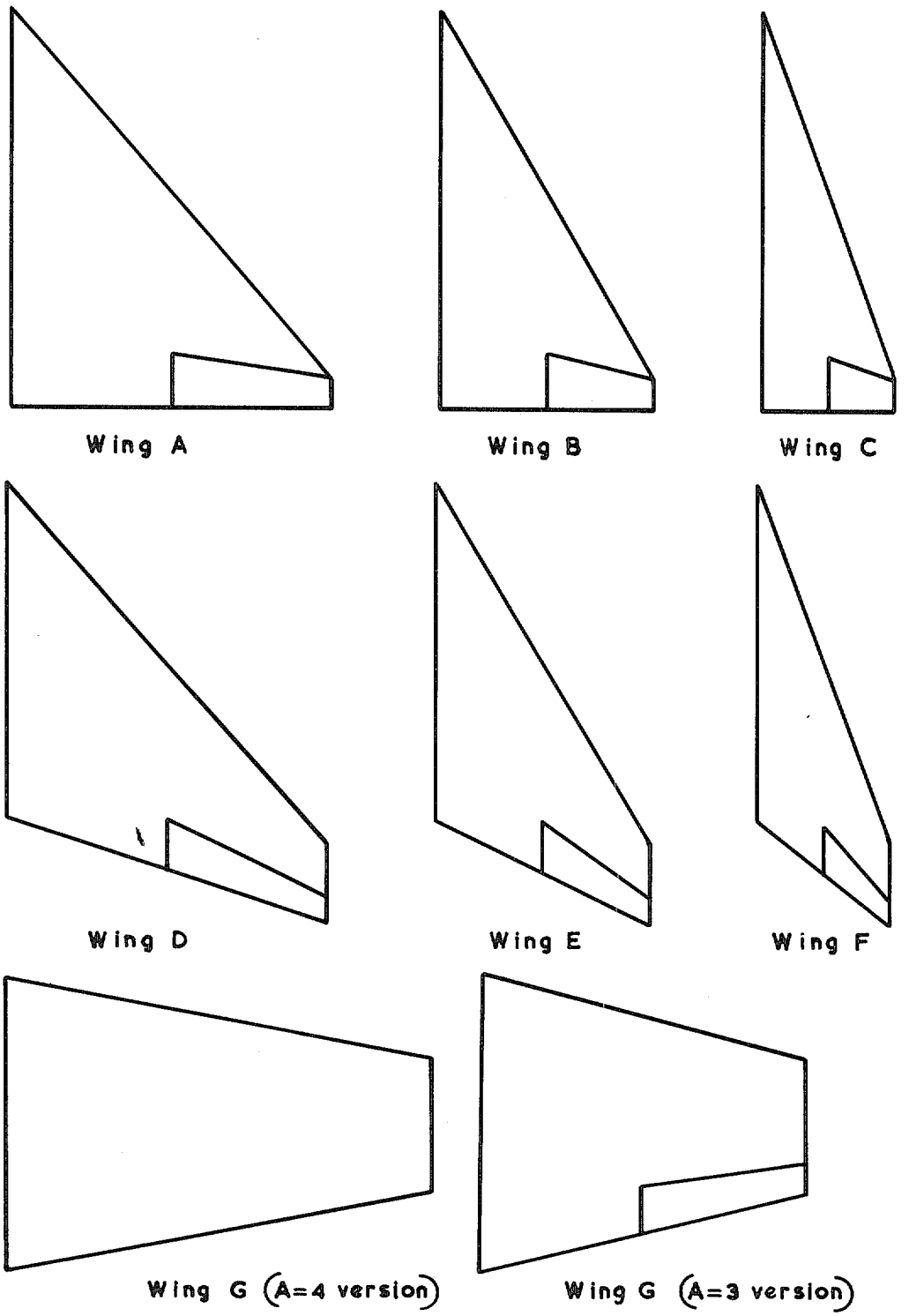

FIG. 1. Wing planforms.

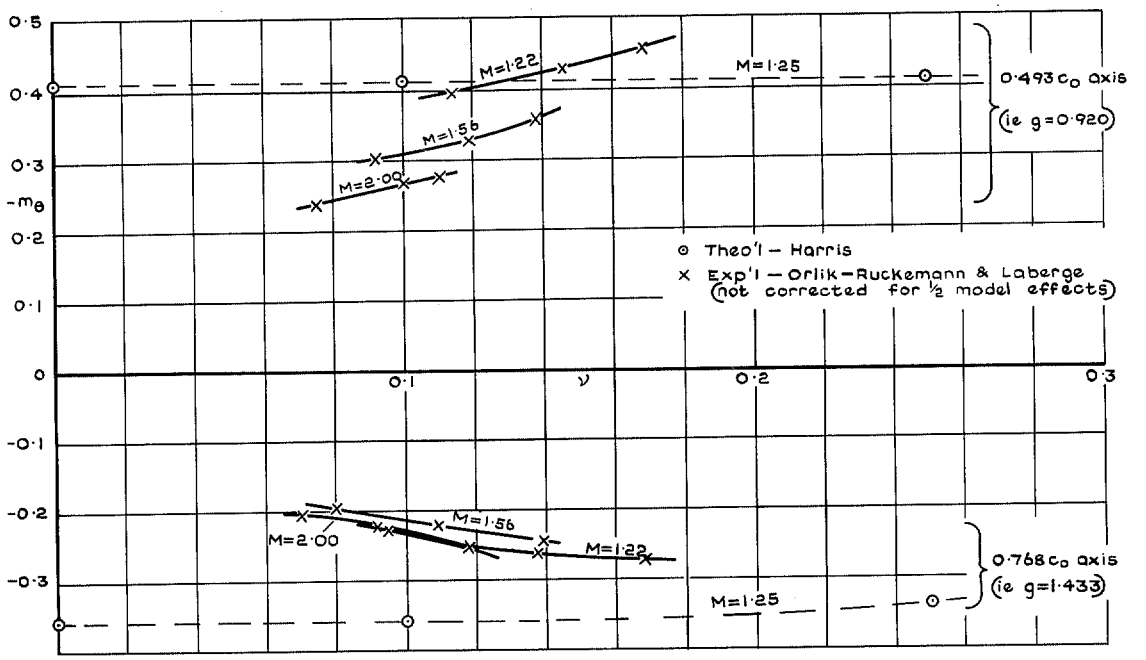

FIG. 2. Wing B – effect of frequency on $(-m_\theta)$.

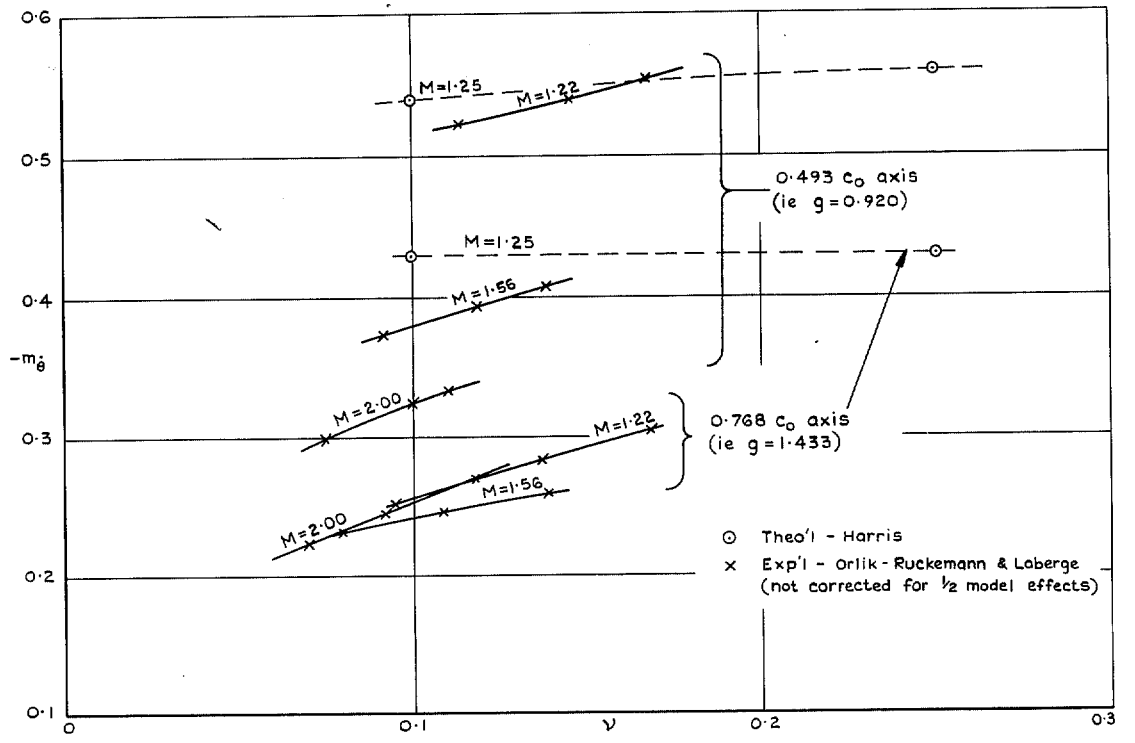

FIG. 3. Wing B – effect of frequency on $(-m_{\dot\theta})$.

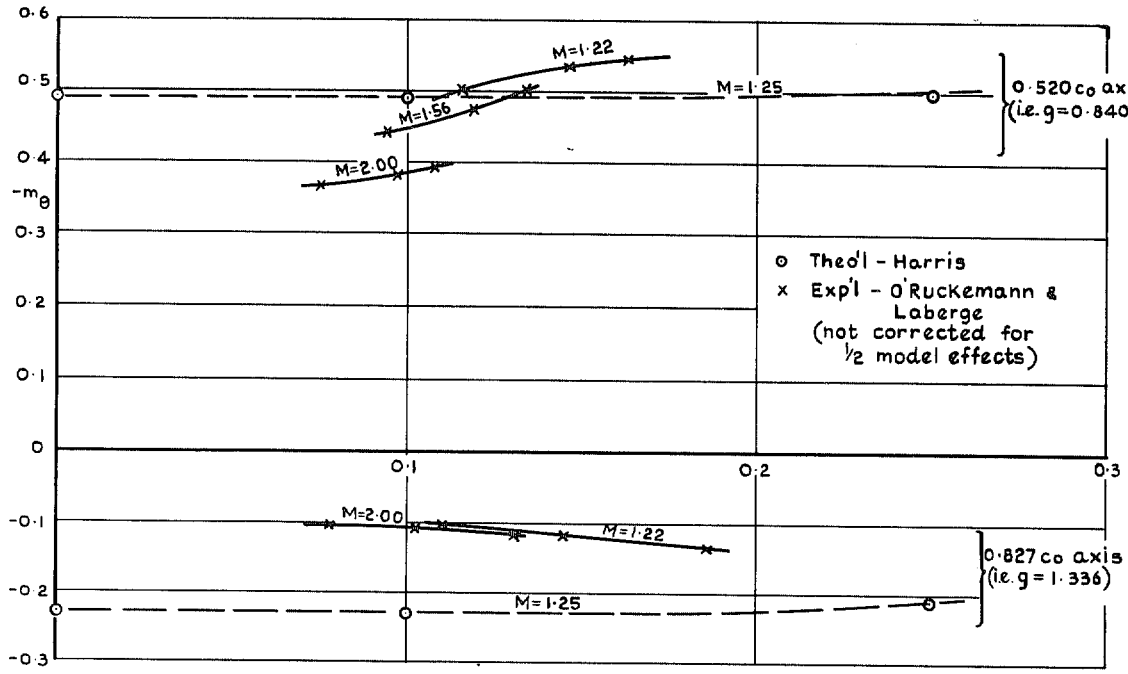

FIG. 4. Wing E – effect of frequency on $(-m_\theta)$.

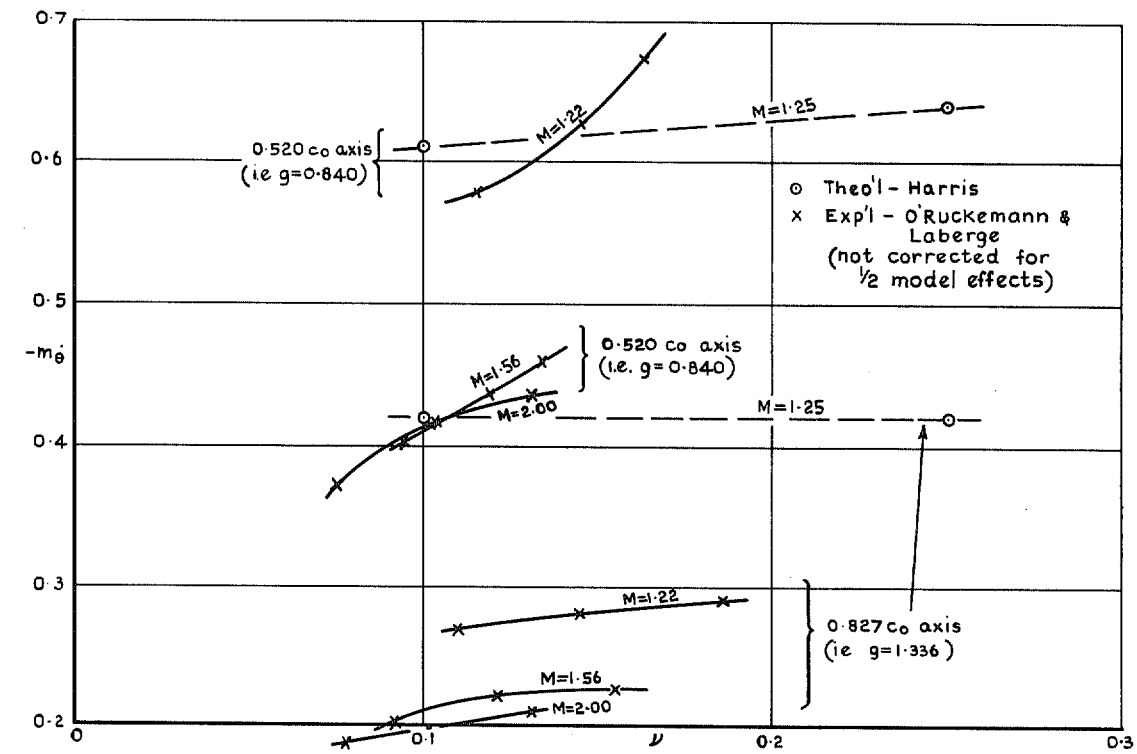

FIG. 5. Wing E – effect of frequency on $(-m_{\dot\theta})$.

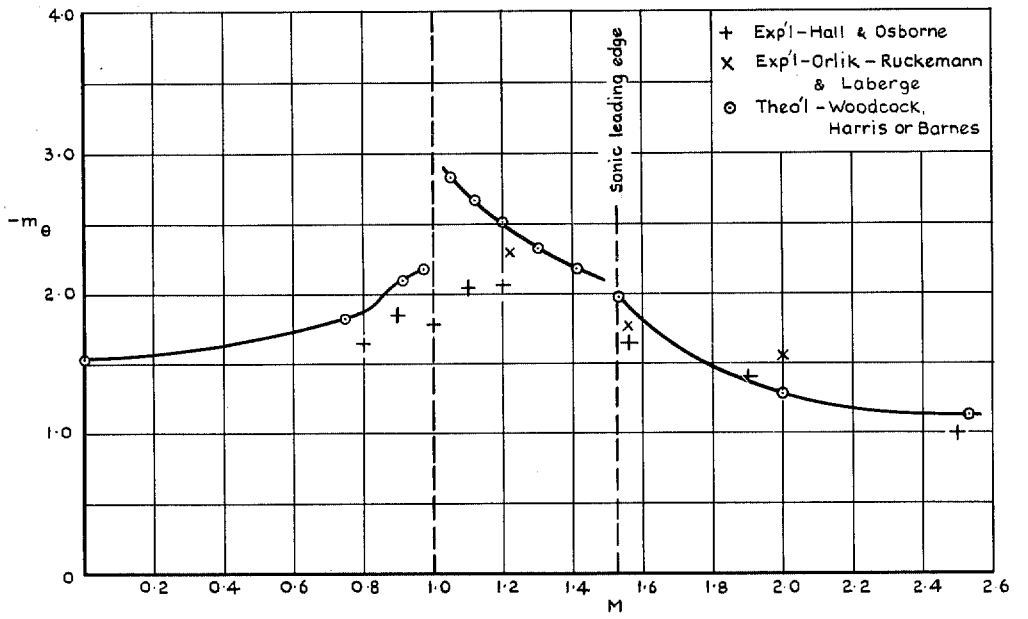

FIG. 6. Variation of $(-m_\theta)$ with M. Wing A, $v = 0$, axis at apex ($g = 0$).

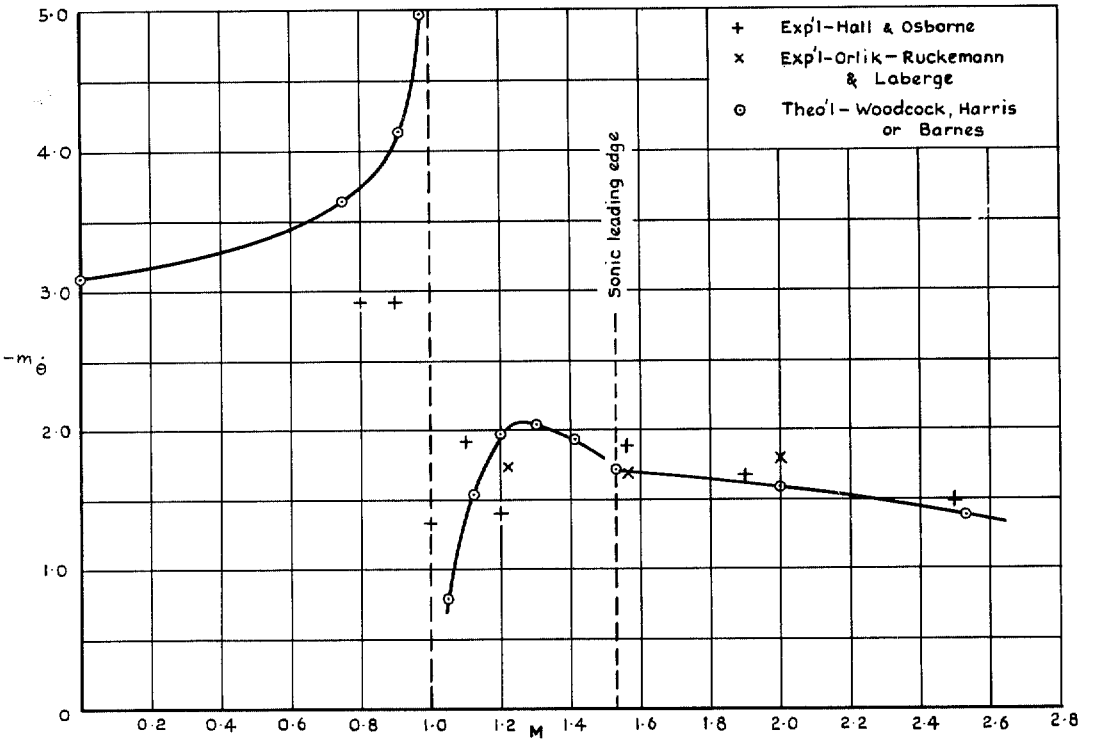

FIG. 7. Variation of $(-m_\theta)$ with M. Wing A, $v = 0$, axis at apex ($g = 0$).

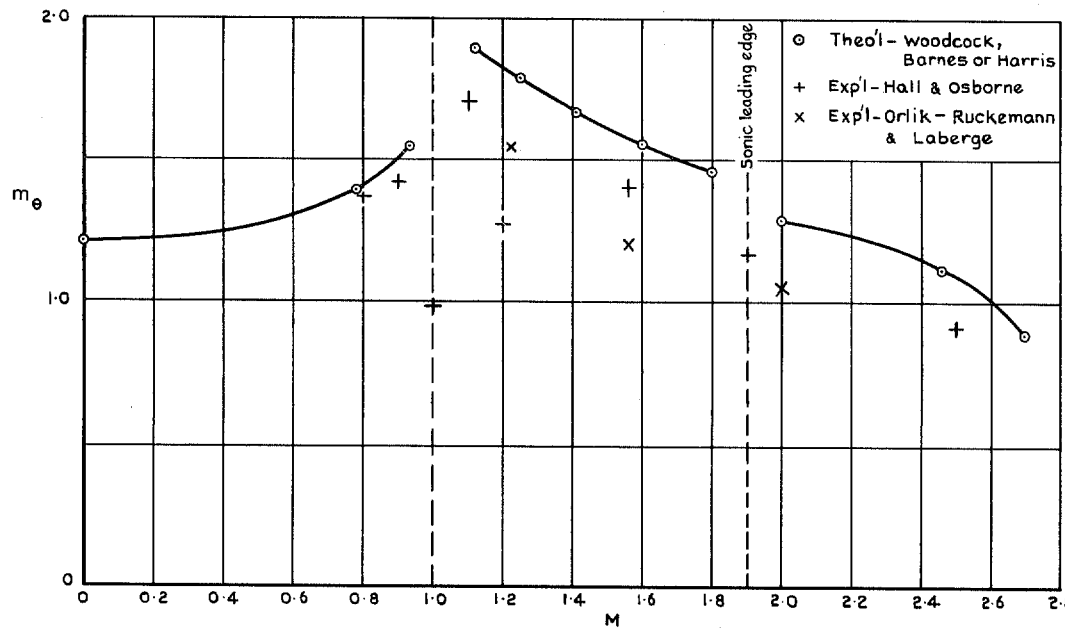

FIG. 8. Variation of $(-m_\theta)$ with M. Wing B, $\nu = 0$, axis at apex ($g = 0$).

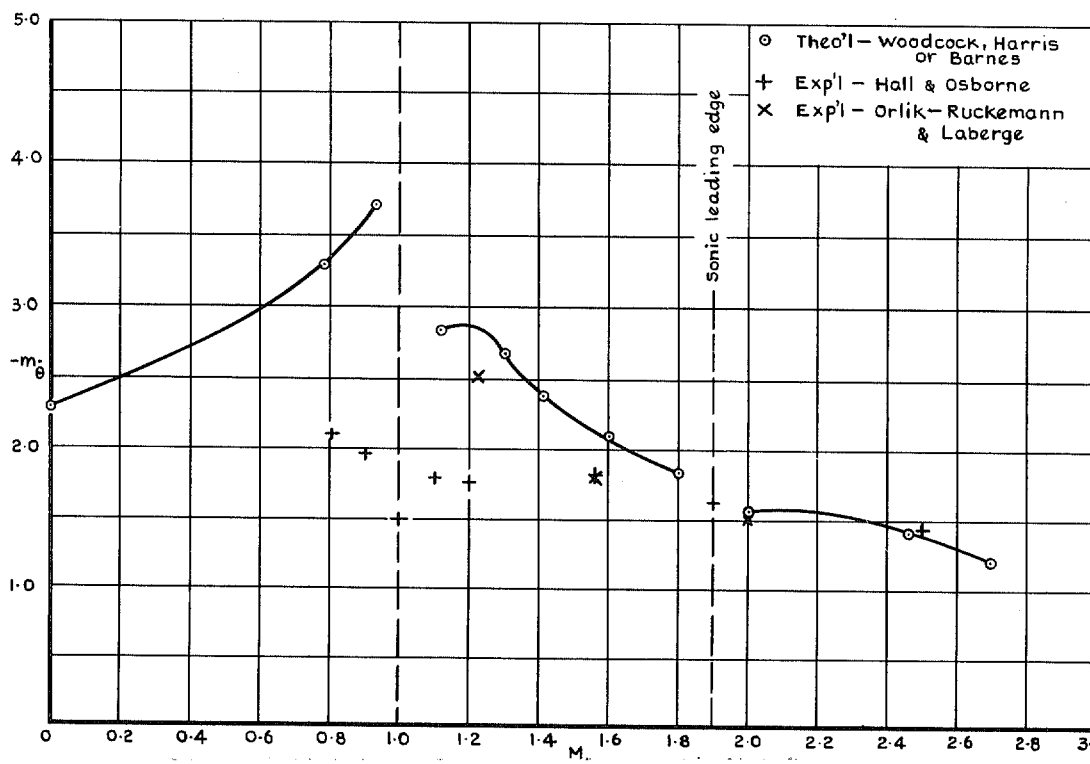

FIG. 9. Variation of $(-m_\theta)$ with M. Wing B, $\nu = 0$, axis at apex ($g = 0$).

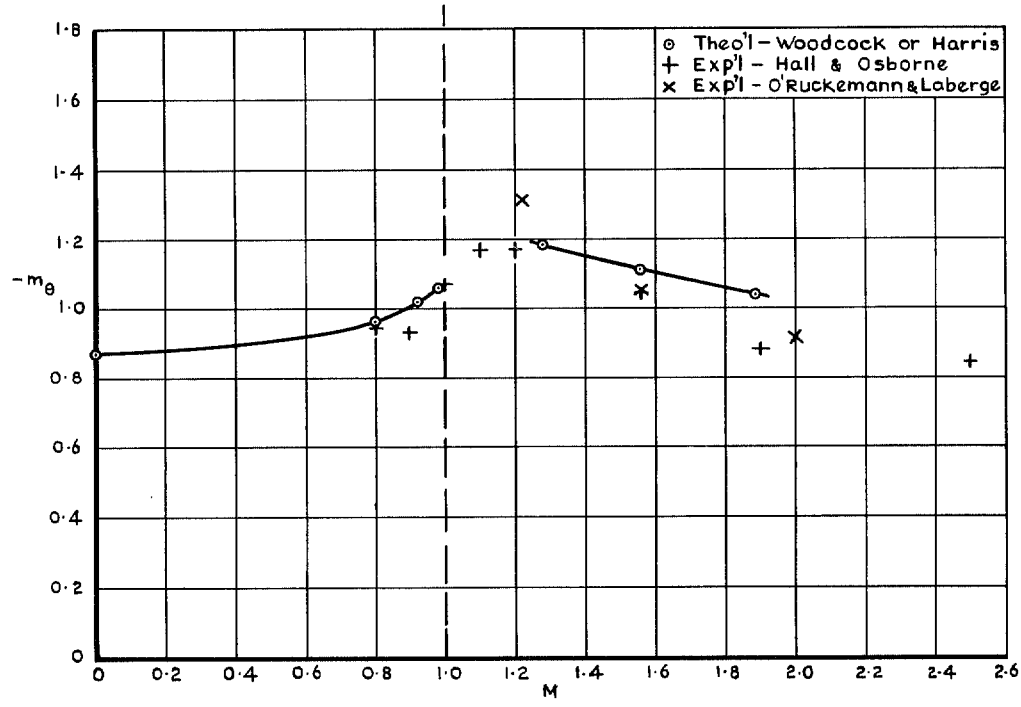

FIG. 10. Variation of $(-m_\theta)$ with M. Wing C, $v = 0$, axis at apex ($g = 0$).

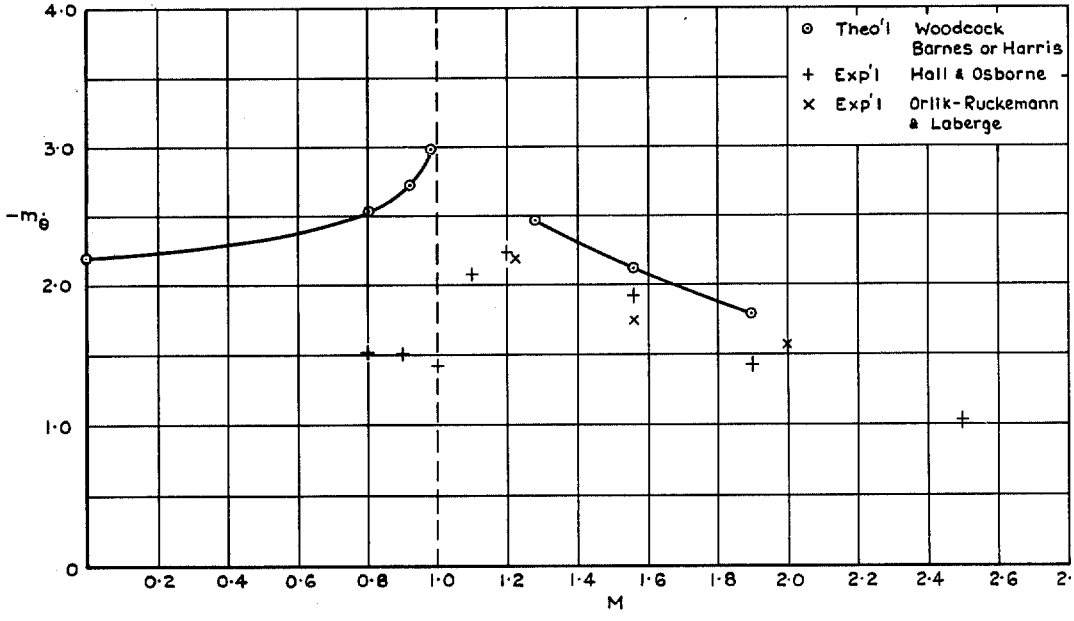

FIG. 11. Variation of $(-m_\theta)$ with M. Wing C, $v = 0$, axis at apex ($g = 0$).

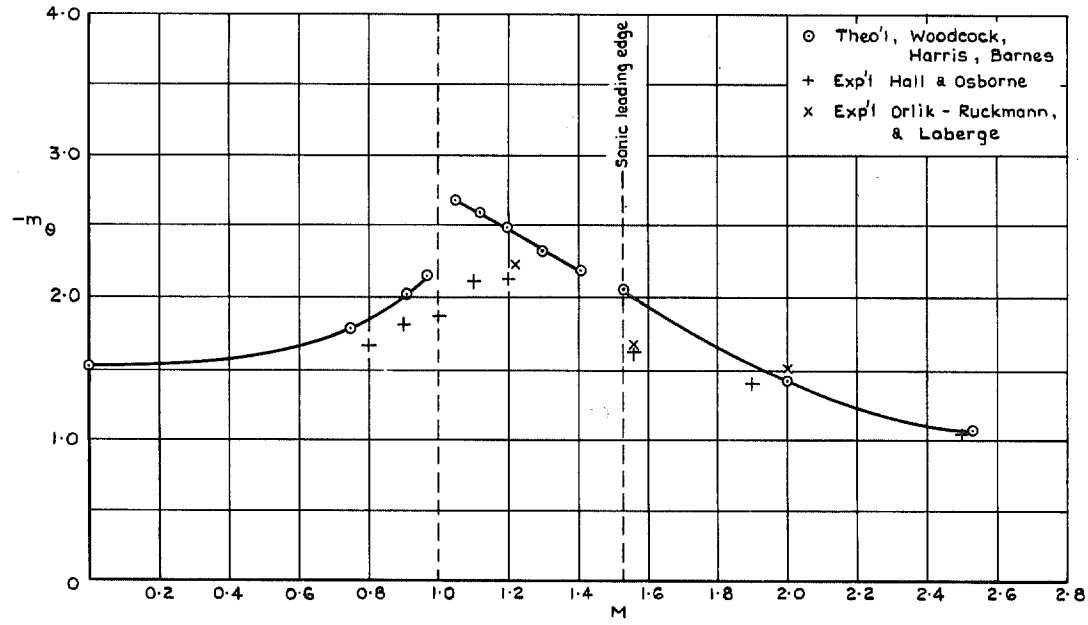

FIG. 12. Variation of $(-m_\theta)$ with M. Wing D, $v = 0$, axis at apex $(g = 0)$.

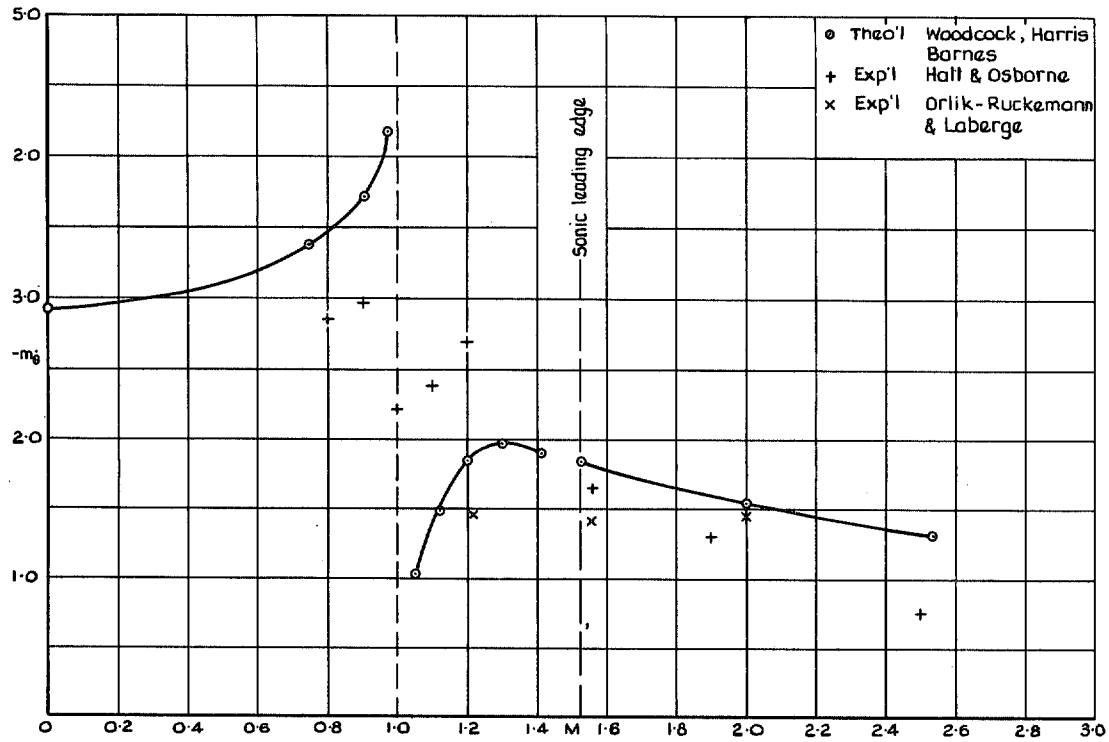

FIG. 13. Variation of $(-m_{\dot\theta})$ with M. Wing D, $v = 0$, axis at apex $(g = 0)$.

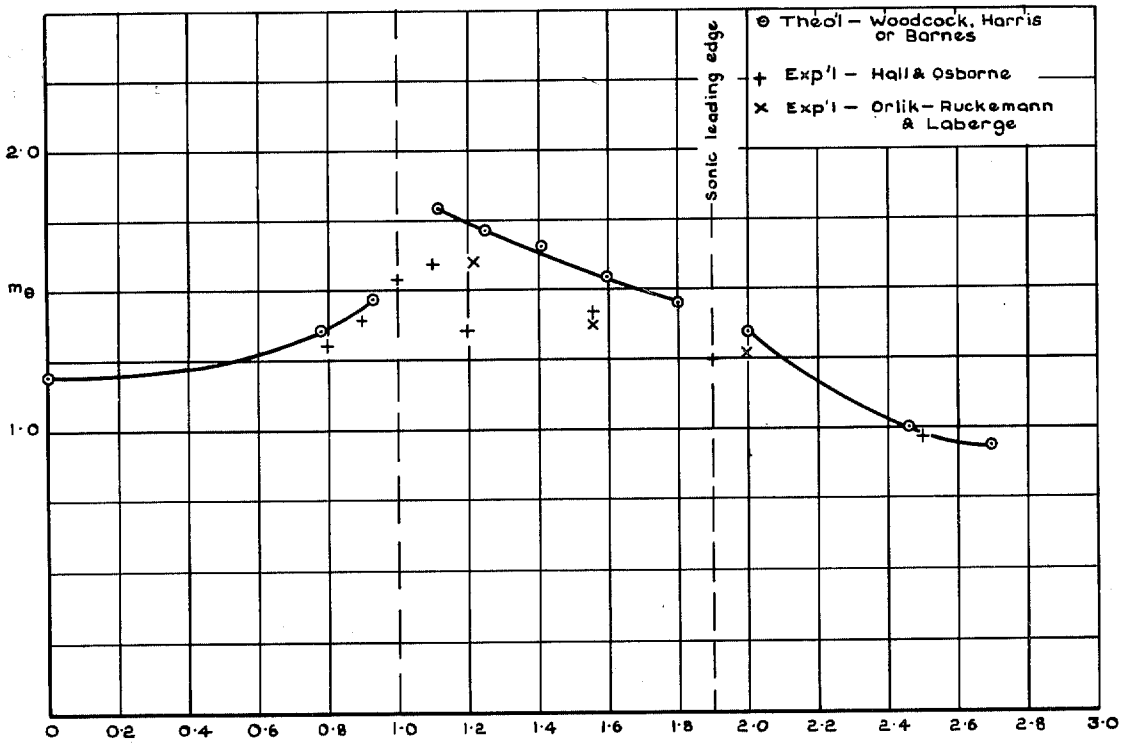

FIG. 14. Variation of $(-m_\theta)$ with M. Wing E, $v = 0$, axis at apex ($g = 0$).

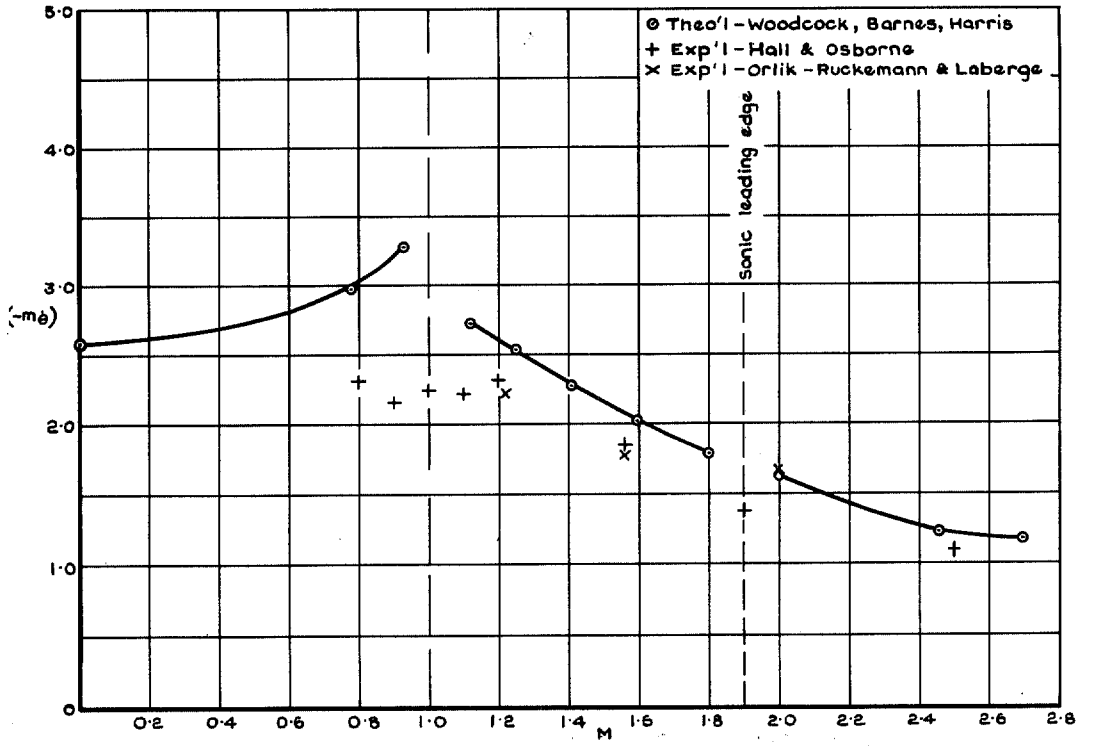

FIG. 15. Variation of $(-m_\theta)$ with M. Wing E, $v = 0$, axis at apex ($g = 0$).

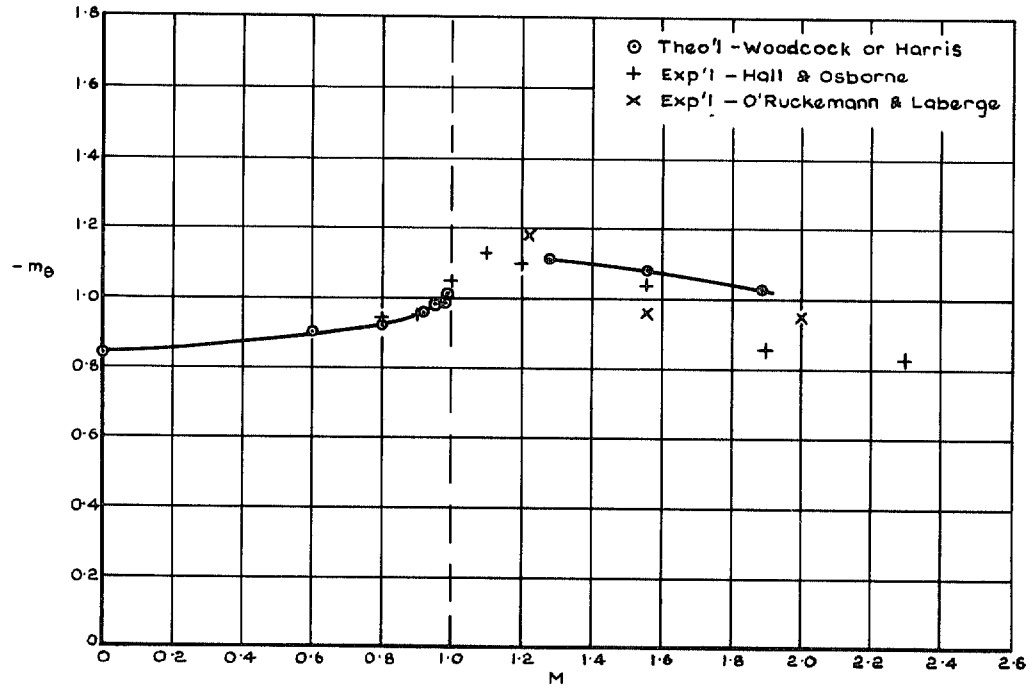

FIG. 16. Variation of $(-m_\theta)$ with M. Wing F, $v = 0$, axis at apex ($g = 0$).

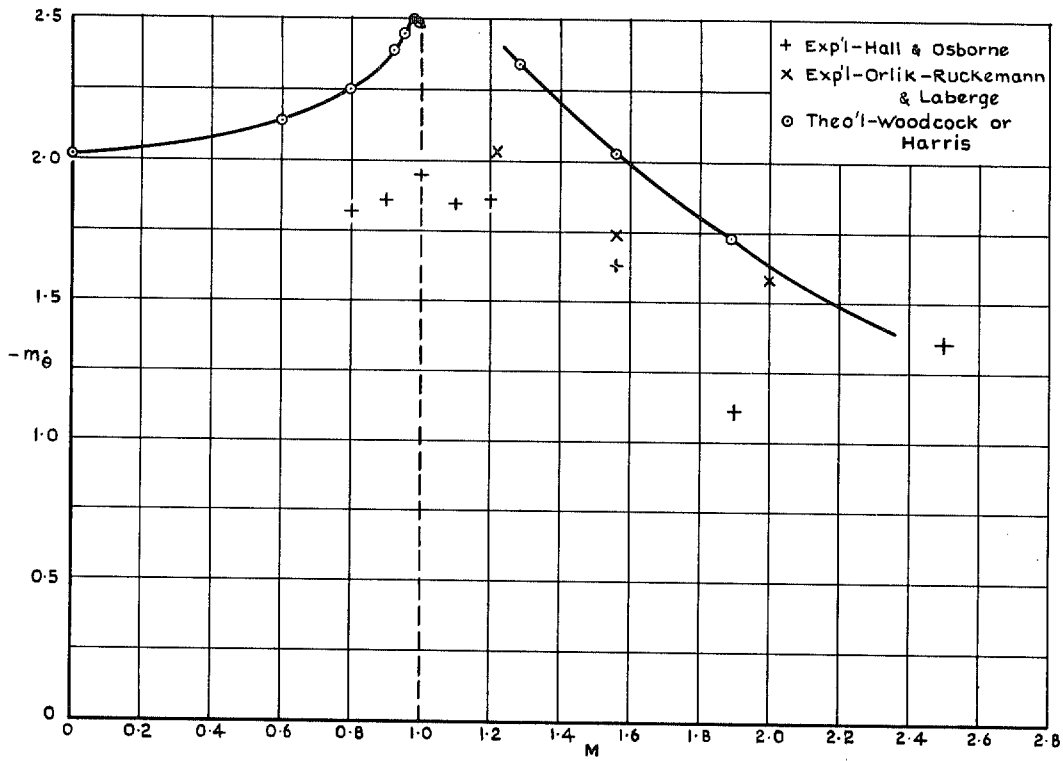

FIG. 17. Variation of $(-m_{\dot\theta})$ with M. Wing F, $v = 0$, axis at apex ($g = 0$).

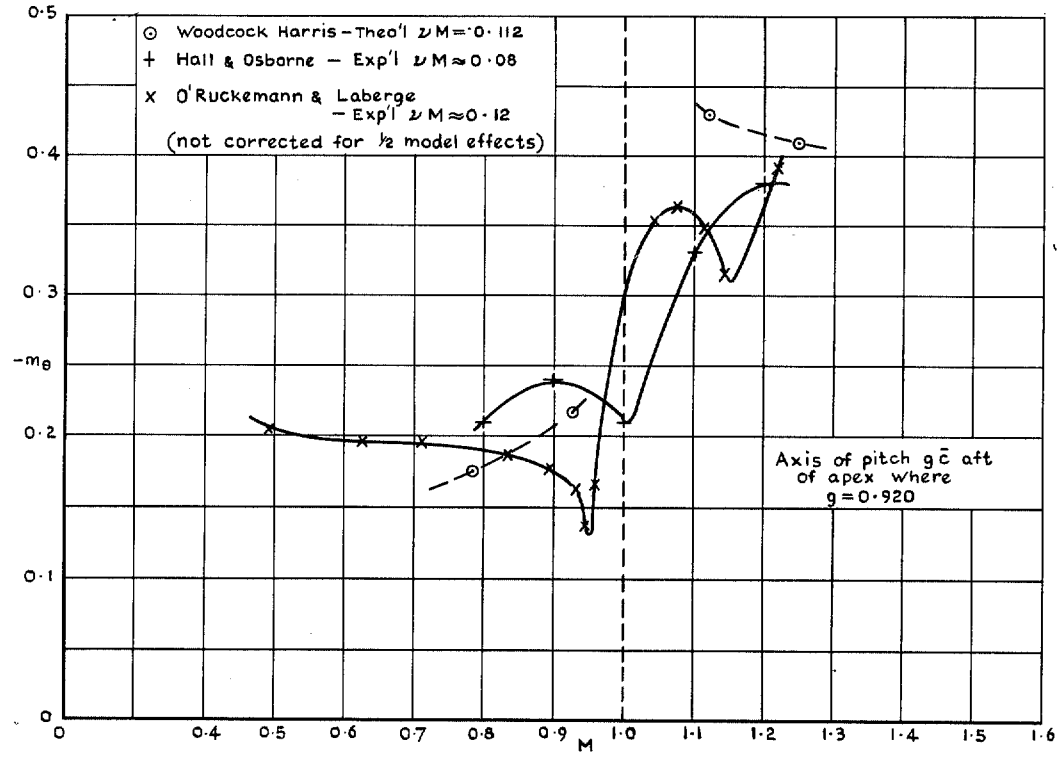

FIG. 18. Variation of $(-m_\theta)$ with M. Wing B, axis 0·493 c_0, $vM \approx 0{\cdot}1$.

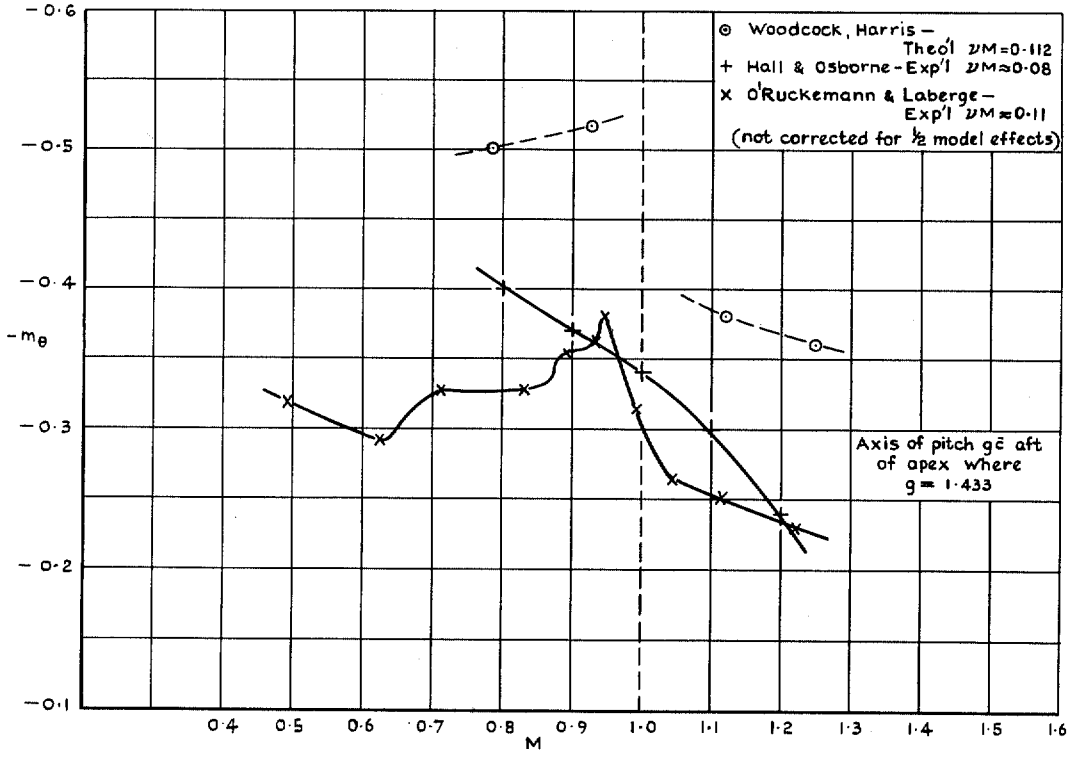

FIG. 19. Variation of $(-m_\theta)$ with M. Wing B, axis 0·768c_0, $vM \approx 0{\cdot}1$.

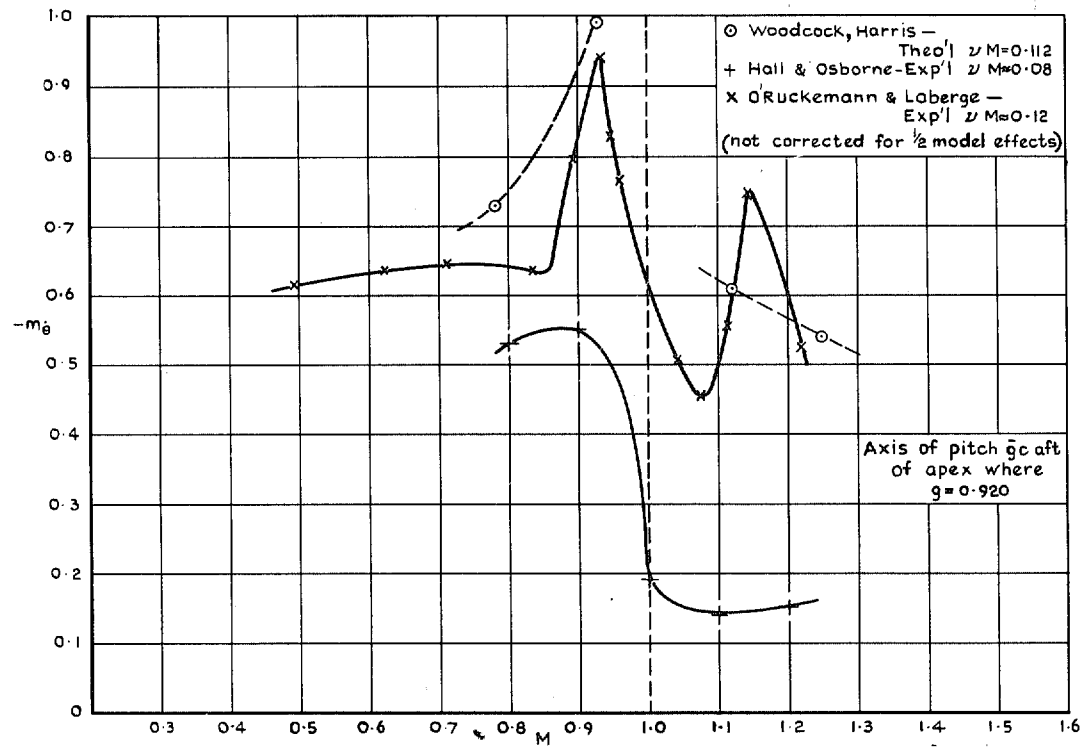

FIG. 20. Variation of $(-m_{\dot{\theta}})$ with M. Wing B, axis $0{\cdot}493c_0$, $\nu M \approx 0{\cdot}1$.

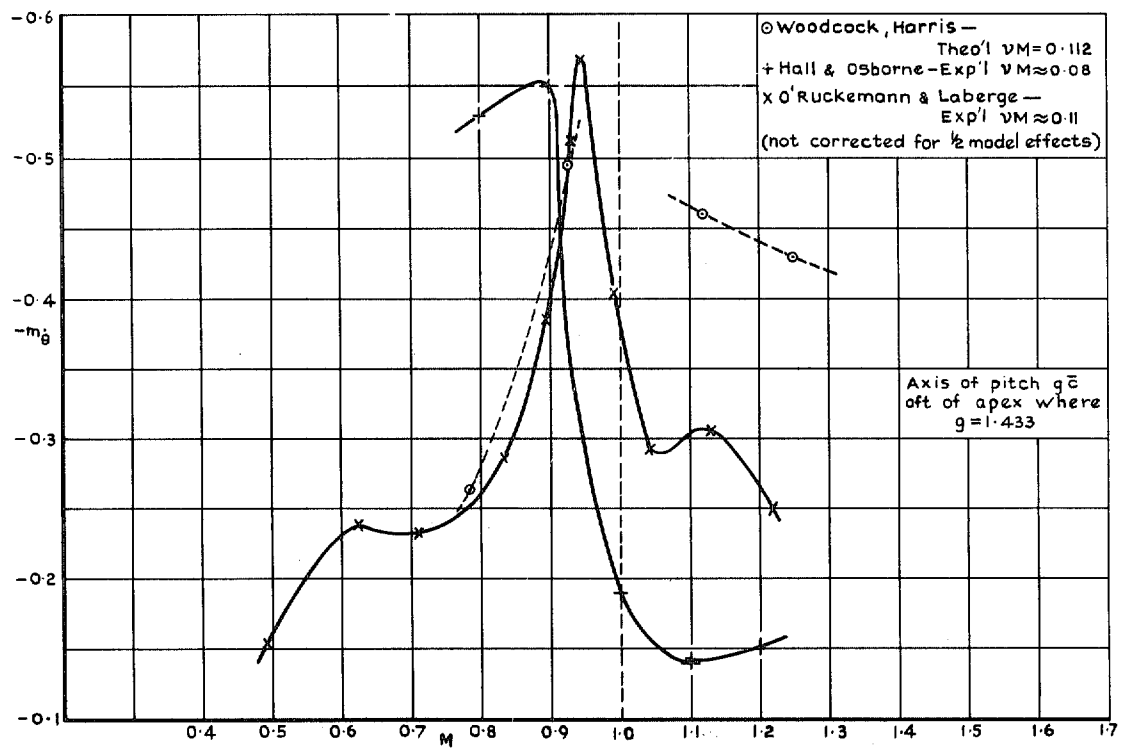

FIG. 21. Variation of $(-m_{\dot{\theta}})$ with M. Wing B, axis $0{\cdot}768c_0$, $\nu M \approx 0{\cdot}1$.

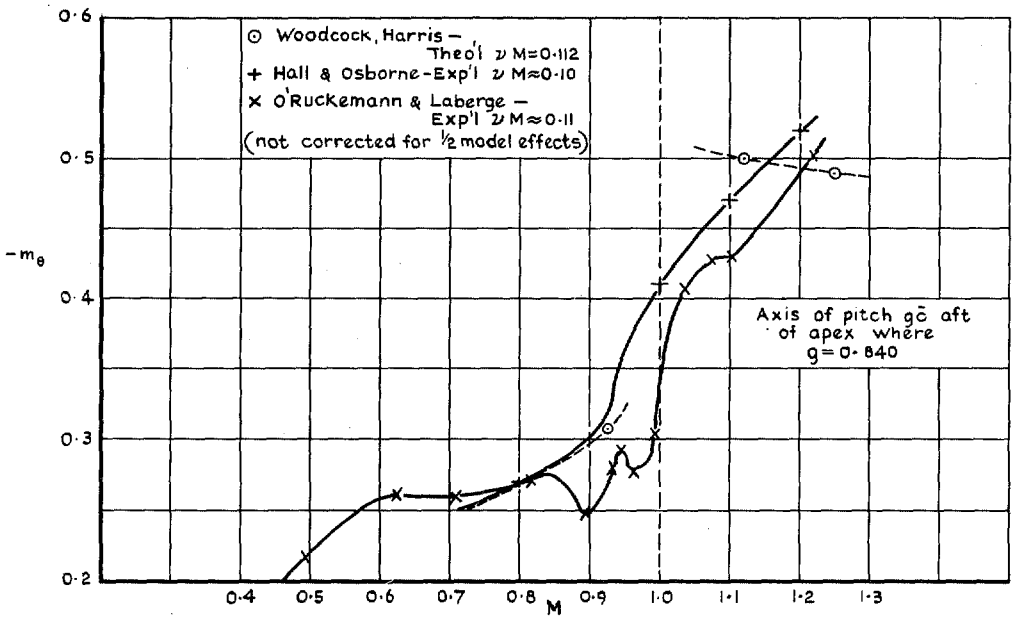

FIG. 22. Variation of $(-m_\theta)$ with M. Wing E, axis $0{\cdot}520c_0$, $\nu M \approx 0{\cdot}1$.

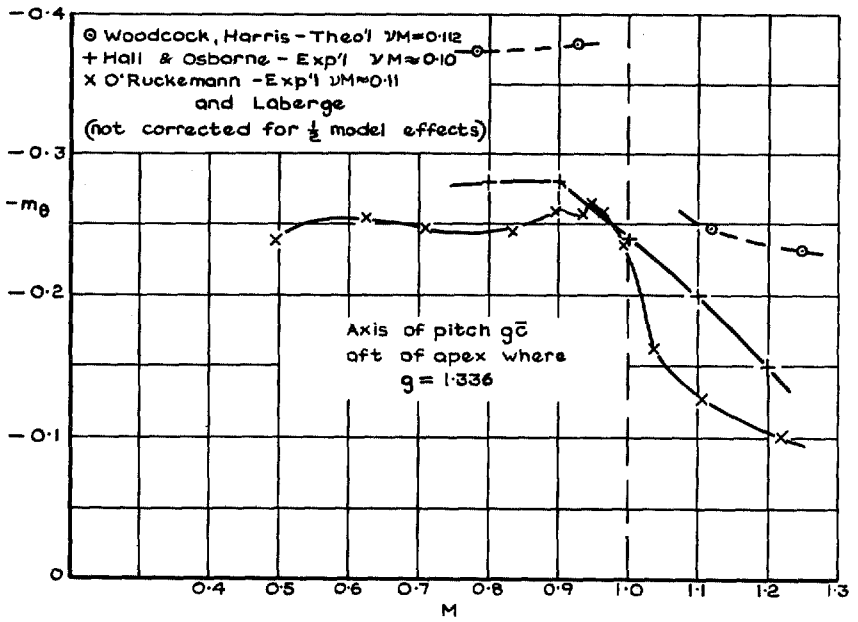

FIG. 23. Variation of $(-m_\theta)$ with M. Wing E, axis $0{\cdot}827c_0$, $\nu M \approx 0{\cdot}1$.

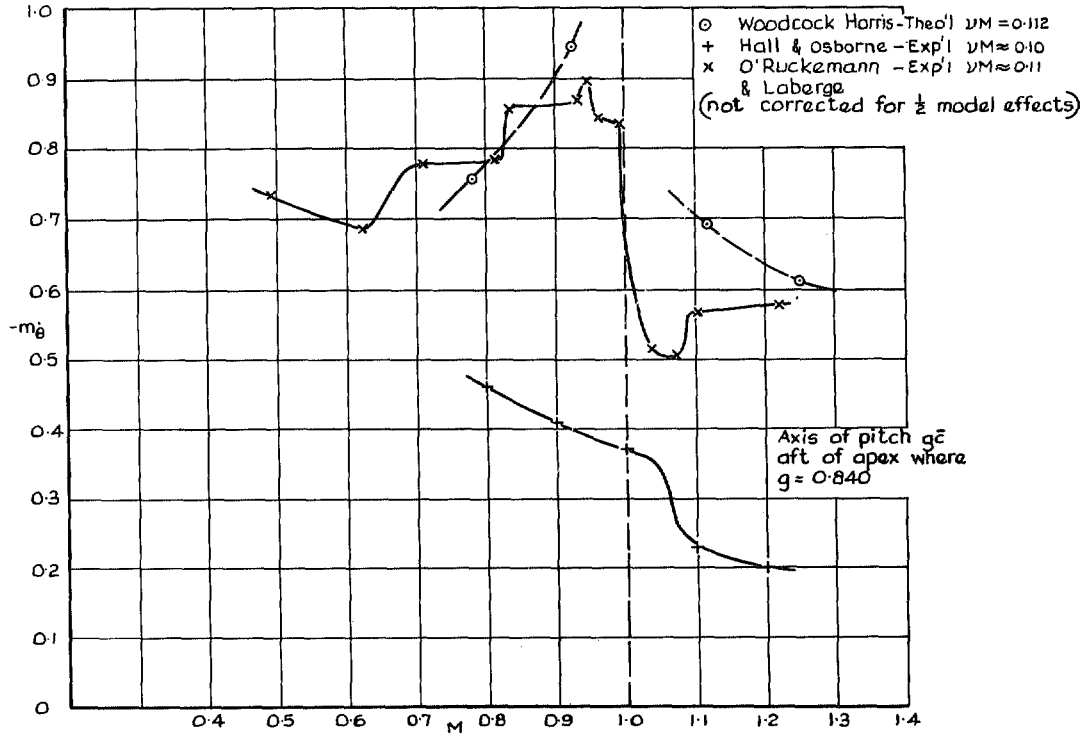

FIG. 24. Variation of $(-m_{\dot{\theta}})$ with M. Wing E, axis $0{\cdot}520c_0$, $\nu M \approx 0{\cdot}1$.

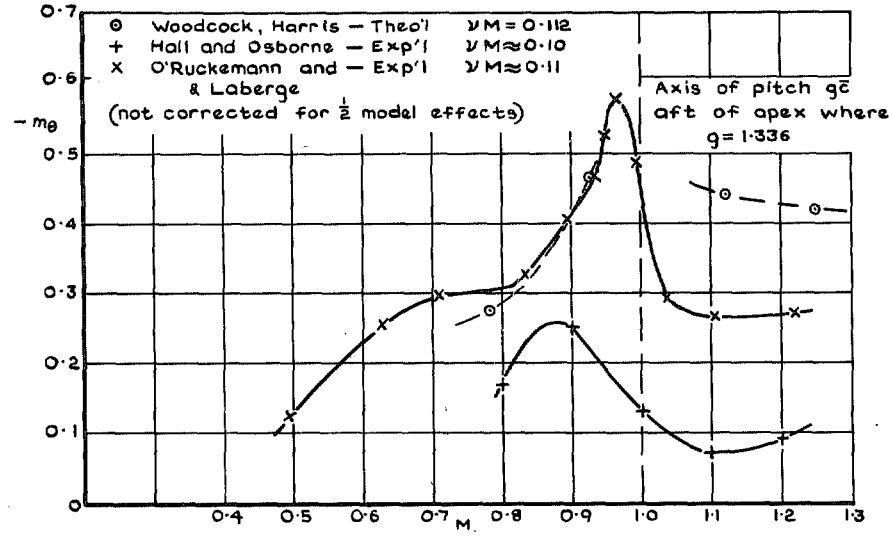

FIG. 25. Variation of $(-m_{\dot{\theta}})$ with M. Wing E, axis $0{\cdot}827c_0$, $\nu M \approx 0{\cdot}1$.

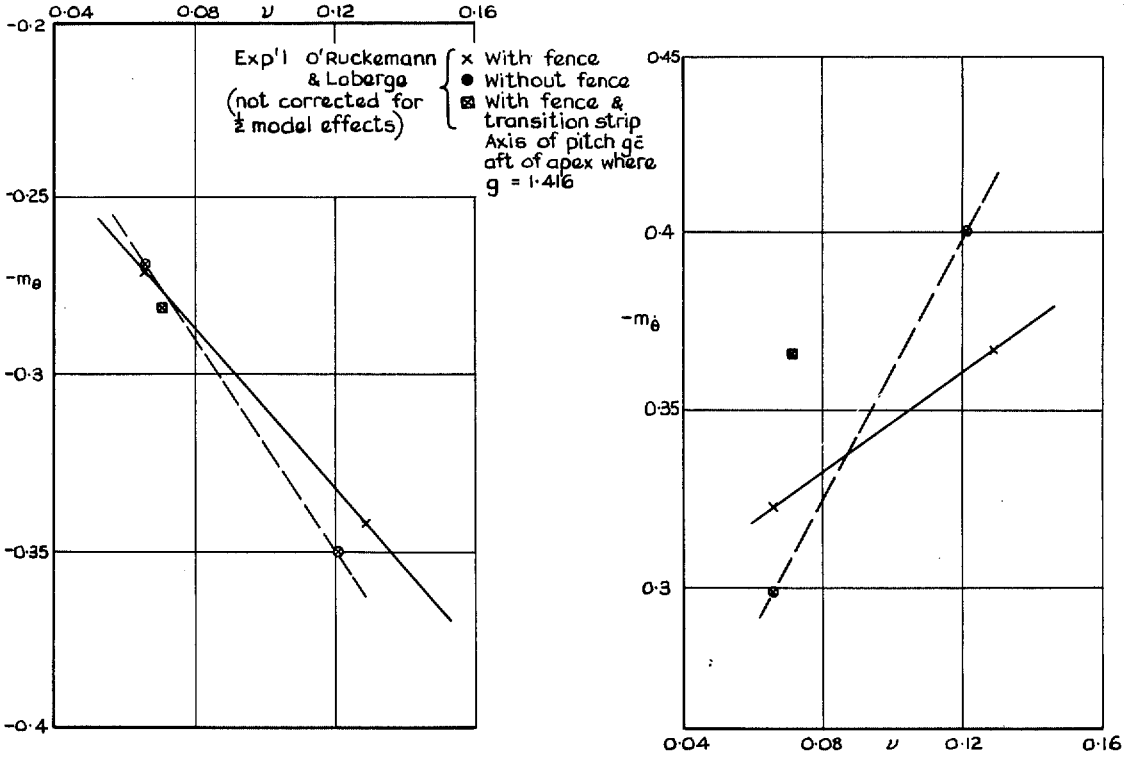

FIG. 26. Effect of fences and transition. Wing A, $M = 1{\cdot}56$, axis $0{\cdot}759c_0$.

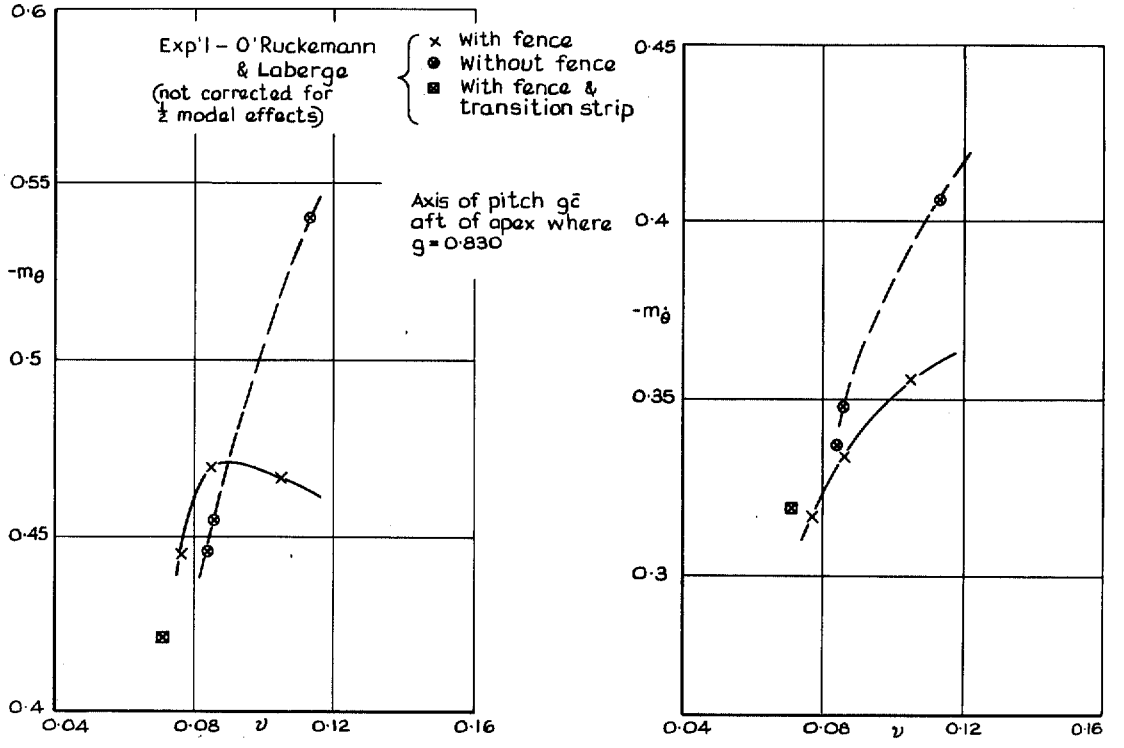

FIG. 27. Effect of fences and transition. Wing A, $M = 2{\cdot}0$, axis $0{\cdot}445c_0$.

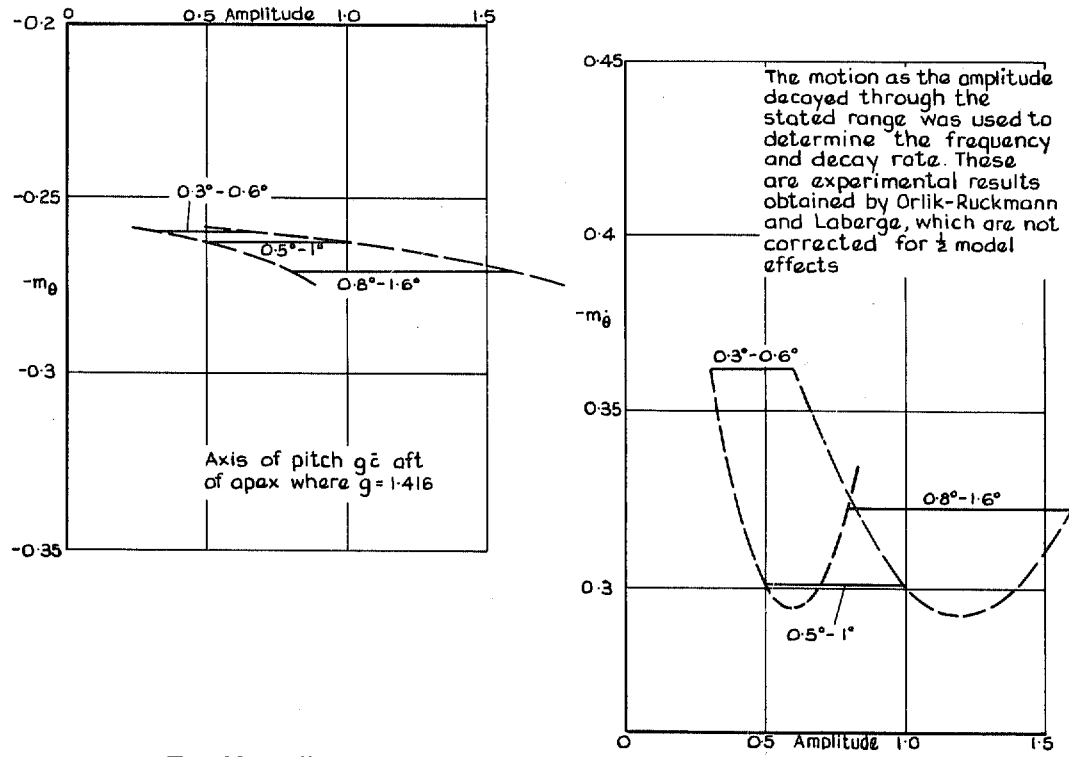

FIG. 28. Effect of amplitude. Wing A, $M = 1{\cdot}56$, $\nu = 0{\cdot}066$, axis $0{\cdot}759c_0$.

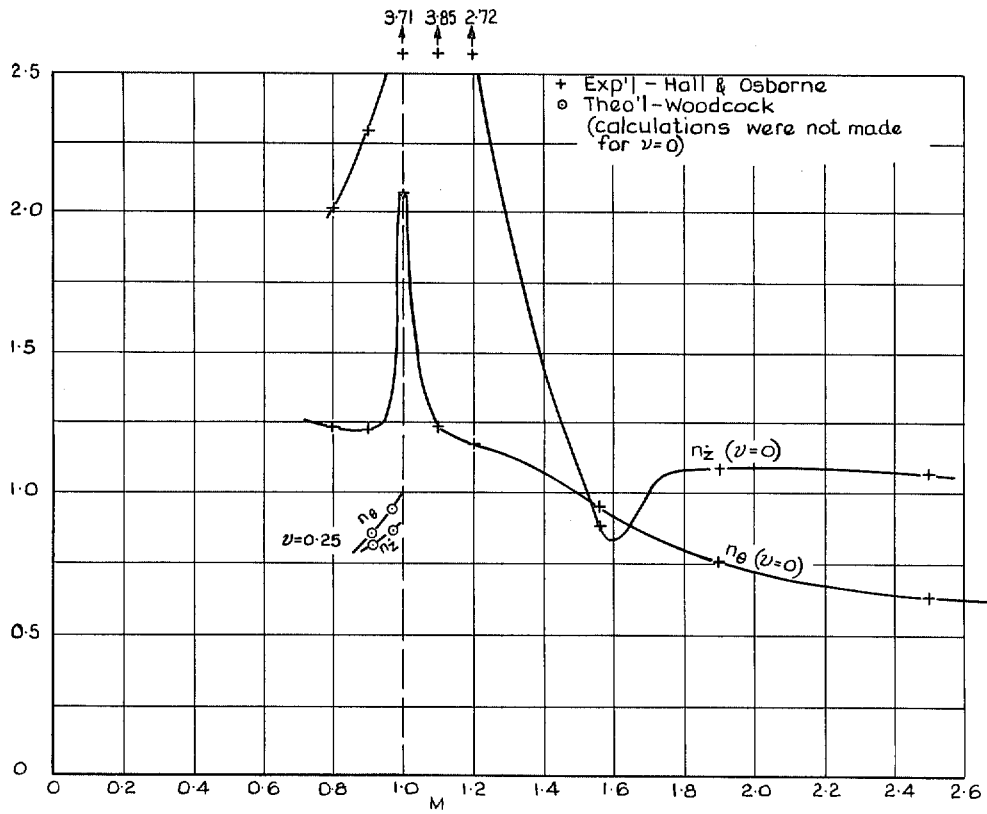

FIG. 29. Variation of $n_{\dot{z}}$ and n_θ with M. Wing A, axis at apex ($g = 0$).

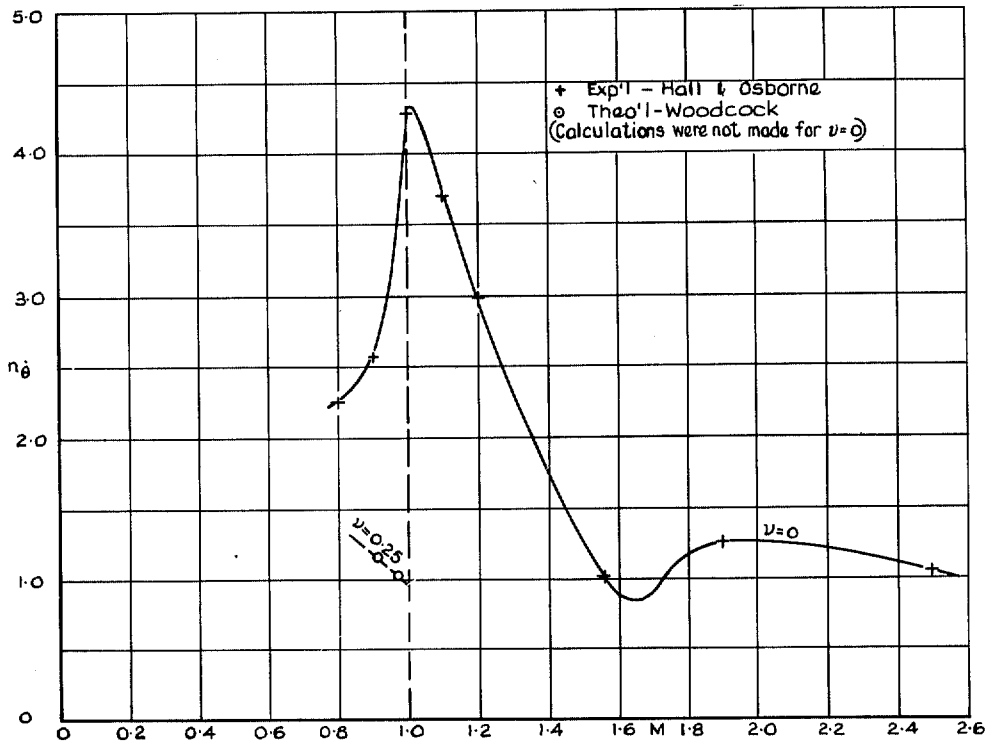

FIG. 30. Variation of n_θ with M. Wing A, axis at apex ($g = 0$).

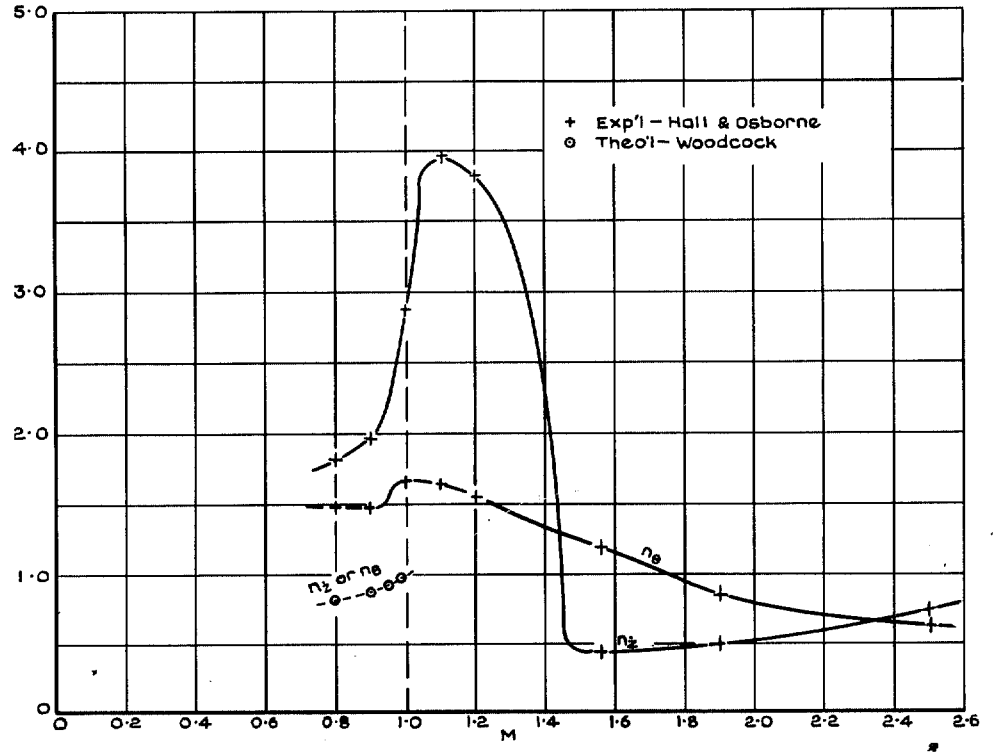

FIG. 31. Variation of n_z and n_θ with M. Wing G ($A = 3$ version), axis at apex ($g = 0$), $\nu = 0$.

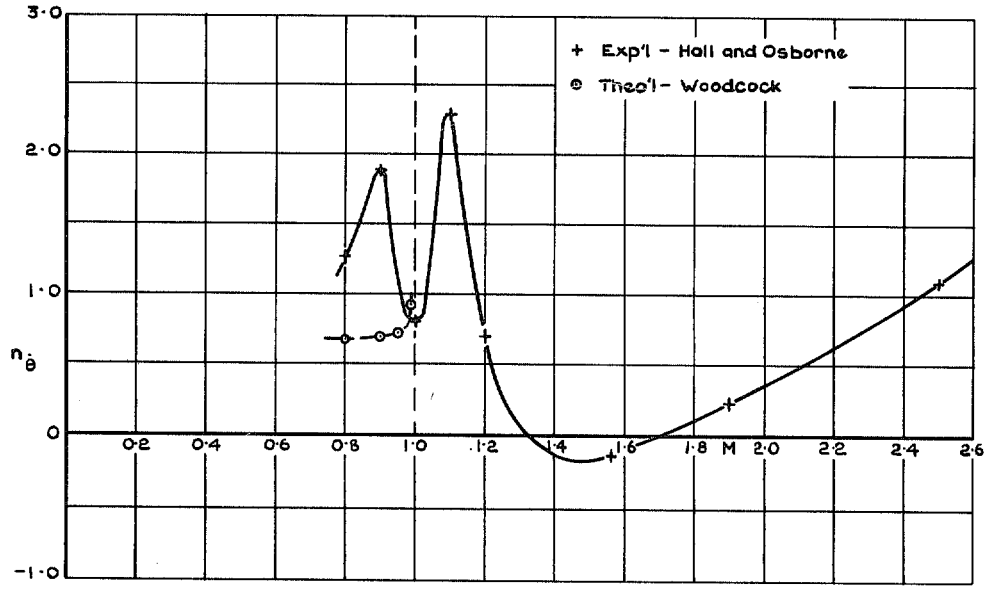

FIG. 32. Variation of $n_{\dot{\theta}}$ with M. Wing G ($A = 3$ version), axis at apex ($g = 0$), $v = 0$.

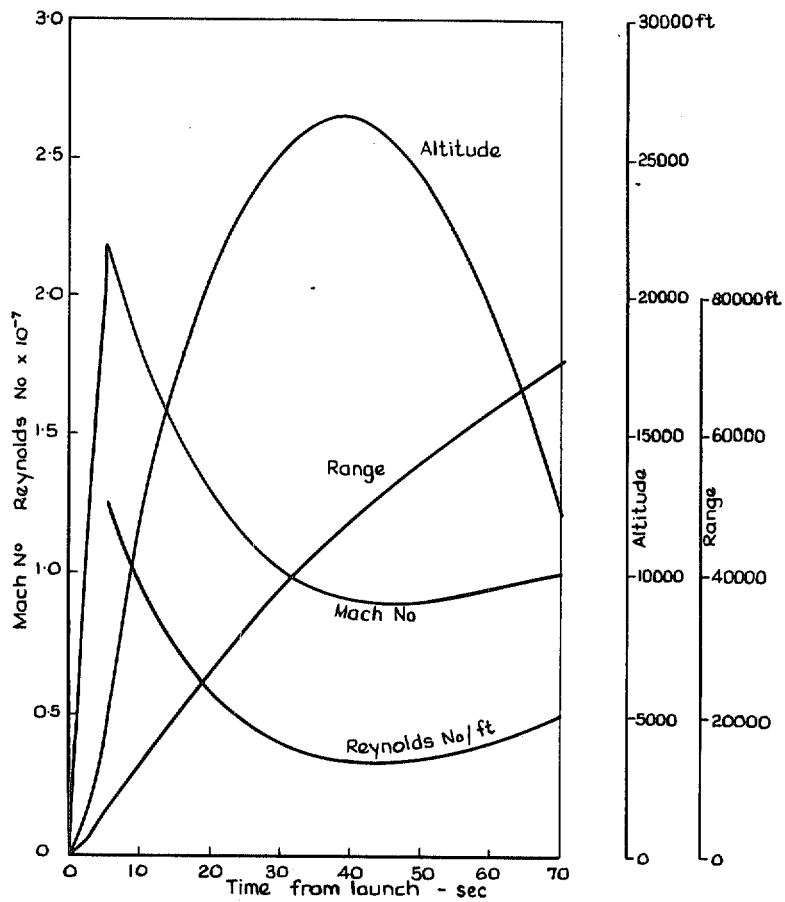

FIG. 33. Typical performance of Koorigal test vehicle.

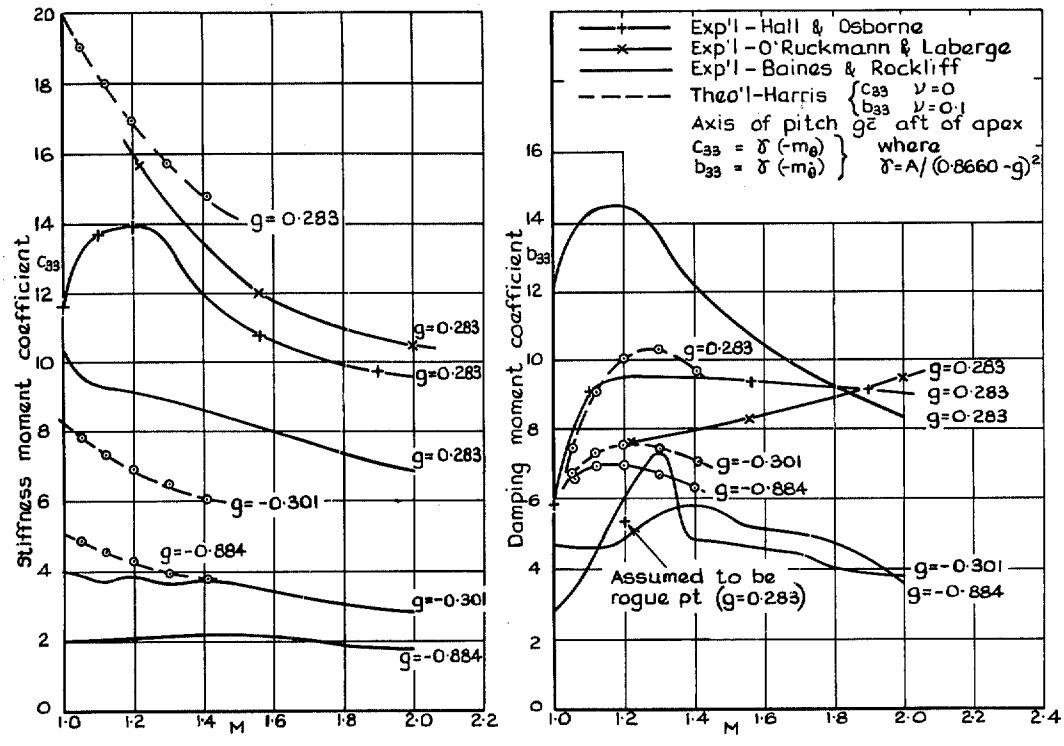

FIG. 34. Free-flight results compared with theory. Wing A, supersonic (without transition strip).

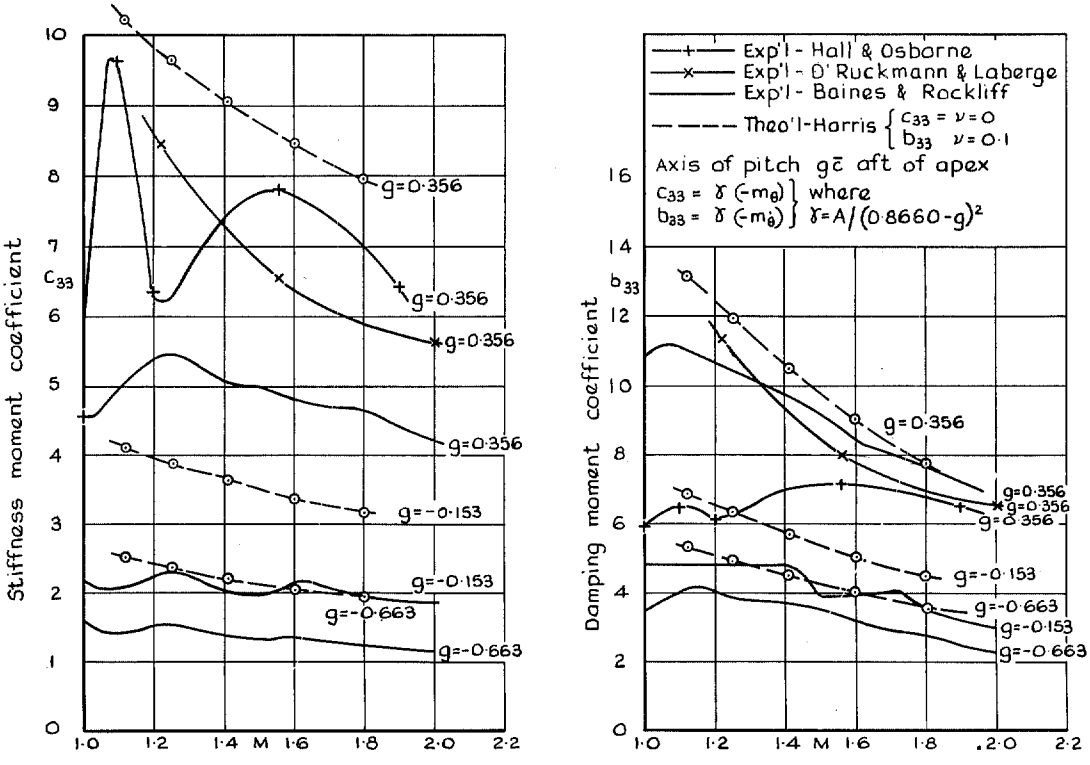

FIG. 35. Free-flight results compared with theory. Wing B, supersonic.

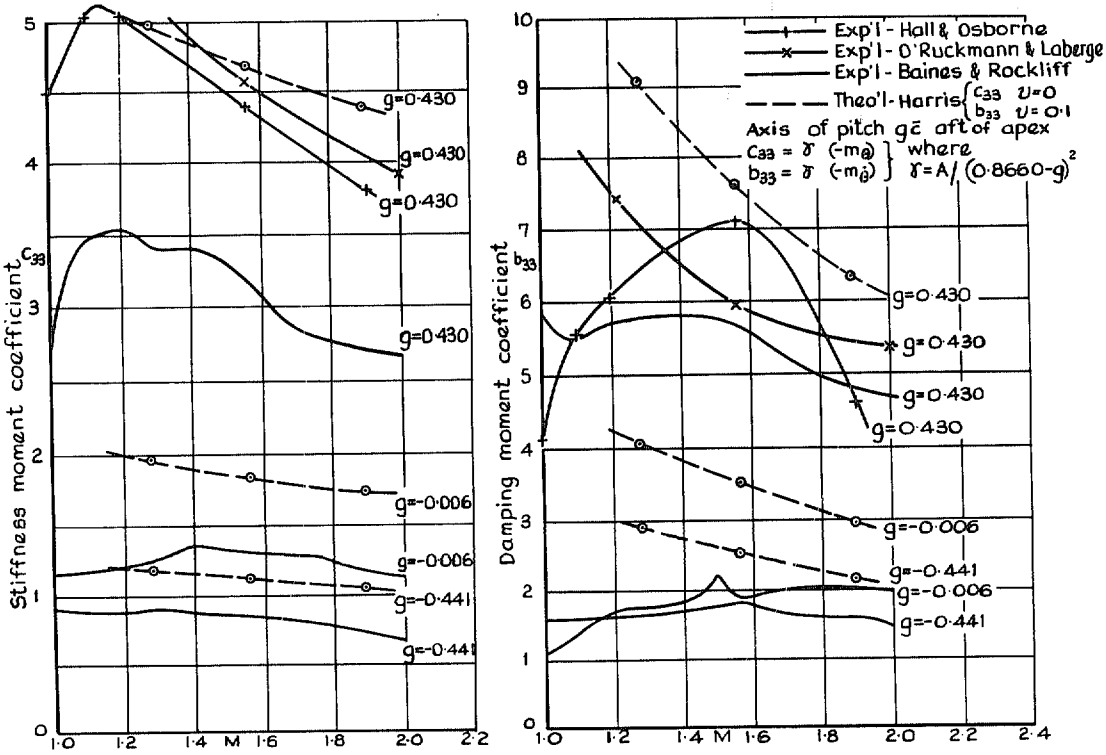

FIG. 36. Free-flight results compared with theory. Wing C, supersonic.

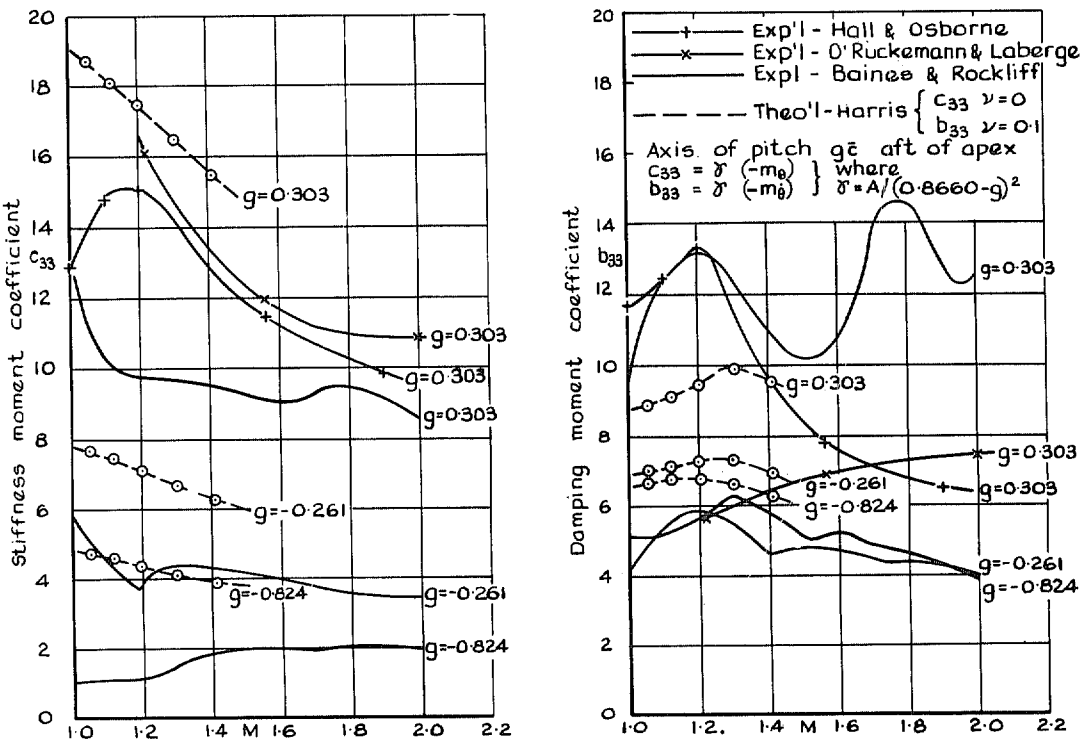

FIG. 37. Free-flight results compared with theory. Wing D, supersonic.

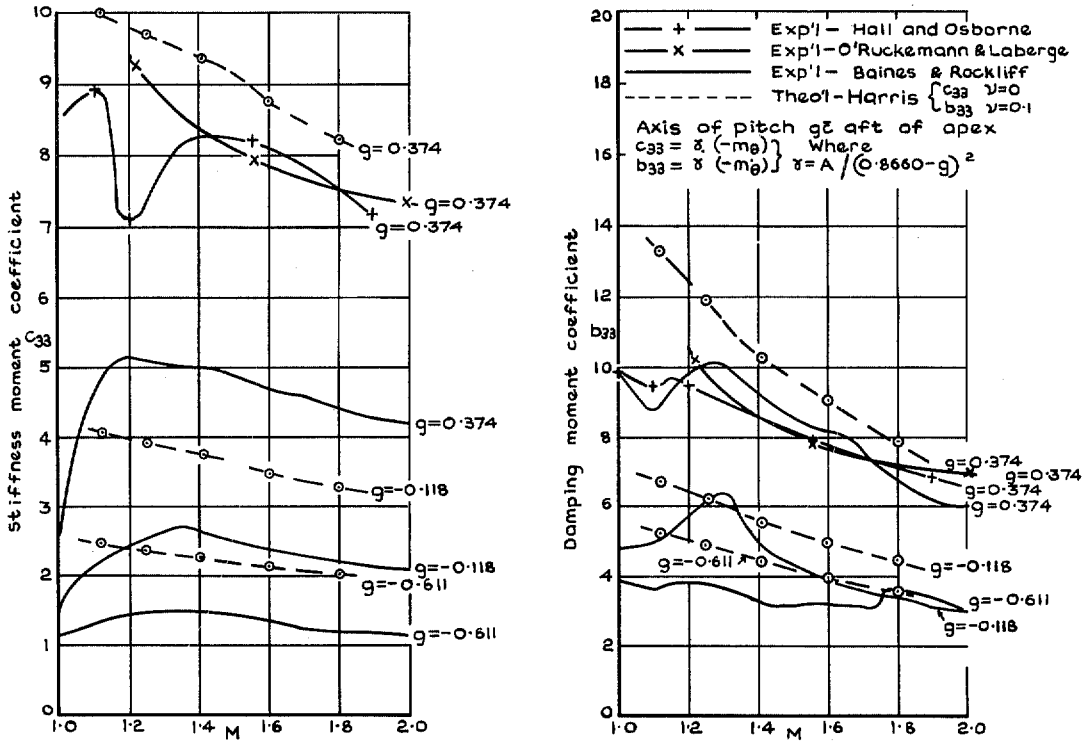

FIG. 38. Free-flight results compared with theory. Wing E, supersonic.

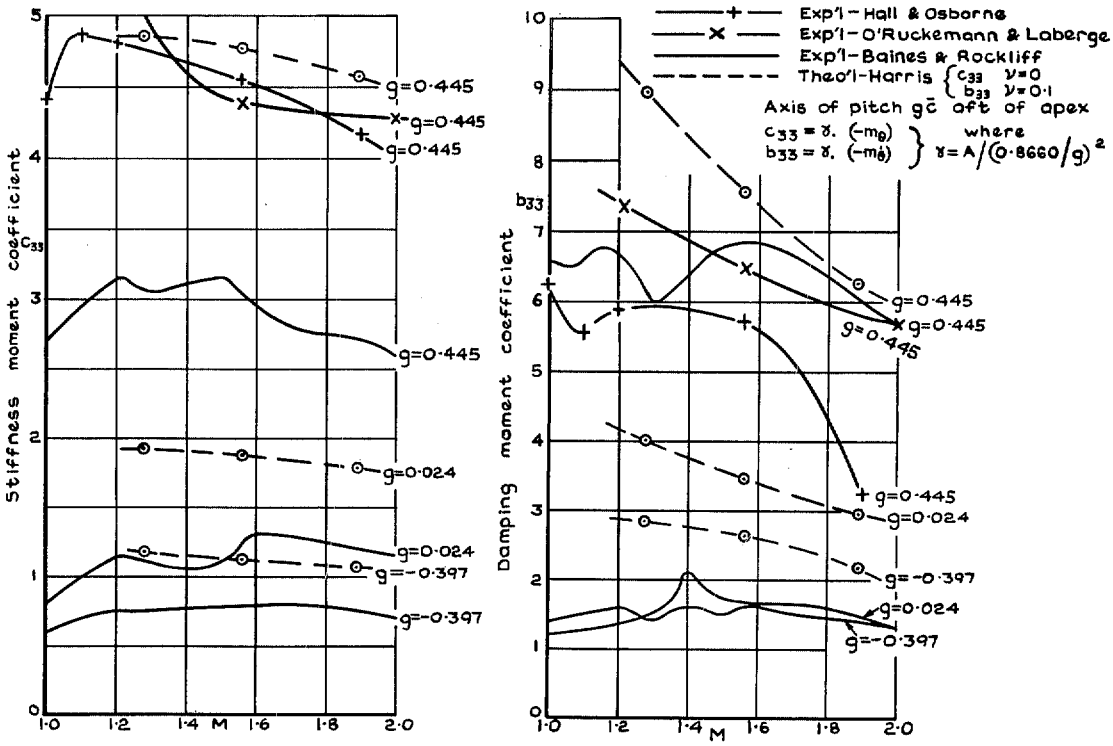

FIG. 39. Free-flight results compared with theory. Wing F, supersonic.

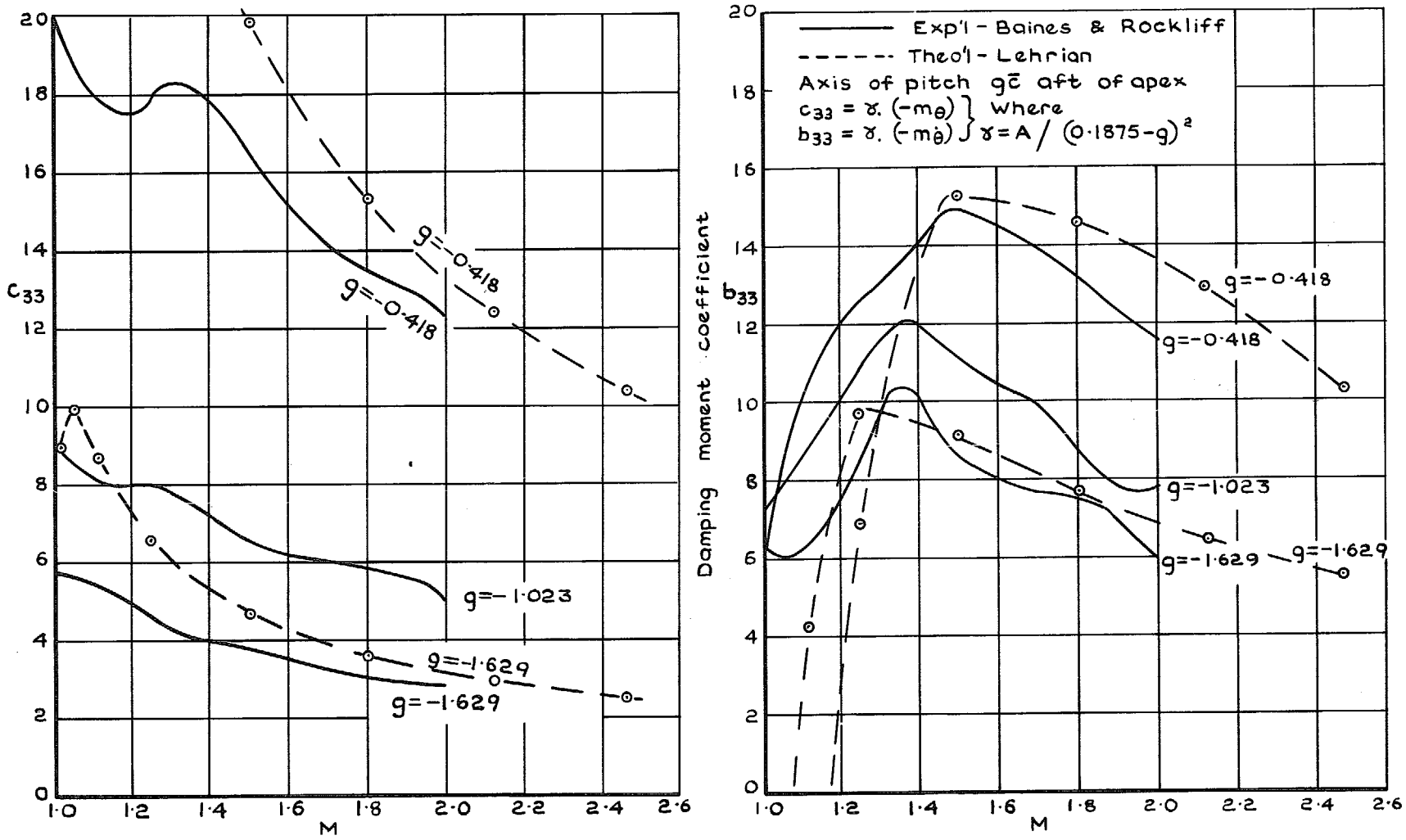

FIG. 40. Free-flight results. Wing G ($A = 4$ version), supersonic.

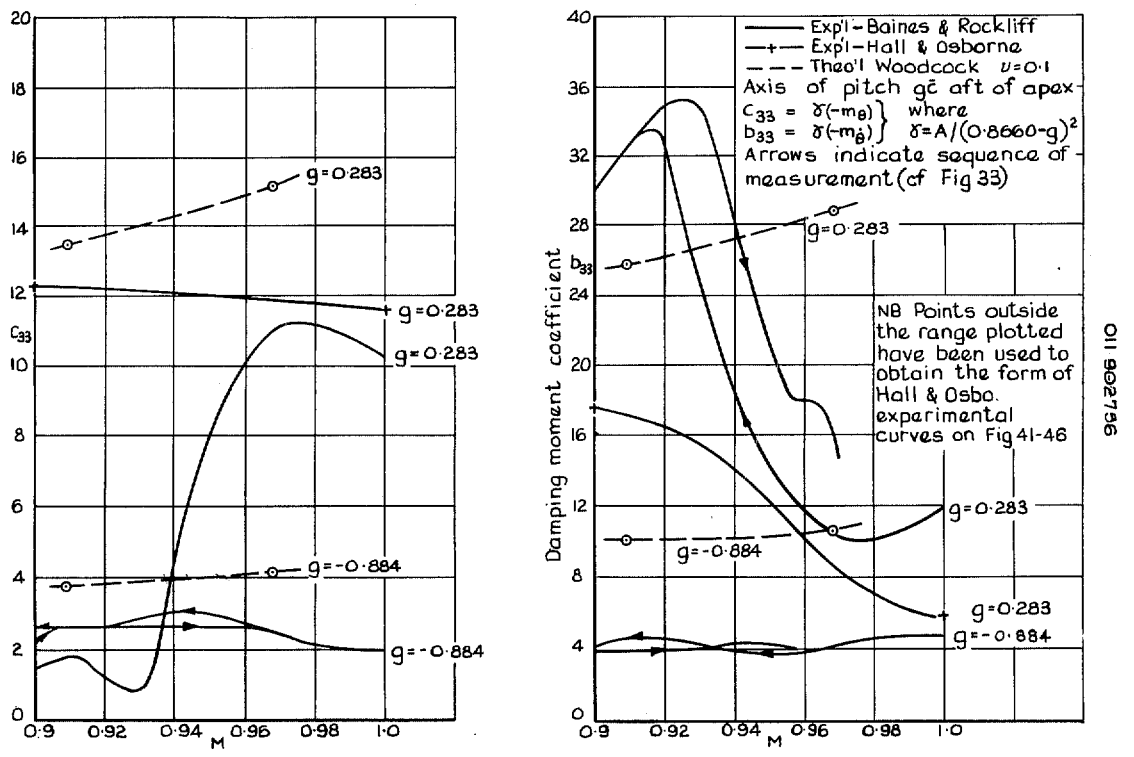

FIG. 41. Free-flight results compared with theory. Wing A, subsonic (without transition strip).

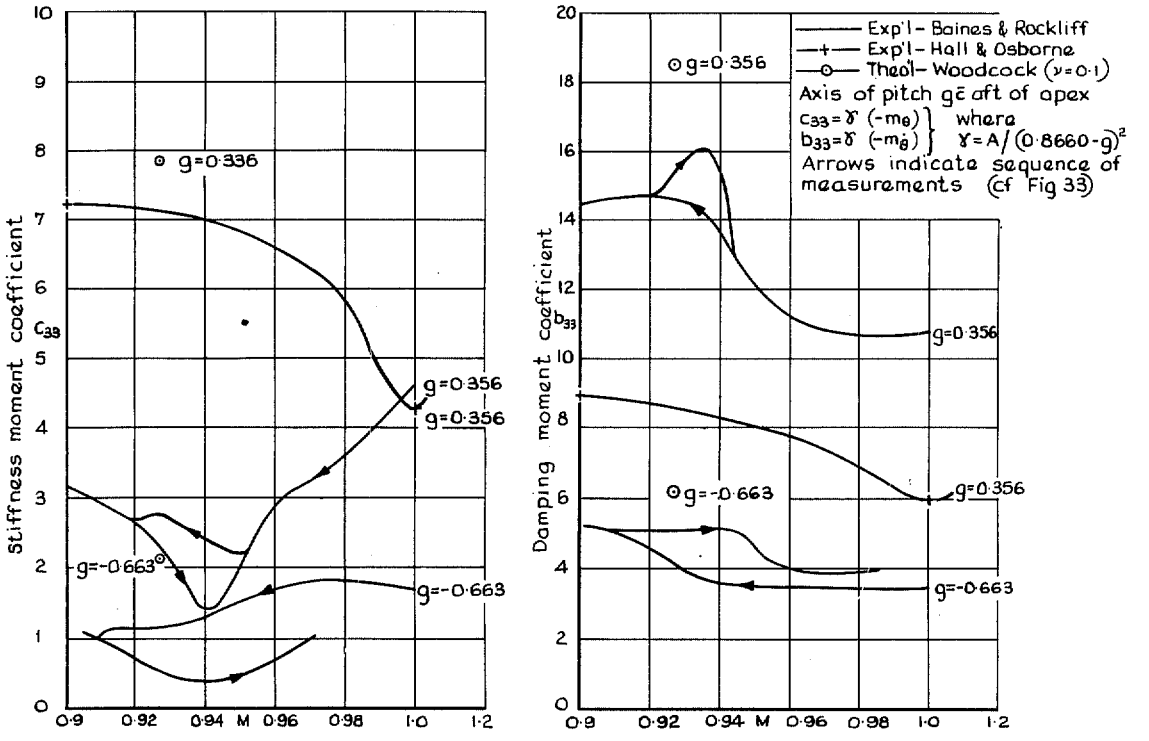

FIG. 42. Free flight results compared with theory. Wing B, subsonic.

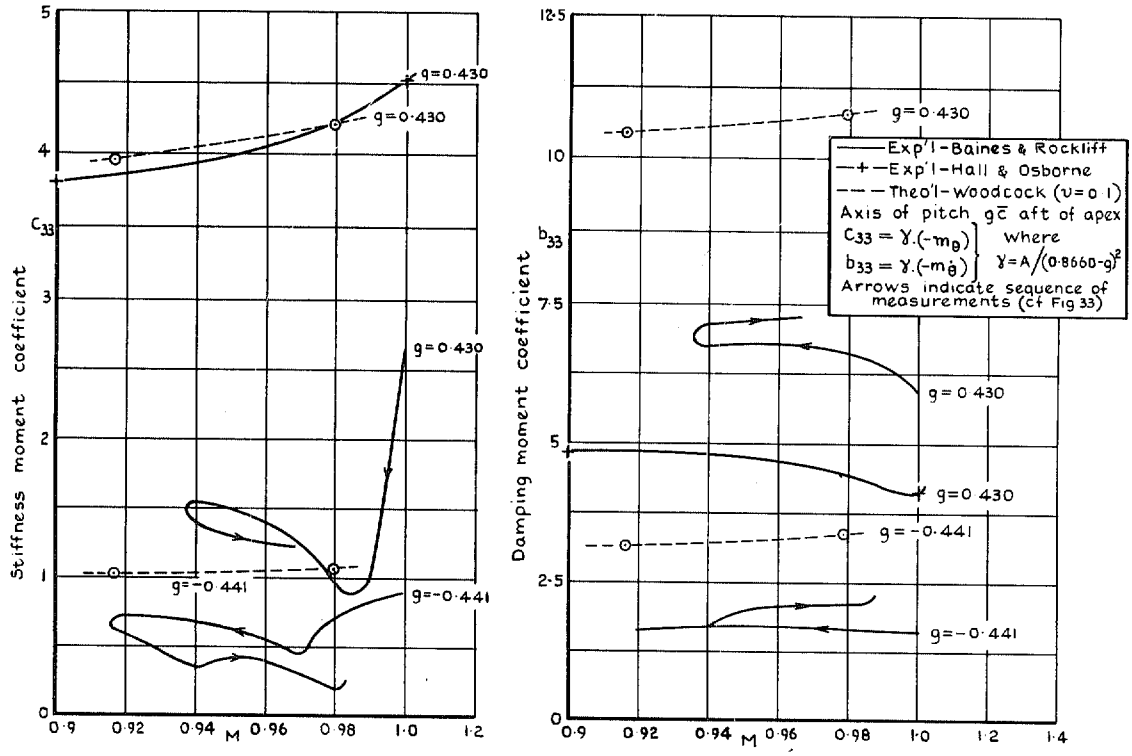

FIG. 43. Free flight results compared with theory. Wing C, subsonic.

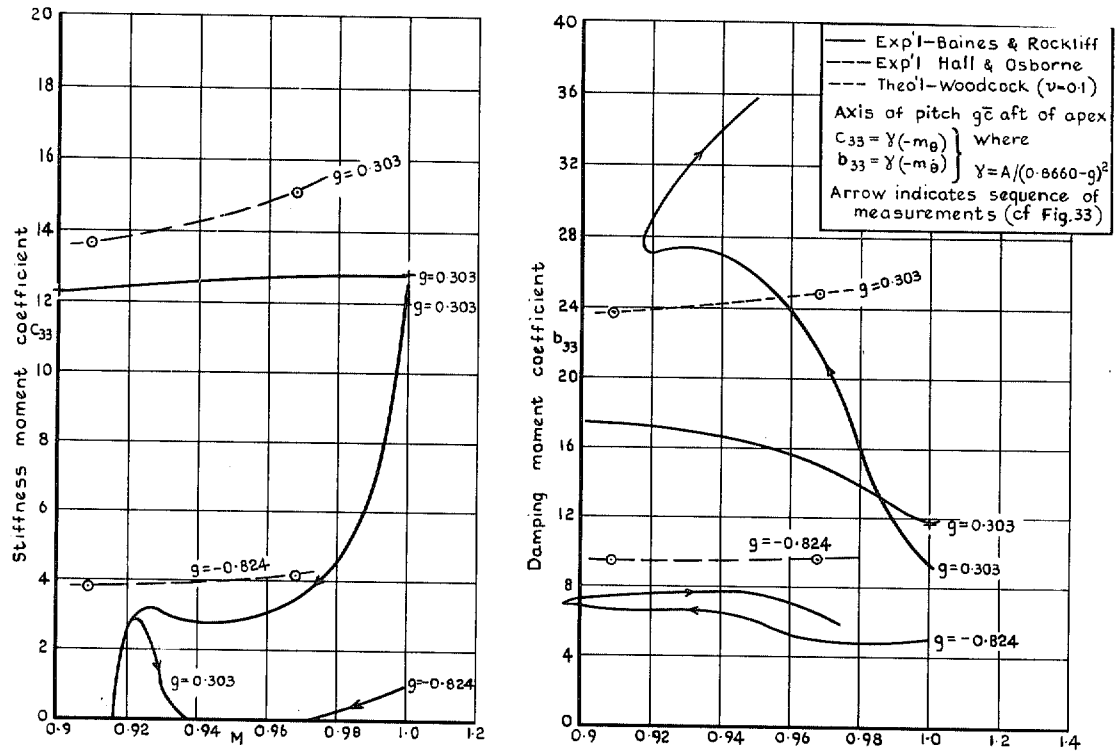

FIG. 44. Free flight results compared with theory. Wing D, subsonic.

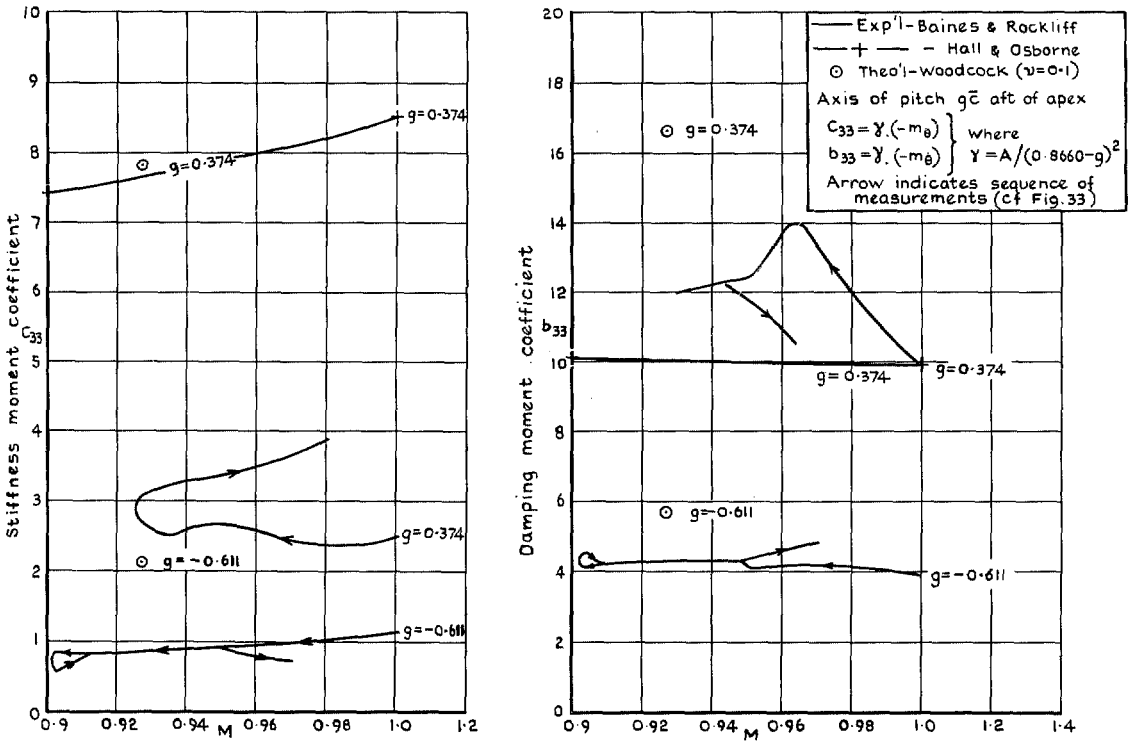

FIG. 45. Free flight results compared with theory. Wing E, subsonic.

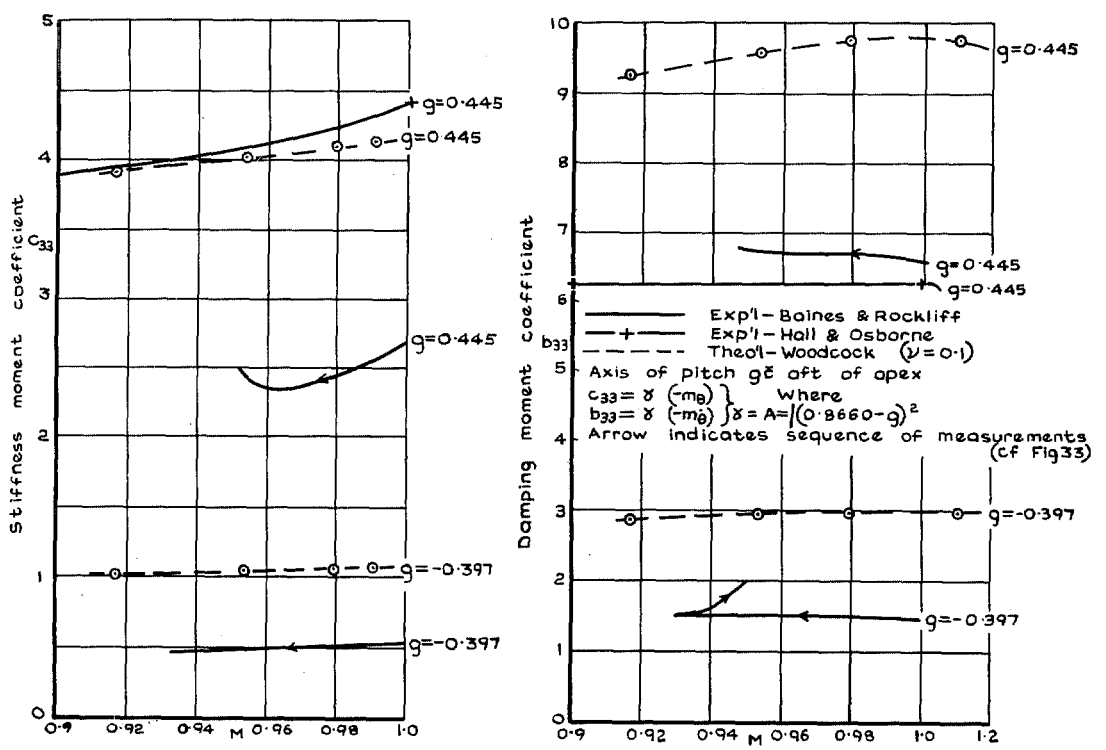

FIG. 46. Free flight results compared with theory. Wing F, subsonic.

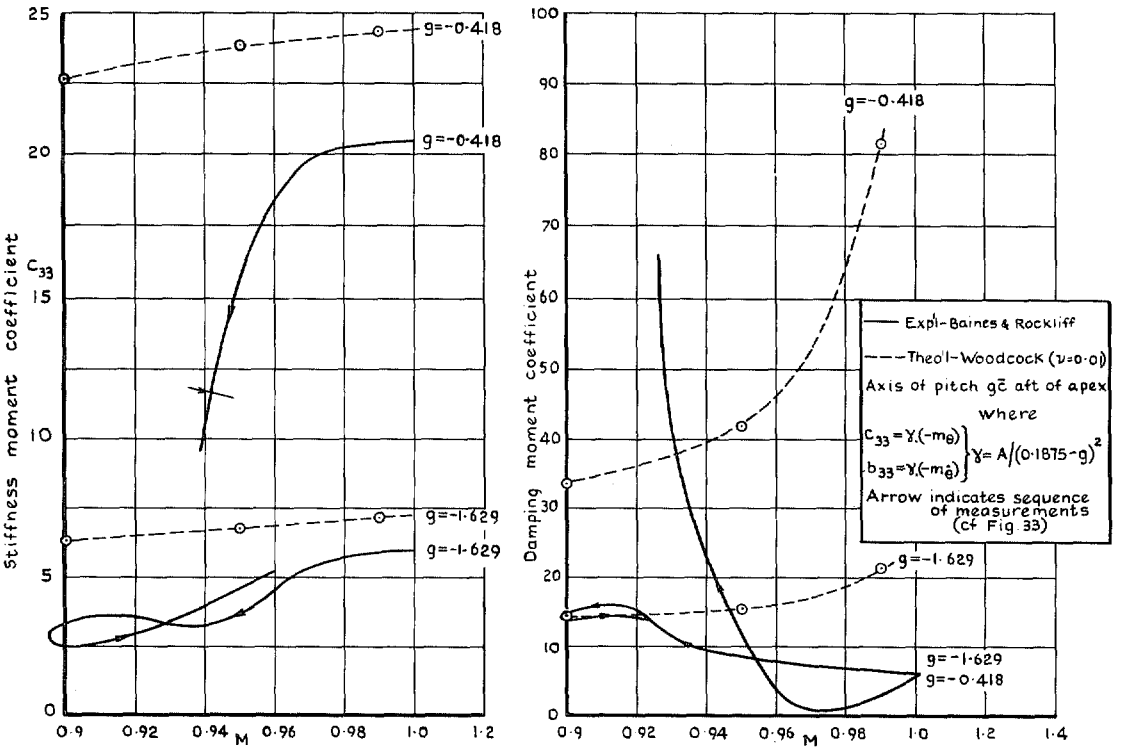

FIG. 47. Free flight results compared with theory. Wing G ($A = 4$ version), subsonic.

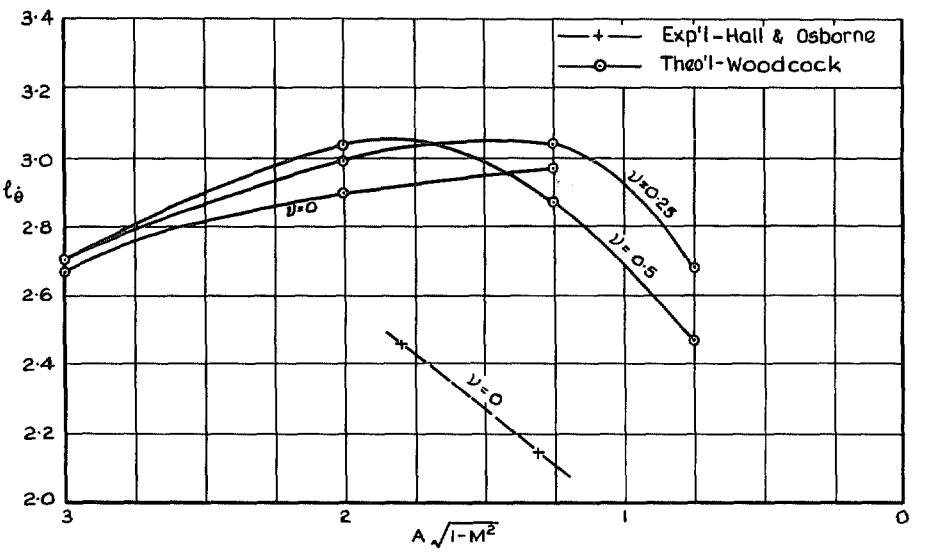

FIG. 48. Variation of $l_{\dot\theta}$ with $A\sqrt{1-M^2}$. Wing A, axis at apex ($g = 0$).

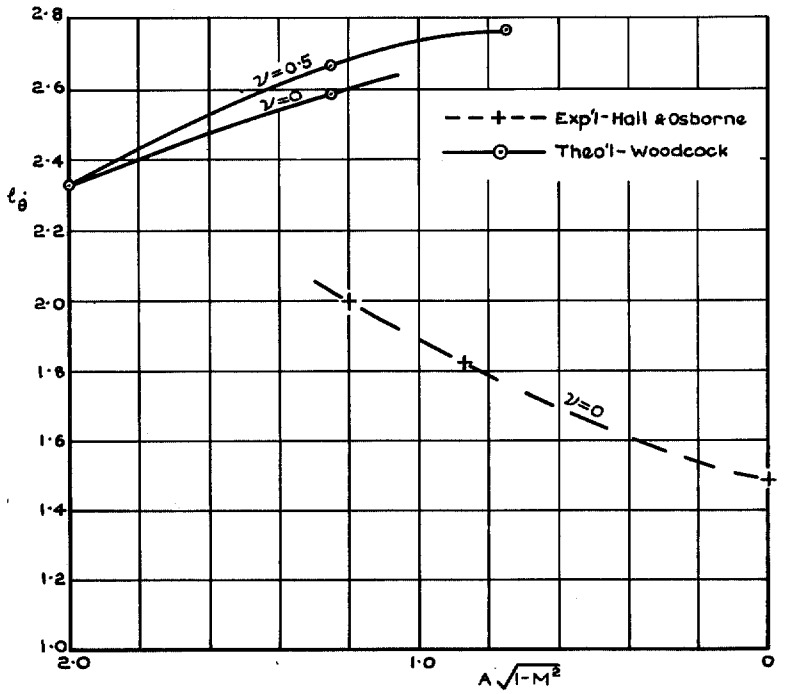

FIG. 49. Variation of $l_{\dot{\theta}}$ with $A\sqrt{1-M^2}$. Wing B, axis at apex ($g = 0$).

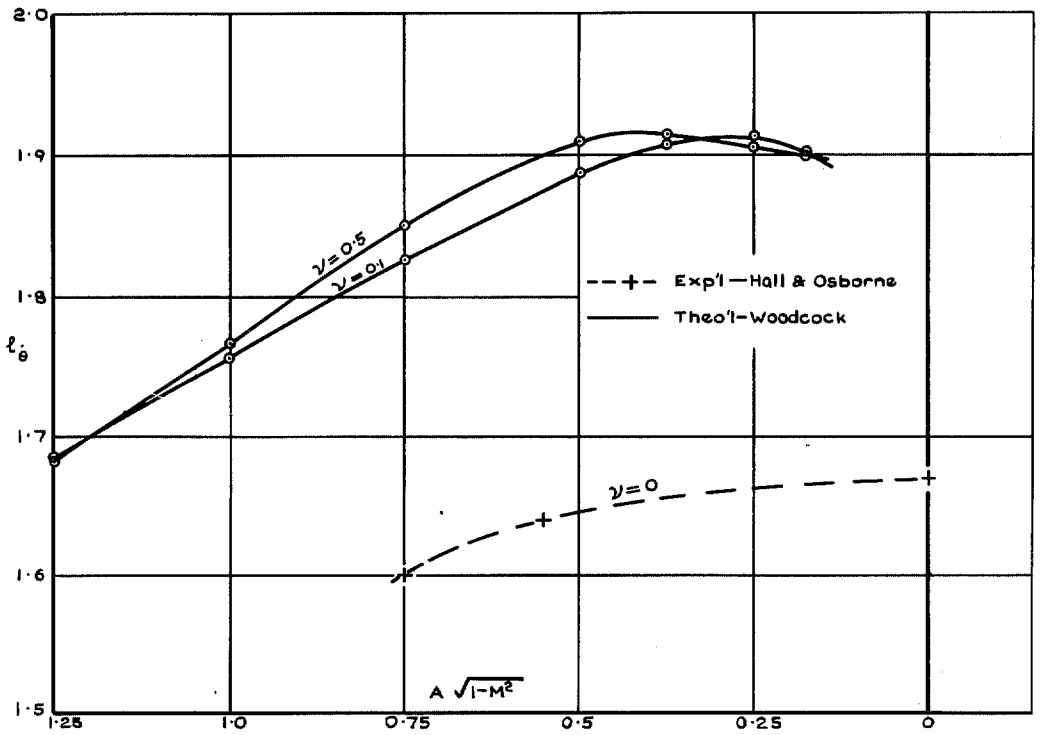

FIG. 50. Variation of $l_{\dot{\theta}}$ with $A\sqrt{1-M^2}$. Wing F, axis at apex ($g = 0$).

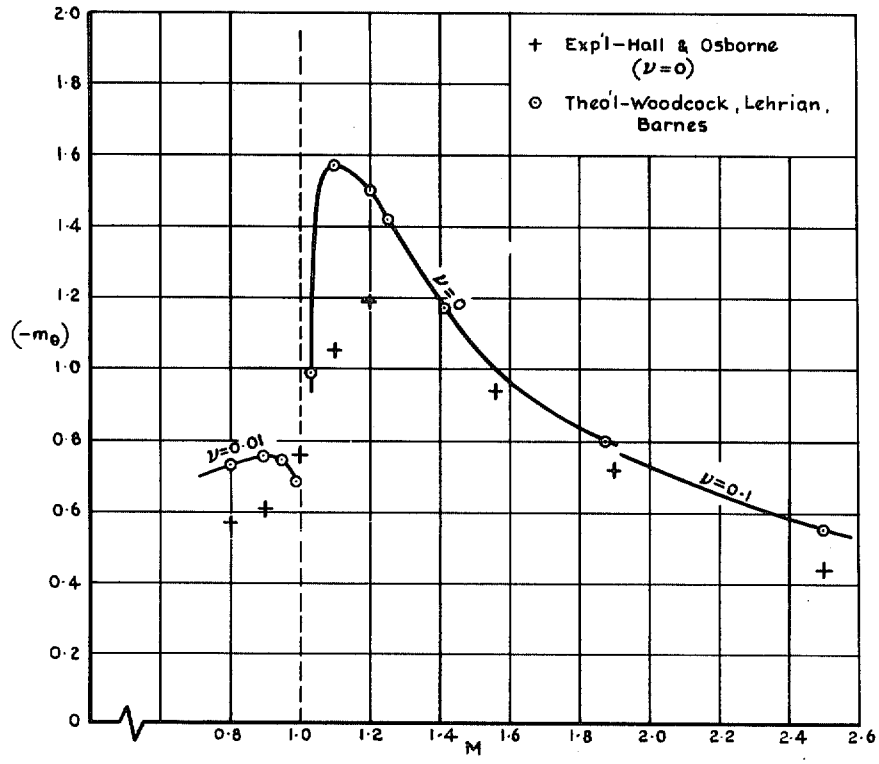

FIG. 51. Variation of $(-m_\theta)$ with M. Wing G ($A = 3$ version) axis at apex ($g = 0$).

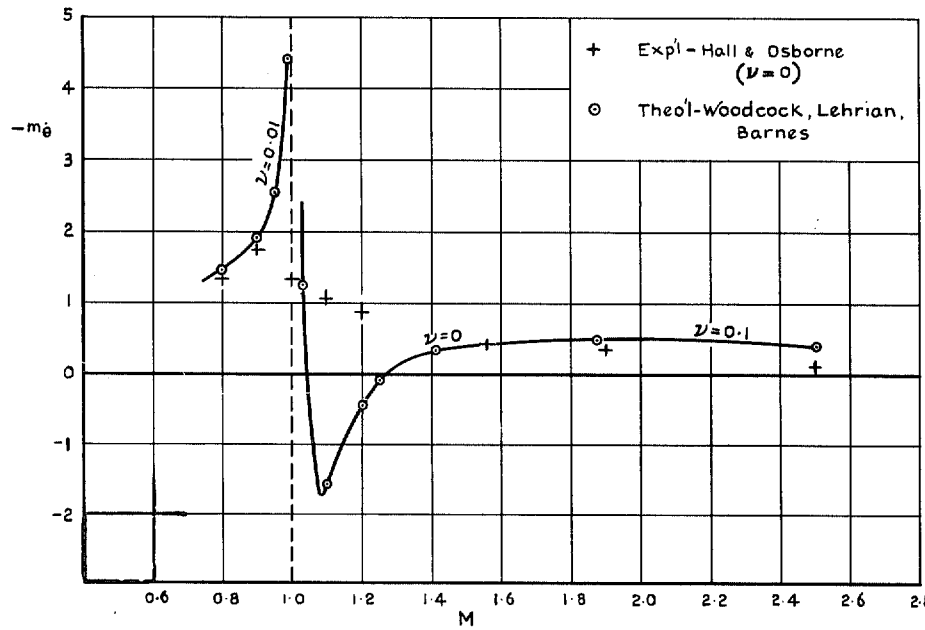

FIG. 52. Variation of $(-m_{\dot\theta})$ with M. Wing G ($A = 3$ version), axis at apex ($g = 0$).

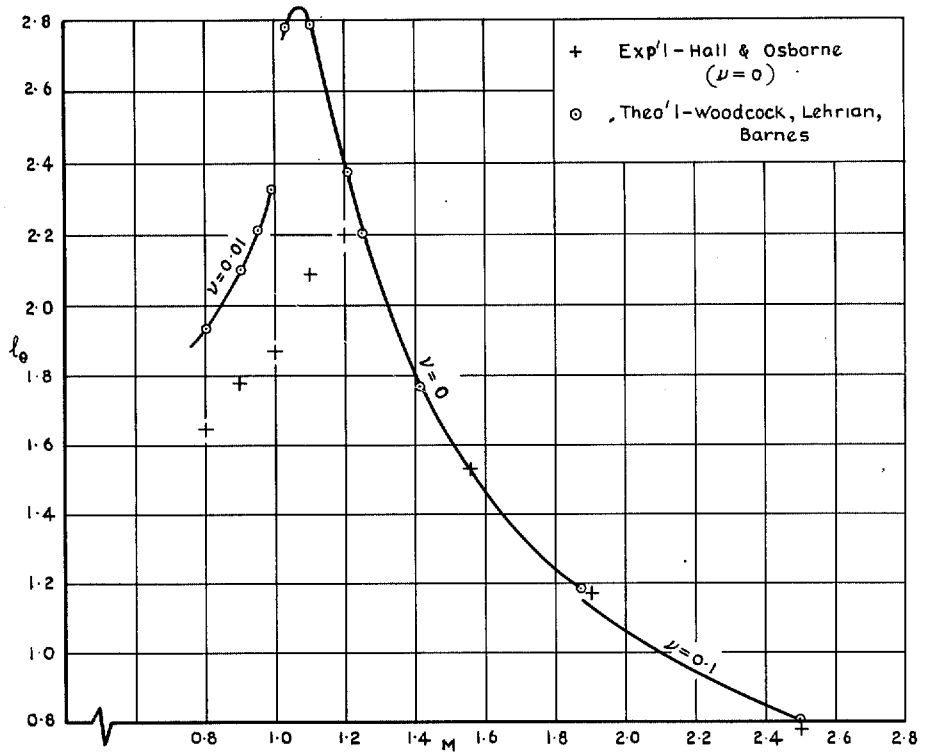

FIG. 53. Variation of l_θ with M. Wing G ($A = 3$ version), axis at apex ($g = 0$).

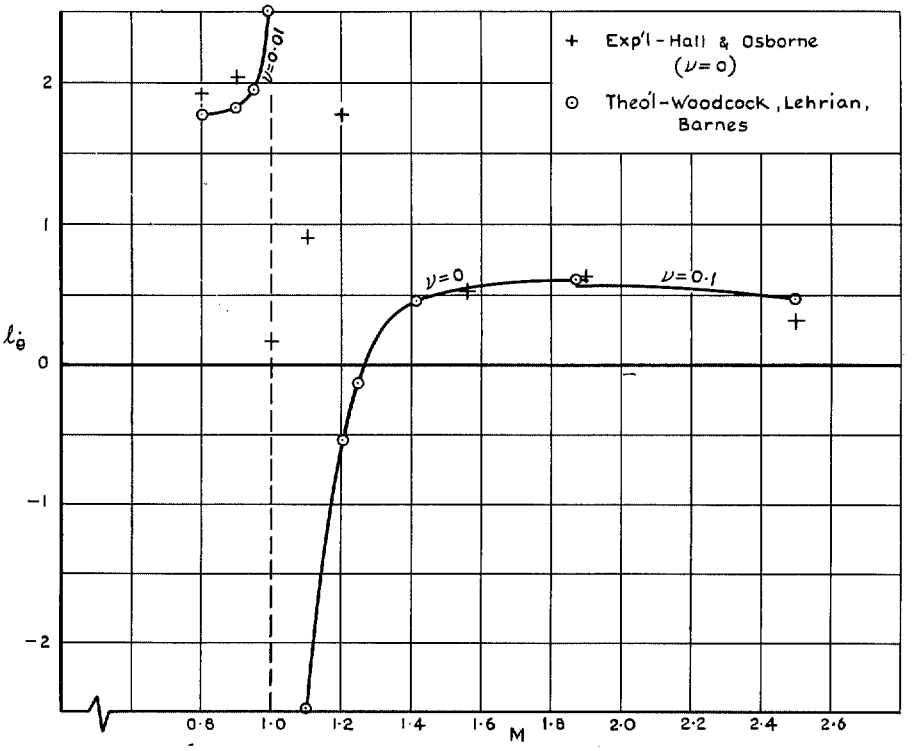

FIG. 54. Variation of l_θ with M. Wing G ($A = 3$ version), axis at apex ($g = 0$).

Printed in Wales for Her Majesty's Stationery Office by Allens Printers (Wales) Limited

Dd. 135646 K.5

Published by
HER MAJESTY'S STATIONERY OFFICE

To be purchased from
49 High Holborn, London W.C.1
13A Castle Street, Edinburgh 2
109 St. Mary Street, Cardiff CF1 1JW
Brazannose Street, Manchester M60 8AS
50 Fairfax Street, Bristol BS1 3DE
258 Broad Street, Birmingham 1
7 Linenhall Street, Belfast BT2 8AY
or through any bookseller

S.O. Code No. 23–3581